Thesis presented to the Instituto Tecnológico de Aeronáutica, in partial fulfillment of the requirements for the degree of Doctor of Science in the Graduate Program of Physics, Field of Nuclear Physics.

Estevão Alves Teixeira

MONTE CARLO MODEL OF DEUTERON EMISSION IN PRE-EQUILIBRIUM NUCLEAR REACTIONS

Thesis approved in its final version by signatories below:

Prof. Dr. Brett Vern Carlson

Advisor

Prof. Dr. Emília Villani

Pro-Rector of Graduate Courses

Campo Montenegro
São José dos Campos, SP - Brazil
2023

Cataloging-in Publication Data
Documentation and Information Division

Teixeira, Estevão Alves
Monte Carlo model of deuteron emission in pre-equilibrium nuclear reactions / Estevão Alves Teixeira.
São José dos Campos, 2023.
142f.

Thesis of Doctor of Science – Course of Physics. Area of Nuclear Physics – Instituto Tecnológico de Aeronáutica, 2023. Advisor: Prof. Dr. Brett Vern Carlson.

1. Nuclear reactions. 2. Pre-equilibrium. 3. Monte Carlo. I. Instituto Tecnológico de Aeronáutica. II. Title.

BIBLIOGRAPHIC REFERENCE

TEIXEIRA, Estevão Alves. **Monte Carlo model of deuteron emission in pre-equilibrium nuclear reactions**. 2023. 142f. Thesis of Doctor of Science – Instituto Tecnológico de Aeronáutica, São José dos Campos.

CESSION OF RIGHTS

AUTHOR'S NAME: Estevão Alves Teixeira
PUBLICATION TITLE: Monte Carlo model of deuteron emission in pre-equilibrium nuclear reactions.
PUBLICATION KIND/YEAR: Thesis / 2023

Estevão Alves Teixeira
São José dos Campos, SP – Brazil

MONTE CARLO MODEL OF DEUTERON EMISSION IN PRE-EQUILIBRIUM NUCLEAR REACTIONS

Estevão Alves Teixeira

Thesis Committee Composition:

Prof. Dr.	Manuel Malheiro	Presidente	-	ITA
Prof. Dr.	Brett Vern Carlson	Advisor	-	ITA
Prof. Dr.	Maurício Pazianotto	Membro Interno	-	ITA
Prof. Dr.	Luiz Chamon	Membro Externo	-	USP
Prof. Dr.	Felipe Canto	Membro Externo	-	UFRJ

ITA

For the advancement of science and the
appreciation of education in Brazil.

Acknowledgments

I would like to thank all professors for their dedication to teaching, all scientists for their hard work and inspiration, and all people involved in the process of advancing science.

I also would like to thank my wife, Renata Cardoso, my mother, Silvaneth Lima, along with my stepfather, Jorival Lima, and my father, João Teixeira, for supporting me. All of them provided me with the foundation to get my doctorate degree.

My special thanks go to my advisor, Prof. Brett V. Carlson, for everything! The discussions, the patience, and the way he treats his students. Prof. Brett's knowledge goes beyond my imagination, and I had the privilege to work with him during these last six to seven years.

For last, I also say thanks to all friends I made at ITA, to prof. Manuel Malheiro, a person that always talks to me and gives me support, and prof. Carlos Bertulani for accepting my application and for all help provided during my one-year scholarship in the USA.

Play the song as loud as possible,
closing your eyes and singing....

Woah, oh, oh-oh, oh
Woah, oh, oh-oh, oh
Woah, oh, oh-oh, oh
Woah, oh, oh-oh, oh

— Viva La Vida - **(Live)** - Coldplay

Abstract

Pre-equilibrium reactions induced by nucleons are important in applications of nuclear physics, applications for aerospace technologies, atmospheric and space physics, as well as for astrophysics studies. One-fifth of the particles emitted in pre-equilibrium nuclear reactions are composites, such as deuterons, tritiums, and alpha particles. Iwamoto and Harada proposed a semi-classical model for pre-equilibrium nuclear reactions describing direct mechanisms. Deuterons can be produced by a direct reaction mechanism called pickup. Our goal is to implement their model of deuteron emission in the Blann Hybrid-Monte Carlo model to analyze data of proton-induced reactions having deuterons as emitted particles. The unified model phase-space is investigated to understand its restrictions. DWUCK and an eikonal approximation were used to compare with the unified model results. A semi-classical distorted-wave model is used to relate the unified model with the DWBA theory. The theoretical foundation for a Monte Carlo implementation is proposed. We compare our cross-section and angular distribution results with the ones from DWUCK4 for a ground-state to ground-state reaction and also for a sum of all orbits involved in each reaction. We have studied the (p,d) and (n,d) reactions for ^{40}Ca, ^{120}Sn, and ^{208}Pb. We can conclude that we have satisfactory results for all cases studied. The application of the Monte Carlo theoretical foundation and a deep understanding for the results obtained in this study are suggestions for future research.

Resumo

Reações de pré-equilíbrio são reações que ocorrem antes que o sistema atinja o equilíbrio, entre aproximadamente 10^{-22} e 10^{-18} segundos. Reações deste tipo, induzidas por nucleons, são importantes em várias aplicações da física nuclear, tecnologias aeroespaciais, física atmosférica e espacial, além também ser de interesse de estudos em astrofísica. Aproximadamente 20% das partículas emitidas em reações de pré-equilíbrio são partículas compostas, como deuterons, trítios e partículas alfas. Iwamoto e Harada propuseram um modelo semiclássico para descrever os mecanismos diretos de emissão de deuterons em reações de pré-equilíbrio. Deuterons podem ser produzidos pelo mecanismo chamado de "*pickup*". Nosso objetivo foi de implementar o modelo unificado de Iwamoto e Harada no modelo híbrido Monte Carlo de Blann para analisar dados de reações induzidas por prótons incidentes tendo dêuterons como partícula emitida (p,d). Investigamos o espaço de fase do modelo unificado para entender suas restrições e limitações. Utilizamos DWUCK e a aproximação eikonal para comparar com os resultados do modelo unificado. Um modelo semiclássico utilizando ondas distorcidas (*Distorted Wave*) para espalhamento inelástico de nucleóns foi usado para aproximar o modelo unificado da teoria de ondas distorcidas, *DWBA*. Neste trabalho, propomos o nosso modelo e a base teórica para aplicação dos cálculos usando o método Monte Carlo. Comparamos os resultados obtidos para as seções de choque e distribuições angulares do nosso modelo com os resultados obtidos do DWUCK. Apresentamos os resultados para as reações do tipo (p,d) e (n,d) para três casos: ^{40}Ca, ^{120}Sn, e ^{208}Pb. Todos os resultados obtidos foram satisfatórios. Sugerimos a aplicação da base teórica para implementação do método Monte Carlo e estudos para aprofundar o entendimento dos resultados obtidos neste trabalho para serem realizados em pesquisas futuras.

List of Figures

List of Tables

List of Abbreviations and Acronyms

DWBA	Distorted-Wave Born Approximation
EM	Exciton model
MSC	Multi-Step Compound reactions
MSD	Multi-Step Direct reactions
HMS	Hybrid-Monte Carlo model
UM	Iwamoto and Harada unified model
DDHMS	Double Differential Hybrid-Monte Carlo Simulation
DWUCK	It is a acronym for: **D**istorted-**W**ave, **U**niversity of **C**olorado, and **K**unz
SCDW	Semi-classical distorted-wave model of nucleon inelastic scattering to continuum

List of Symbols

p	Proton;
d	Deuteron;
p	Particle number;
h	Hole number;
n	Exciton number;
E_p	Proton energy;
E_d	Deuteron energy;
$P_{\alpha\beta}$	Probability that an incident nucleon (α) scatters with another nucleon (β);
σ_{nn}	Free nucleon-nucleon scattering cross-section;
ϵ'	Nucleon energy above the Fermi energy plus the depth of the potential well below the Fermi energy;
A	Atomic mass;
N	Neutron number;
Z	Proton number;
ρ_n	Exciton state density;

E	Excitation energy;
g	Single-particle state density;
ϵ_F	Fermi energy;
U	Final energy / Potential;
ϵ	internal excitation energy;
$P(\epsilon)$	Probability distribution;
T_n	Weighted table for n quasiparticle configuration;
e	Energy after emission for a nucleon / Asymptotic kinetic energy;
Q	Energy released from the reaction, Q value.
λ_c	Emission rate for a nucleon to the continuum;
σ_{abs}	Absorption cross-section;
S	Nucleon spin;
μ	Reduced nucleon mass;
λ_+	Scattering transition rate;
ρ_{av}	Average nuclear density;
σ_{NN}	Average nucleon-nucleon cross-section;
v	Nucleon velocity;
k_{mfp}	Mean free path multiplication factor;
λ_{mfp}	Mean free path in the nuclear medium;
P_ν	Probability to emit a nucleon into the continuum;

Γ	Total width;
$\Gamma^{\uparrow}$	Emission width;
$\Gamma^{\downarrow}$	Scattering width;
p_F	Fermi momentum;
g_s	Spin multiplicity;
g_{lev}	Single-particle nuclear level density;
ϵ_s	Exit energy immediately outside the nucleus, above the Coulomb barrier;
v_f	Relativistic velocity;
$\rho_{n\to m}$	Transition density of $n \to m$;
ω	Matrix element of the interaction between plane wave states;
$P_{p,pauli}$	Pauli exclusion factor for p;
ρ_0	Neutron or proton density inside the nucleus;
R	Radius of the nucleus;
$\vec{R}_d$	Deuteron center of mass coordinate;
$\vec{P}_d$	Deuteron center of mass momentum;
σ_d	Ground state of the hamiltonian for the deuteron;
F_{lm}	Formation factor for l and m nucleons;
l	Number of nucleons above the Fermi energy / phase space radius;
m	Number of nucleons below the Fermi energy;

ϵ_d	Observed deuteron energy;
ϵ_0	Ground state energy of the deuteron / oscillator;
ΔR	Unified model parameter;
$\omega^*_{n(l,m)}$	Level density of the residual nucleus;
$\omega(p,h,E)$	Level density of the nucleus before its decay;
f_β	Scattering amplitude;
$\langle\vec{K}\|T^{(1)}\|\vec{K}\rangle$	Transition amplitude;
$\Phi^{(\pm)}$	Incoming (+) and outgoing (-) wave-functions
$d\lambda$	Differential pickup rate;
E_{njl}	State energy;
E_x	Nucleus state excitation energy;
σ_T	Total cross-section of nucleon-nucleon scattering in the free space at two-nucleon system;
T_{DWBA}	DWBA amplitude;
ϕ_h	Occupied orbital in the initial nucleus;
ϕ_p	Unoccupied orbital of continuum state of the initial nucleus;
ρ_n	Total nucleon density;
E_{tot}	Level energy;
V_C	Coulomb potential;
Y	Correction factor;

Contents

1 Introduction

1.1 Motivation

Nucleon induced pre-equilibrium reactions are important in the description and modeling of accelerator-driven-system, rapid-reactors, particle-beam radiotherapy, as well as for applications for aerospace technologies, such as the study of radiation damage on electronic, radiation protection for astronauts, and for modeling of particle detection systems. It is also important for atmospheric and space physics, and also for astrophysics studies.

In nucleon induced reaction, with incident energy above 30 MeV, about 20% of the nucleon-induced pre-equilibrium emission rate corresponds to composite particles such as deuterons, tritium, and alpha particles. The pre-equilibrium process provides reasonable results for reaction cross-sections with incident energies between 10 and 220 MeV. One can define pre-equilibrium reaction as those that occur before the system reaches equilibrium, a time scale approximately between 10^{-22} and 10^{-18} seconds.

In Fig. 1.1, one can see the emission spectra for a p+^{56}Fe reaction at 61.5 MeV. Each data set represents the emission spectrum for a different kind of particle. The one in black, the first data set from the top, represents the emission spectrum for protons (p). The red one is for deuterons (d), the green one for tritium (t), the blue one for helium-3 (h), and the purple one for alpha particles (a).

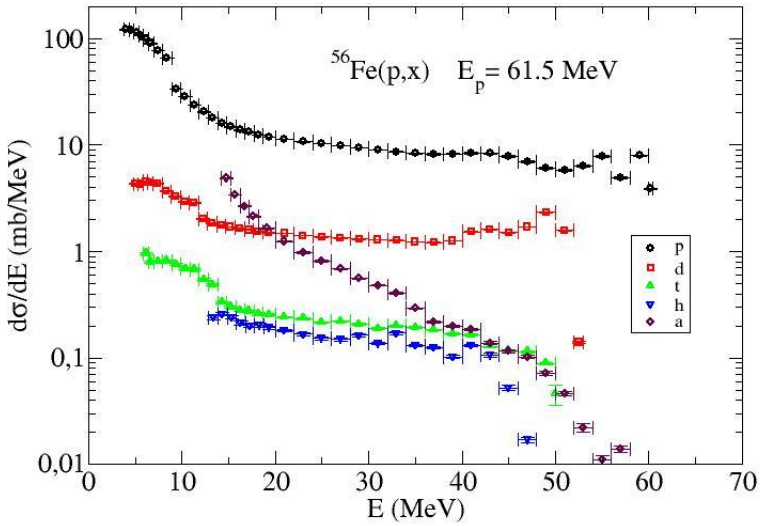

FIGURE 1.1 – Emission spectra of p+^{56}Fe at 61.5 MeV from Bertrand e Peelle (1973).

One can observe that the deuteron emission spectrum has a magnitude of about 20% of the proton emission spectrum. The spectra for tritium and helium-3 have similar values but are approximately two orders of magnitude below the proton values and decrease even more with increasing energy. For alpha particles, the initial spectrum, at about 15 MeV, has higher values than the deuteron one with a value of 4.9 mb/MeV. However, the alpha particle spectrum decreases considerably with increasing energy. In this work, we will discuss only deuteron emission.

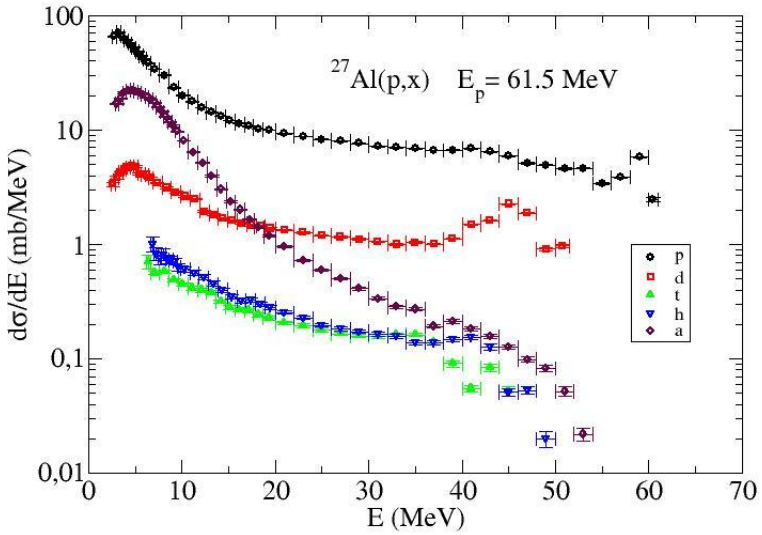

FIGURE 1.2 – Emission spectra of p+^{27}Al at 61.5 MeV from Bertrand e Peelle (1973).

In Fig. 1.2, the emission spectra of p+^{27}Al is shown. This target has about half the mass of ^{56}Fe. The emission spectra of p+^{120}Sn is shown in Fig. 1.3. ^{120}Sn is a target with about twice the mass of ^{56}Fe. It is clear that, in all three cases, the deuteron emission spectrum is close to 20% of the proton emission spectrum independently of the target mass and charge. Furthermore, the other particle emission spectra show similar emission rates with respect to the proton one as seen in the p+^{56}Fe reaction, with exception of the tritium (t) and helium-3 (h) spectra for ^{120}Sn.

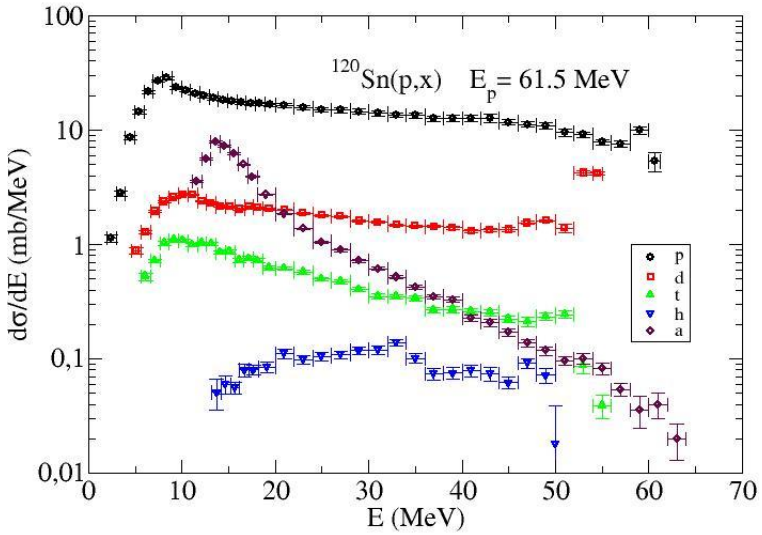

FIGURE 1.3 – Emission spectra for p+^{120}Sn at 61.5 MeV from Bertrand e Peelle (1973).

Before talking about the deuteron formation mechanisms, we define some models we will talk about. The exciton model is a semi-classical model created by (GRIFFIN, 1966) to analyze pre-equilibrium nuclear reactions. The Hybrid model is a model developed by Blann (BLANN, 1971) and later extended to a new model called the Hybrid-Monte Carlo model (BLANN, 1996), which calculates the exclusive spectra and yields of precompound reactions. The unified model, or the Iwamoto and Harada model (IWAMOTO; HARADA, 1982), is a model used for describing pre-equilibrium reactions with composite particle emissions, for example, deuterons, tritiums, and alpha particles. We will further discuss them on the next section.

An important mechanism for deuteron formation is called "pickup". In this kind of reaction, an incident nucleon takes another nucleon from the target nucleus to form the deuteron. Another important deuteron formation mechanism is called "coalescence" (BUTLER; PEARSON, 1963; SCHWARZSCHILD; ZUPANCIC, 1963; NAGLE *et al.*, 1996). In this case, the deuteron is formed from two fast nucleons which were emitted close to each other in phase space. In the context of the pre-equilibrium reaction exciton model (KONING; DUIJVESTIJN, 2004), Iwamoto and Harada developed a model that unifies both deuteron formation mechanisms (IWAMOTO; HARADA, 1982; SATO *et al.*, 1983; KONOBOEYEV; KOROVIN, 1996). Inspired by their model, we tried to modify their model to apply it in the

Hybrid-Monte Carlo Simulation model.

In (SATO *et al.*, 1983), Sato, Iwamoto and Harada discussed the angle-integrated energy spectra for pre-equilibrium emission of tritium, helium-3 and deuterons. As they used the "never come back" approximation, their energy spectra calculations did not contain equilibrium and quasi-equilibrium components. They started with the 2p1h (2 particles and 1 hole) state and they summed all contributions until the 6p5h state. They also mentioned that the states above 4p3h had insignificant contributions to the high energy spectra. The other relevant parameters of the exciton model, such as the single-particle level density, the spreading width, nucleon absorption cross-section, the complex particle and the target nucleus radius, were the same as in (IWAMOTO; HARADA, 1982).

In Fig. 1.4, we show the proton, deuteron, tritium, helium-3 (Note that here the helium-3 notation change to ^{3}He instead of h), and alpha particle spectra in proton induced reactions on ^{197}Au (left) and ^{54}Fe (right), respectively. The incident proton energy is 62 MeV. K Sato, Iwamoto and Harada concluded that the data was well reproduced by their calculations even with the discrepancies seen in the high energy part, especially for deuteron emission.

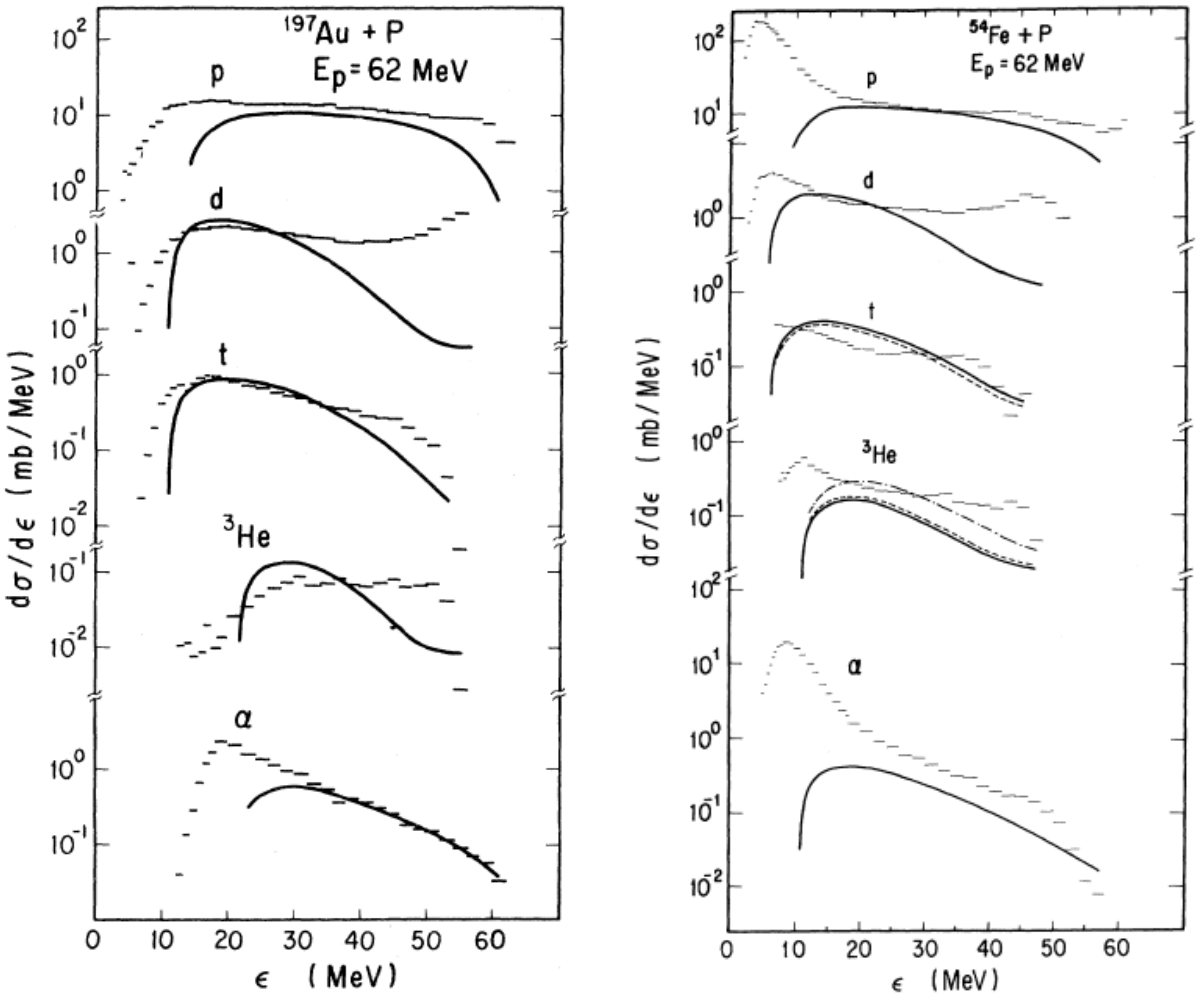

FIGURE 1.4 – Proton, deuteron, tritium, ^{3}He, and alpha particle angle-integrated energy spectra for proton induced reactions for ^{197}Au (left) and ^{54}Fe (right) with $E_p = 62$ MeV from Sato, Iwamoto e Harada (SATO *et al.*, 1983). The bars represent the experimental values. The line represents the results from K. Sato, Iwamoto and Harada calculations. For our discussion, one may ignore the dashed curves.

For all reactions in Fig. 1.4, the ^{197}Au results show a better agreement with the experimental data than the ^{54}Fe ones. This is consistent with the idea that a Fermi gas model provides a better description of Sato, Iwamoto and Harada formation factor in heavier systems. For Sato, Iwamoto and Harada, deuteron emission is dominated by the pickup component. The underestimate of this cross-section in Fig. 1.4 is huge. The other emitted particles will not be discussed in this work.

Broeders e Konobeyev (2005), proposed an alternative approach to the pre-equilibrium energy distribution for nucleon-induced reactions at intermediate energies. Their approach combined the emission mechanisms, pickup, coalescence and knock-out, into a unique

model. According to them, in a knock-out process, the emitted particle is "knocked out" (emitted) from the target by the interaction of the incident particle with the target. The incident particle excites a "preformed" particle on the target resulting in its emission from the nucleus.

The Sato, Iwamoto and Harada model (SATO *et al.*, 1983) was used in their work to describe the pickup and coalescence components starting from a 2p1h exciton configuration. However, the knock-out component was formulated using the Pauli principle for the nucleon-deuteron interaction inside the nucleus. With that, they developed an alternative approach based on pickup and coalescence models from the exciton model (SATO *et al.*, 1983) and the hybrid model (BLANN; VONACH, 1983).

They also assumed that non-equilibrium deuteron emission in nucleon induced reactions was due to: i) pickup from a low energy nucleon below the Fermi energy right after the initial exciton state (2p1h) formation, ii) coalescence between two excited nucleons with energies above the Fermi energy level, iii) knock-out of a pre-formed deuteron, or iv) a direct process resulting in deuteron formation and emission. These contributions from each deuteron formation component were calculated using formation factors from Sato, Iwamoto and Harada model (SATO *et al.*, 1983).

In Fig. 1.5, we have pickup (F(1,1)), coalescence (F(2,0)), and (KO) contributions for deuteron emission spectra on ^{54}Fe and ^{197}Au with $E_p = 61.5$ MeV. It is interesting to note that Broeders and Konobeyev included knock-out contribution beyond those that Sato, Iwamoto and Harada included in their work, (SATO *et al.*, 1983). We can also see in Fig. 1.5 that the pickup and coalescence contributions are small and that the knock-out contribution dominates most of the high energy part of the spectra. This contribution was not part of the results of (SATO *et al.*, 1983). The direct pickup process (D) is a process where the nucleon is picked up without the formation of the 2p1h configuration. As Broeders e Konobeyev (2005) state, its final state is the 0p1h.

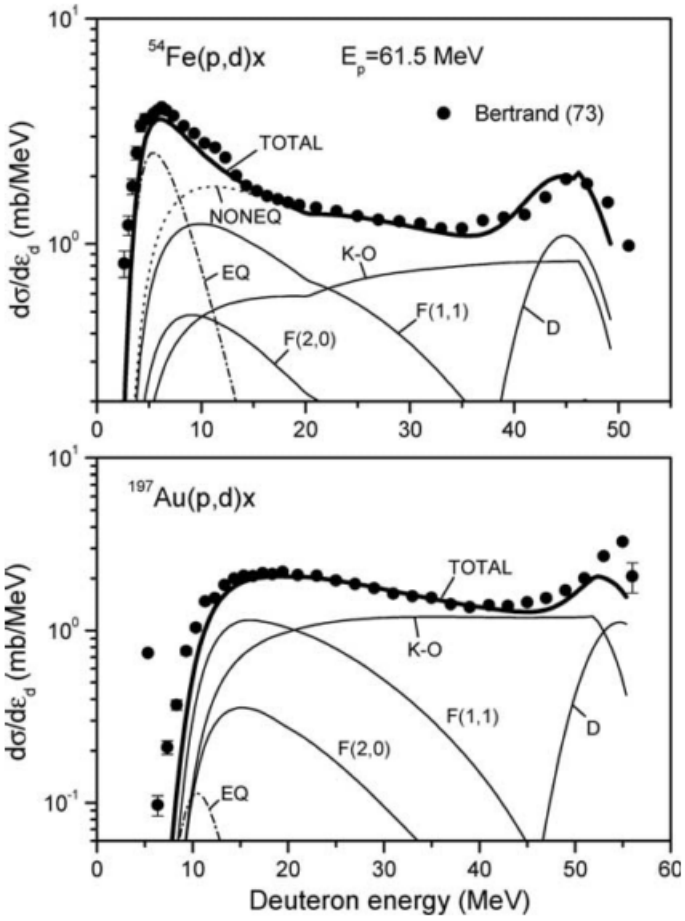

FIGURE 1.5 – Contributions of different nuclear processes for deuteron emission in proton induced reactions on p+^{54}Fe and p+^{197}Au with E_p = 61.5 MeV. EQ is equilibrium emission, (F(1,1)) is pickup nucleon from a (2p1h) exciton state, (F(2,0)) is two excited nucleon coalescence, knock-out is (KO) and direct pickup is (D). The sum of all non-equilibrium components is denoted as (NONEQ) and the total spectrum as (TOTAL). The black circles represent the experimental data obtained from (BERTRAND; PEELLE, 1973). The deuteron energy shown is in laboratory coordinates. Figure taken from (BROEDERS; KONOBEYEV, 2005).

Thus, the description of pre-equilibrium emission of composite particles is needed in order to improve our understanding of nucleon-induced reactions. As we have pointed out, pre-equilibrium nuclear reactions are important and they can impact many important areas of science. By creating a model to simulate this kind of composite particles emission, we will be able to improve our understanding of this type of reaction. Furthermore, it will help other researchers in their endeavors to describe nuclear experimental data.

1.2 Goals

EMPIRE, (HERMAN *et al.*, 2007), is a well-known software used for theoretical investigations of nuclear reactions and for nuclear data evaluation. EMPIRE is constituted of several modules, two of which are the PCROSS module (based on the exciton model), and the DDHMS module (based on the Hybrid-Monte Carlo model). Both models are used for pre-equilibrium nuclear reactions.

Our goal in this project is to implement our semi-classical distorted-wave model into the Hybrid-Monte Carlo Simulation (HMS) for pre-equilibrium nuclear reactions, (BLANN, 1996). The HMS calculates the emission distribution of the emitted nucleons both in energy and angles. We intend to implement our model in the DDHMS (Double Differential Hybrid-Monte Carlo Simulation) module in the nuclear reaction code EMPIRE, (HERMAN *et al.*, 2007). This module executes the pre-equilibrium calculation inside this code. Our final goal is that our code will expand EMPIRE in order to analyse (p,d) reactions.

1.3 Structure of this work

This thesis is organized in five chapters. We start with the introduction. In the second chapter, we review the literature. In the third chapter, we discuss about the distorted-wave born approximation (DWBA) and the eikonal approximation. In the fourth chapter, we discuss about the semi-classical distorted-wave model, introducing the theoretical basis for the Monte Carlo evaluation of the scattering series, and we talk about the results we have obtained for the cross-sections and the angular distributions for deuteron pickup. In the last chapter, we made our conclusions about this thesis. In the appendix, we present a published proceedings, a discussion about the potentials used in our studies, and a study we made to understand the limitations of the unified model from Iwamoto and Harada by redefining its phase space, a discussion about inelastic scattering with DWBA, and the energy levels used in DWUCK for the results obtained on chapter 4.

2 Literature Review

In this chapter, we review previous work on the subject of the thesis. We start by talking about nuclear reaction mechanisms and their differences. Of the three mechanisms that we will present, the pre-equilibrium reaction mechanism will be the center of our attention. Following our discussion of this mechanism, we discuss the differences between the classical and the quantum-mechanical theories used to describe it, as well as several models created to study pre-equilibrium reactions.

Three models are important for our work: the exciton model, the hybrid-Monte Carlo model, and the unified model. We will discuss them in turn after the introduction. This discussion is important for understanding the source of our ideas, our goals, and what we want to achieve with this work.

2.0.1 Introduction

According to Koning and Akkermans, (KONING *et al.*, 1999), there are three different types of a nuclear reaction mechanisms in a reaction induced by a light-ion: the direct, compound, and pre-equilibrium nuclear ones. We can define these mechanisms by the time in which the reaction takes place and by the characteristics that each mechanism produces in the data. Fig. 2.1, from (KONING *et al.*, 1999), gives an idea of the energy spectrum of a reaction A(a,b)B with an incident energy of several tens of MeV. The differences between the mechanisms can be seen in the spectrum. One can also see that the angular distribution transition to isotropy by the decrease of the outgoing energies.

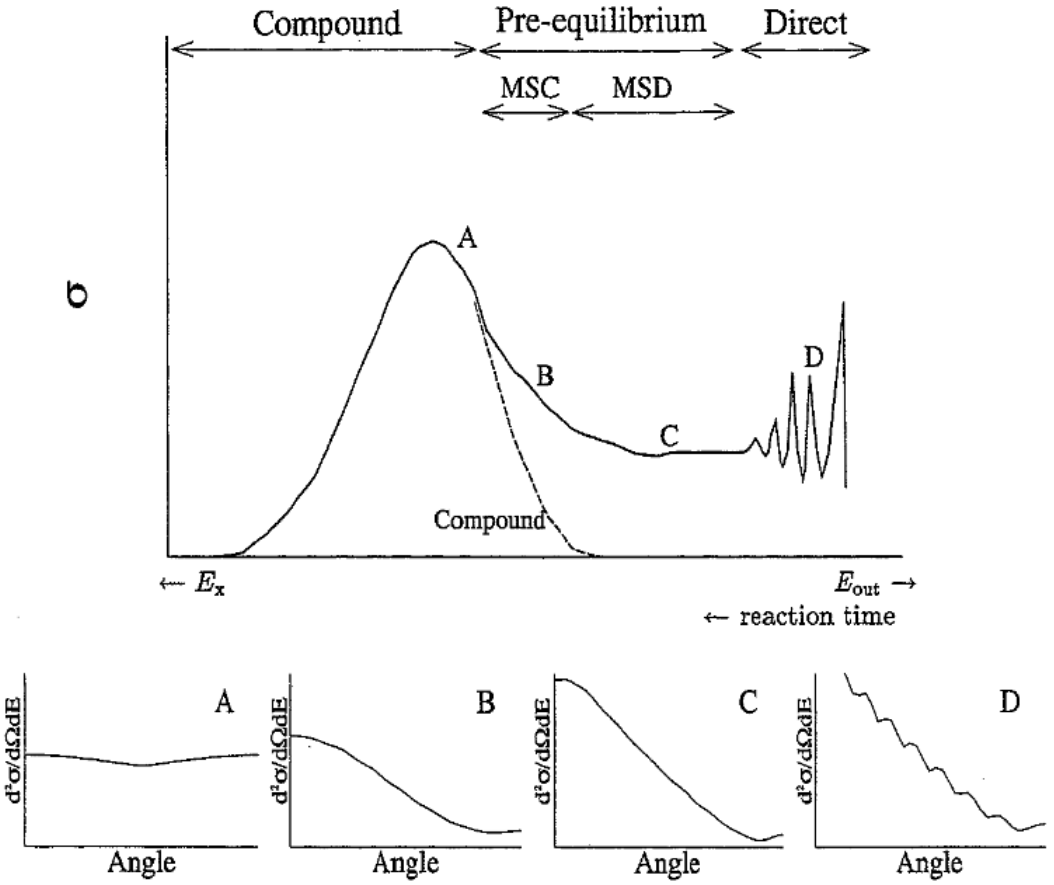

FIGURE 2.1 – Representation of a typical energy spectrum of a reaction A(a,b)B with an incident energy of several tens of MeV from (KONING *et al.*, 1999).

In a direct reaction, the process occurs in a short period of time, $\sim 10^{-22}$ seconds, and, as we can see in part D of Fig. 2.1, the associated angular distribution is forward peaked with an oscillatory behavior. Koning *et al.* (1999) says that the forward-peaked angular distribution is expected to be due by the pre-equilibrium phase. Compound process takes longer than a direct process, $\sim 10^{-18}$ seconds. This process is predominant at low energies (below 10 MeV). The compound nucleus is formed when the target nucleus captures the incident particle. Different from a direct process, which occurs mostly in a one-step process, the compound emission process occurs after the nucleus reaches equilibrium.

Intermediate between compound and direct processes are the pre-equilibrium processes. In pre-equilibrium reactions, the composite nucleus emits particles before reaching the statistical equilibrium. These reactions can be described in a time-dependent process. In the exciton model, the occupation probability of the configurations with the same number of particles and holes can be determined by a master equation, which results are predictions of the energy distribution of emitted particles. We are not going to discuss

about the master-equation model in this work.

A pre-equilibrium process takes features from both compound and direct processes. As (KONING *et al.*, 1999) state, "It is imagined that the incident particle step-by-step creates more complex states of the compound system and gradually loses its memory of the initial energy and direction". The pre-equilibrium processes provide reasonable results for reaction cross-sections with incident energies between 10 and 220 MeV.

While explaining the differences between the classical and quantum-mechanical pre-equilibrium reaction theories, Koning and Akkermans, (KONING *et al.*, 1999), state that most classical models are phenomenological ones. These models, like the one that we will discuss in one of the next subtopics, the unified model from Iwamoto and Harada, take into account a master equation which represents the probability of particle transitions. The exciton number (n), which represents the number of particles (p) and holes (h), is used to account for the states, as many particle-holes are involved in the process.

Although proven to be quite successful, the exciton model was criticized due to its classical treatment of the compound and direct mechanisms. A quantum-mechanical model for the pre-equilibrium mechanism is more appropriate. Two quantum-mechanical models were proposed, the multi-step compound (MSC) and the multi-step direct (MSD) ones.

MSC reactions mostly occur in an energy range a little above the one that is characteristic of the compound nucleus and are restricted to energies between 10 and 20 MeV. MSD reactions are said to provide most of the pre-equilibrium cross-section.

One interesting way to look at the differences between MSC and MSD models is that on compound reactions the reaction keeps on by the bound configurations of the system. When it proceeds by the unbound configurations, one can think of that as the MSD reactions.

Among the differences between the classical and quantum treatments, in which the MSC combines quantum-mechanical perturbation theory with statistical postulates, is that the MSC mechanism yields symmetrical angular distributions while the exciton model has practical problems due to its systematical underestimation of the double-differential cross-section at backward angles. For the MSD, as Koning and Akkermans, (KONING *et al.*, 1999), say, "the crucial feature of the MSD process is that one can make a meaningful

distinction between a leading fast particle and the residual one".

Despite these differences, the classical and quantum-mechanical models, are important to supply data for practical use. Pre-equilibrium reactions are important to provide nuclear data for fusion reactor-design calculations, for the analysis of applications that require accelerators, and for other scientific purposes.

Since Griffin's pioneering work, (GRIFFIN, 1966), many papers were published and several pre-equilibrium models were developed. The most used models were the exciton models developed, and the hybrid model. In this work, we will not talk about the hybrid model, but we will discuss the hybrid-Monte Carlo Simulation model instead. We will explain pre-equilibrium nuclear reaction models developed to analyze nuclear reaction data where a fast particle is emitted before reaching equilibrium. This fast particle is emitted before its degrees of freedom have reached the compound nucleus equilibrium. These reactions are characterized by having a small number of excitons.

In the next subsections, we will talk about different pre-equilibrium models. With a brief introduction, we start with the exciton model. Then, we discuss the Hybrid-Monte Carlo model from Blann, and the Unified model of Iwamoto and Harada.

2.1 Exciton model

The exciton model (EM) was introduced by Griffin in 1966, (GRIFFIN, 1966), to analyze pre-equilibrium nuclear reactions and later elaborated in more detail. The EM is a semi-classical model that classifies states of the system by the exciton number (the number of particles + holes) and by the excitation energy E. The exciton number (n) is equal to the sum of the number of excited particles (p) above the Fermi energy and the number of holes (h) below the Fermi energy.

The EM assumes that the system reaches equilibrium by multiple two-body interactions. Particle-hole configurations with the same exciton number and excitation energy are assumed to be equally probable. As a result of these two-body interactions, the number of excitons changes in time. With that, one can account for the evolution of the scattering process just by counting the exciton number.

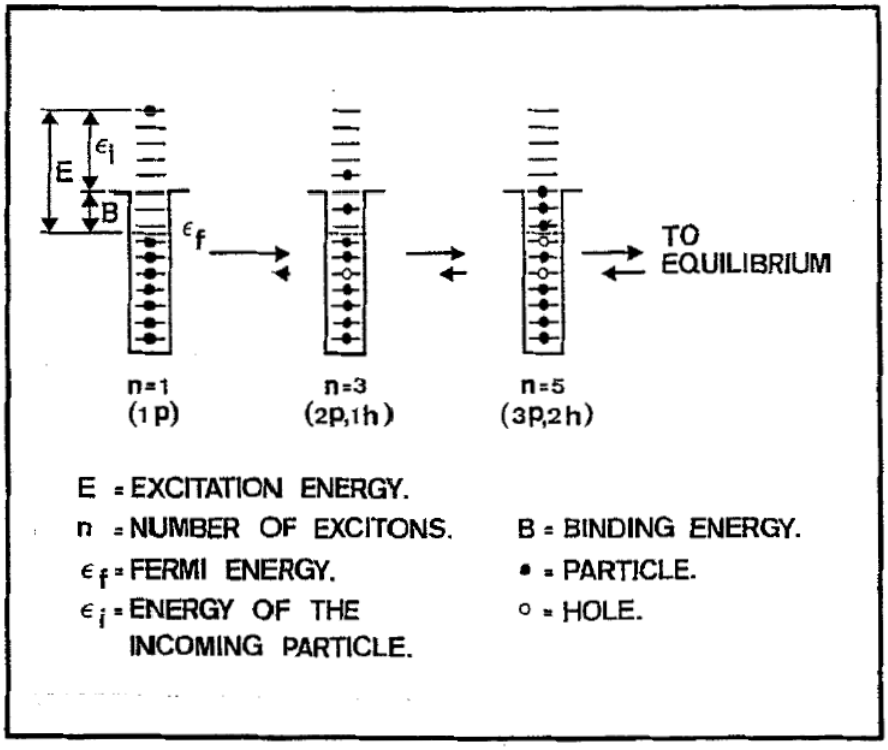

FIGURE 2.2 – Reaction process described by the EM. The symbols are described on the figure. This figure was taken from (KONING *et al.*, 1999).

In Fig. 2.2, one can see an $n = 1$ state starting with a projectile particle with energy above the Fermi energy. As it interacts with the target nucleus, the system undergoes a $\Delta n = +2$ transition to a (2p,1h) state. As the other particles interact (following the right arrows), the system undergoes further transitions $\Delta n = +2$ transitions until it reaches equilibrium. On the other hand, following the left arrows, a particle can be emitted causing the system to undergo a $\Delta n = -1$ transition. This transition is caused by a nucleon in an unbound single-particle state being emitted. There is one more type of internal transition, the $\Delta n = -2$, in which the system changes its configuration by reducing the exciton number, (KONING *et al.*, 1999; CLINE; BLANN, 1971).

As Koning and Akkermans state, "in principle the exciton model enables to compute the emission cross-sections in an unified way, without introducing arbitrary adjustments between equilibrium and pre-equilibrium contributions", (KONING *et al.*, 1999). With that, we will continue our discussion of pre-equilibrium models. The hybrid model, mentioned before, can be considered as a variation of the EM. We will not discuss it here as we will discuss the Hybrid-Monte Carlo Simulation Model in the next section.

2.2 Hybrid-Monte Carlo Simulation Model

In (BLANN, 1996), Blann developed a new formulation of the hybrid model to resolve the principal inconsistencies and limitations of earlier precompound decay models, such as the exciton model, which assumed that the states of any p-particle h-hole density are equally occupied. As Bisplinghoff demonstrated, this is only the case for the initial 2p1h density, (BISPLINGHOFF, 1986).

The hybrid model was developed considering multiple precompound decay, (BLANN; VONACH, 1983). However, it was restricted to two or fewer emissions of precompound nucleons from each nuclide. This became a serious limitation for high energies models.

To improve the description and solve the hybrid model limitations, the Hybrid-Monte Carlo Simulation (HMS) model was developed. The restriction on emissions of precompound nucleons was removed on the HMS. It has a validity range up to about 280 or 400 MeV, depending on the effective pion threshold and on the pion production. The model was inserted on the nuclear reaction code ALICE, and later, on the DDHMS module, in EMPIRE, (BLANN, 1996).

2.2.1 Formulations

To prepare the Monte Carlo sampling, a collision partner for the incident nucleon is chosen. It can be a proton or a neutron. A two particle-one hole state is than selected from a weighted table of the energies above the Fermi energy of the scattered nucleons, and of the hole left by the excited nucleon. The next step is to define whether the nucleons are emitted or re-scatter. These steps are followed repeatedly until the nucleus is in a near equilibrium state.

In the next subsections, we will show the steps of the HMS formulation. This discussion is based on (BLANN, 1996).

2.2.2 Collision partners

There are four kinds of collisions between nucleons in the HMS: (n,n), (n,p), (p,n), and the (p,p). The probability that an incident neutron scatters with another neutron, is

energy dependent, is given as

$$P_{nn}(\epsilon') = \frac{\sigma_{nn}(\epsilon')(A-Z)}{\sigma_{nn}(\epsilon')(A-Z) + \sigma_{np}(\epsilon')Z}, \tag{2.1}$$

with

$$P_{np} = 1 - P_{nn}, \tag{2.2}$$

with ϵ' being the nucleon energy above the Fermi energy plus the depth of the potential well below the Fermi energy, where n represents a neutron and p a proton. The free nucleon-nucleon scattering cross-sections are given by the σ's, while A and Z are the atomic mass and proton number of the target. The probability for an incident protons colliding can be calculated analogously as eq. (2.1).

The probabilities give values for which the model will choose a result from weighted tables. These values, as they are probabilities, are between 0 and 1. All events, such as scattering or emission, and which collision partner will be chosen, are governed by the results in these tables.

2.2.3 Weighted tables

Precompound models used exciton state densities given by

$$\rho_n(E) = \frac{g(gE)^{n-1}}{p!h!(n-1)!}, \tag{2.3}$$

where g is the single-particle state density, p the number of particles, h the number of holes, and E the excitation energy.

A more detailed calculation for $n = 2$ (1p1h) excitons, where $n = p + h$, furnishes

$$\rho_2(E) = g(g\epsilon_F) \qquad \text{if} \qquad E > \epsilon_F, \tag{2.4a}$$

$$\rho_2(E) = g(gE) \qquad \text{if} \qquad E \leq \epsilon_F. \tag{2.4b}$$

with ϵ_F, the Fermi energy, limiting the density of states.

For $n = 3$ (2p1h), with $E \geq \epsilon_F$, we have

$$\rho_3(E) = \frac{g^3[\epsilon_F(2E - \epsilon_F)]}{4}. \tag{2.5}$$

Using eq.(2.4) and eq.(2.5), one can create weighted tables in order to retrieve the energy ϵ for a nucleon above the Fermi energy. The excitation energy E will be represented as $U = E - \epsilon$, with U as the final energy and ϵ as the internal excitation energy.

With that, a nucleon at energy ϵ is found in a three exciton probability distribution by

$$P(\epsilon)d\epsilon = \frac{\rho_2(E - \epsilon)gd\epsilon}{\rho_3(E)}. \tag{2.6}$$

In this weighted table given by eq. (2.6), each interval is given by $\epsilon + \Delta\epsilon$. All intervals summed from 0 to E will give unity. A random number will identify the interval defined by eq. (2.6) in a table prepared by

$$T_3(\epsilon', E) = \int_{\epsilon=0}^{\epsilon'} \frac{\rho_2(E - \epsilon)gd\epsilon}{\rho_3(E)}, \tag{2.7}$$

for a three quasiparticle configuration, and

$$T_2(\epsilon', E) = \int_{\epsilon=0}^{\epsilon'} \frac{g^2 d\epsilon}{\rho_2(U)}, \tag{2.8}$$

for a two quasiparticle configuration, with $U = E - \epsilon'$.

One must compute T_3 and T_2 for all composite system excitation energies E' to use during the deexcitation cascade.

2.2.4 Probabilities of emission and rescattering

The last step is the calculation of the emission and rescattering probabilities. They will define if a nucleon will be emitted or rescatter. If they were to rescatter, all processes will be repeated until the remaining nucleons reach equilibrium.

The energy e after emission for a nucleon, with energy ϵ above the Fermi energy, in a potential well, is given by

$$e = \epsilon - Q, \tag{2.9}$$

with Q being the energy released from the reaction, the Q value.

2.2.4.1 Rate of emission and rescattering

The emission rate for a nucleon to the continuum, with energy e, according to the hybrid precompound decay model, is given by the Weisskopf expression,

$$\lambda_e(e) = (constant)\frac{\sigma_{abs}(e)e(2S+1)\mu}{g(\epsilon)}, \tag{2.10}$$

with σ_{abs} the absorption cross-section, e the emitted nucleon energy, S the nucleon spin, μ the reduced nucleon mass, and g the single-particle density at internal excitation energy ϵ. The constant comes from phase space factors.

In addition to emission, a nucleon can also rescatter within the nucleus. The scattering transition rate is given by

$$\lambda_+(\epsilon) = \rho_{av}\sigma_{NN}\frac{v}{k_{mfp}}. \tag{2.11}$$

$\lambda_+(\epsilon)$ takes into account the nucleon velocity in the nucleus and the nuclear density. ρ_{av} is the average nuclear density, σ_{NN} is the average nucleon-nucleon cross-section, v is the nucleon velocity, and k_{mfp} is a mean free path multiplication factor. Blann observes in (BLANN, 1996) that k_{mfp} takes into account the average value over longer paths on the diffuse nuclear surface, as well as medium modifications of the nucleon-nucleon cross-section. One should also note that $\lambda_+(\epsilon)$ is given by v/λ_{mfp}, when λ_{mfp} is the mean free path in the nuclear medium.

2.2.4.2 Calculation of the Probabilities of emission and rescattering

Once we know the emission and scattering transition rates, we are able to calculate the emission and rescattering probabilities.

The probability to emit a nucleon with energy e into the continuum is given in (BLANN, 1996) as

$$P_\nu(e) = \frac{\lambda_e(e)}{\lambda_e(e) + \lambda_+(\epsilon)}, \tag{2.12}$$

with ν being a proton or a neutron, $\lambda_e(e)$ given by eq. (2.10) and $\lambda_+(\epsilon)$ given by eq. (2.11).

The probability for rescattering is given by the interval $1 - P_\nu(e)$. With that, a random number from 0 to 1 can be used to determine whether a particular cascade exciton will be emitted or if it will rescatter within the nucleus.

The collisions are computed successively until no more nucleons can be emitted, a condition considered as equilibrium. Any further emissions are calculated using a compound nucleus emission model.

2.2.5 Single-particle density and transition rates

Continuing our discussion of Blann's model, we describe in more detail the discussion in (BLANN, 1996) of single-particle densities and transition rates. Blann discusses the emission rate $\lambda_e(\epsilon)$, but merely mentions the scattering rate $\lambda_+(\epsilon)$. In the next subtopic, we will describe single-particle densities, emission and scattering widths, and, lastly, we will discuss transition rates.

To begin our discussion, one must note that energies of composite nuclei states have finite widths. In order to understand this idea, we start with the uncertainty principle, where

$$\Delta E \Delta t \simeq \hbar. \tag{2.13}$$

A state would have an energy width Γ given by $\hbar/\Delta t$. This interval of time can be called a lifetime. As the lifetime is given by the inverse of the decay rate in units of time, λ, we obtain

$$\Gamma = \hbar\lambda. \tag{2.14}$$

Having different partial widths for each type of decay, a nucleus can decay in different ways. To calculate the total width, we sum the partial widths,

$$\Gamma = \sum_i \Gamma_i = \sum \hbar\lambda_i. \tag{2.15}$$

With this idea in mind, we proceed to calculate the single-particle density. After that,

we will discuss emission and scattering widths in more details.

2.2.5.1 Single-particle density

A single-particle state with a definite spin projection is defined by a momentum vector $\vec{p}$ in three dimensions with normalization volume,

$$V = \frac{4\pi}{3} r_0^3 A. \tag{2.16}$$

The particle is confined in this volume and its density is given by

$$g(\vec{p}) = V \frac{d^3p}{(2\pi\hbar)^3}. \tag{2.17}$$

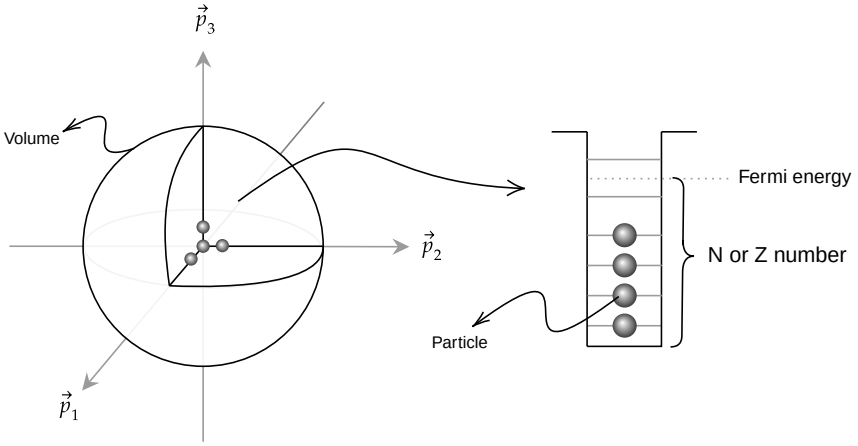

FIGURE 2.3 – A simplistic interpretation of eq. (2.18).

Instead of having one spin projection, we could sum eq. (2.17) over all spin projections and integrate it to the Fermi momentum, p_F. By doing that, one may obtain the neutron number N or proton number Z,

$$g_s V \frac{p_{Fn}^3}{6\pi^2\hbar^3} = N \qquad \text{and} \qquad g_s V \frac{p_{Fp}^3}{6\pi^2\hbar^3} = Z, \tag{2.18}$$

where $g_s = 2$ is the spin multiplicity, $A = N + Z$, and $\frac{4\pi}{3} r_0^3$ is the average volume occupied by a nucleon. For a simplistic interpretation of this equation, see Fig. 2.3.

For typical values, $N = Z = A/2$ and $r_0 = 1.2$ fm, we would have $p_F \approx 250$ MeV/c

and $\epsilon_F \approx 33$ MeV (Fermi energy). When defining $A_{ef} = 2N$ or $2Z$, we would have

$$p_F r_0 = \frac{3}{2}\hbar\left(\frac{\pi}{3}\frac{A_{ef}}{A}\right)^{1/3}. \tag{2.19}$$

One can also express the single-particle density in terms of the energy, $\epsilon = p^2/2m$. This gives us

$$g_s V\frac{d^3p}{(2\pi\hbar)^3} = g_s\frac{2m}{3\pi}p_F\left(\frac{r_0}{\hbar}\right)^3 A\sqrt{\frac{\epsilon}{\epsilon_F}}d\epsilon\frac{d\Omega_p}{4\pi} = g(\epsilon)d\epsilon\frac{d\Omega_p}{4\pi}, \tag{2.20}$$

where $g(\epsilon)$, the single-particle density, is given by

$$g(\epsilon) = g_s\frac{2m}{3\pi}p_F\left(\frac{r_0}{\hbar}\right)^3 A\sqrt{\frac{\epsilon}{\epsilon_F}}. \tag{2.21}$$

2.2.5.2 Single-particle free density and single-particle nuclear level density

The single-particle free density is calculated to account for all particles in the continuum. Instead of using ϵ, the internal excitation energy, we use e, the energy after emission. Blann defines the single-particle free density as

$$\begin{aligned} g_{free}(e)de = g_s\frac{4\pi p^2 dp}{(2\pi\hbar)^3} &= \frac{g_s}{4\pi^2}\left(\frac{2m}{\hbar^2}\right)^{3/2}\sqrt{e}de, \\ &\rightarrow \frac{g_s}{2\pi^2 h^3}\sqrt{e(2m+e)}(m+e)de, \end{aligned} \tag{2.22}$$

where g_s is the spin multiplicity and the second line represents the relativistic value for the single-particle free density.

Using the same idea as our $g(\epsilon)$, eq. (2.21), but for relativistic kinematics, Blann defines the single-particle nuclear level density as

$$\begin{aligned} g_{lev}(\epsilon)d\epsilon = g_s V\frac{4\pi p^2 dp}{(2\pi\hbar)^3} &= \frac{g_s}{3\pi^2}\left(r_0^2\frac{2m}{\hbar^2}\right)^{3/2} A\sqrt{\epsilon}d\epsilon, \\ &\rightarrow \frac{2g_s}{3\pi}\left(\frac{r_0}{\hbar}\right)^3 A\sqrt{\epsilon(2m+\epsilon)}(m+\epsilon)d\epsilon. \end{aligned} \tag{2.23}$$

2.2.5.3 Emission width

Like the rates, the widths can be classified as emission and scattering widths. The widths, as stated before in eq. (2.13), represent an energy width that comes from the uncertainty principle, or in other words, is a way to represent the decay rate in terms of energy.

The emission width $\Gamma^{\uparrow}(\vec{p})$, the energy width in which a particle with momentum $\vec{p}$ can escape from the nucleus, is given in terms of the rate at which flux escapes through the surface of the normalization volume,

$$\frac{\Gamma^{\uparrow}(\vec{p})}{\hbar} V \frac{d^3p}{(2\pi\hbar)^3} = g_s \frac{d^3p_f}{(2\pi\hbar)^3} \int d^3r \hat{r} \cdot \frac{\vec{p_f}}{\mu} \theta(\hat{r} \cdot \hat{p}) \delta(r - R). \tag{2.24}$$

Due to the Q-value of the reaction and the Coulomb barrier, the final momentum p_f deviates from the initial one in magnitude. We rewrite eq. (2.24) using the idea of eq. (2.17) and changing it in terms of single-particle energies,

$$\Gamma^{\uparrow}(\vec{p}) g(\epsilon) d\epsilon \frac{d\Omega_p}{4\pi} = g_s \frac{2\mu\pi R^2}{2\pi^2\hbar^2} \epsilon_s d\epsilon_s \frac{d\Omega_p}{4\pi}. \tag{2.25}$$

where we can see that $\epsilon_s = \epsilon - Q - V_B$ is the exit energy immediately outside the nucleus, above the Coulomb barrier. With that, we can define the asymptotic kinetic energy as

$$e = \epsilon_s + V_B = \epsilon - Q. \tag{2.26}$$

Analyzing for the right side of eq. (2.25), we recognize a well-known approximation for the absorption cross-section, $\sigma_{abs}(e)$, given by

$$\pi R^2 \epsilon_s = e\pi R^2 (1 - V_B/e) \theta(e - V_B) \approx e\sigma_{abs}(e). \tag{2.27}$$

With this approximation, we can rewrite eq. (2.25) as

$$\Gamma^{\uparrow}(\vec{p}) g(\epsilon) d\epsilon \frac{d\Omega_p}{4\pi} = g_s \frac{2\mu e \sigma_{abs}(e)}{2\pi^2\hbar^2} de \frac{d\Omega_p}{4\pi}. \tag{2.28}$$

Finally, we obtain the emission width, as

$$\Gamma^{\uparrow}(\vec{p}) = g_s \frac{2\mu e \sigma_{abs}(e)}{2\pi^2 \hbar^2 g(\epsilon)}, \tag{2.29}$$

with $g(\epsilon)$ given by eq. (2.21). Note that the spin multiplicity, g_s, will cancel out because it is in both the numerator and the denominator (inside $g(\epsilon)$).

Blann, (BLANN, 1996), uses the relativistic velocity to calculate the emission width,

$$v_f = p_f / \sqrt{p_f^2 + m^2} = \frac{\sqrt{e(2m+e)}}{e+m}, \tag{2.30}$$

and the phase space volume, $\sqrt{e(2m+e)}/(e+m)$, rather than the nonrelativistic relative velocity with reduced mass, $p_f/\mu = \sqrt{2e/\mu}$, and phase space volume, $\mu\sqrt{2\mu e}$. With that, the emission width becomes

$$\Gamma^{\uparrow}(\vec{p}) = g_s \frac{(2m+e) e \sigma_{abs}(e)}{2\pi^2 \hbar^2 g_{lev}(\epsilon)}, \tag{2.31}$$

with $g_{lev}(\epsilon)$ given by eq. (2.23). Note that μ could be substituted by the particle mass in order to obtain the correct nonrelativistic limit.

Using the definition of the energy width, eq. (2.14), with the emission width, eq. (2.31), one can calculate the emission rate, already mentioned in section 2.2, as eq. (2.10).

2.2.5.4 Spreading/scattering widths

Instead of being emitted, a particle has a probability to re/scatter within the nucleus. Both the excitation of a 2p1h (Fig. 2.4) or 1p2h (Fig. 2.5) configuration contributes to the width, which gives us the scattering width of a particle (or a hole) of momentum $\vec{p}_1$.

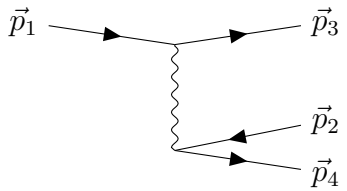

FIGURE 2.4 – Excitation diagram for a 2p1h configuration. The incident particle 1, with momentum $\vec{p}_1$, interacts with particle 2, with momentum $\vec{p}_2$ below the Fermi momentum. Particle 1 is emitted with momentum $\vec{p}_3$ and particle 2 is emitted with momentum $\vec{p}_4$. Particle 2 leaves a "hole" in the system.

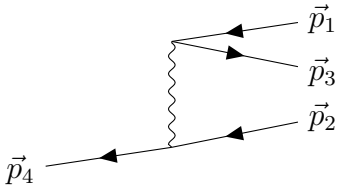

FIGURE 2.5 – Excitation diagram for a 1p2h configuration. A hole 1, with momentum $\vec{p}_1$, interacts with a particle 2, with momentum $\vec{p}_2$ below Fermi momentum. Particle 2 is excited and emitted with momentum $\vec{p_4}$, leaving two holes states in the system.

To begin our calculation, one should understand the role of each particle in our reaction. $\vec{p}_1$ represents the incident particle before the interaction and $\vec{p}_3$ is the same particle but after the collision. $\vec{p}_2$ is a particle above or below the Fermi energy and $\vec{p}_4$ is particle 2 after emission. We focused on two emission mechanisms, one is represented in Fig. 2.4, with $\vec{p}_2$ below the Fermi energy, $\vec{p}_F$, and the second one is represented by Fig. 2.5, with $\vec{p}_2$ above the Fermi energy.

From Fermi's golden rule, we can calculate the scattering width for a particle as

$$\begin{aligned}\Gamma^{\downarrow}_{1p}(\vec{p}_1) = 2\pi\hbar a V^2 \int |U(\vec{q})|^2 (2\pi\hbar)^3 \delta(\vec{p}_1 + \vec{p}_2 - \vec{p}_3 - \vec{p}_4) \\ \times \delta(p_1^2/2m + p_2^2/2m - p_3^2/2m - p_4^2/2m) \\ \times \theta(p_{F2} - |\vec{p}_2|)\frac{d^3p_2}{(2\pi\hbar)^3}\theta(|\vec{p}_3| - p_{F1})\frac{d^3p_3}{(2\pi\hbar)^3}\theta(|\vec{p}_4| - p_{F2})\frac{d^3p_4}{(2\pi\hbar)^3},\end{aligned} \tag{2.32}$$

with particle 4 representing the final particle in a 2p1h reaction. The factor a takes into account indistinguishability. It is equal to 1/2 if the final particles are identical and 1 if they are different.

The nucleon-nucleon interaction, which represents the interaction between the two particles, is defined as

$$U(\vec{q}) = \frac{1}{V}\int d^3r e^{i\vec{q}\cdot\vec{r}} U(\vec{r}), \tag{2.33}$$

where $\vec{q}$ is the transferred momentum, given by

$$\vec{q} = (\vec{p}_3 - \vec{p}_1 - \vec{p}_4 + \vec{p}_2)/2 = \vec{p}_3 - \vec{p}_1, \tag{2.34}$$

when momentum conservation is taken into account.

In order to calculate the integral, we assume that the squared interaction matrix element can be represented by its mean value and taken out of the integral. We will also assume that the squared matrix element is summed over final spins and averaged over initial ones, as it is normally done for an unpolarized cross-section. We thus write for particles,

$$\Gamma^{\downarrow}_{1p}(\vec{p}_1) = 2\pi\langle|U|\rangle^2\rho_{1p\to 2p1h}(\vec{p}_1), \tag{2.35}$$

with

$$\begin{aligned}\rho_{1p\to 2p1h}(\vec{p}_1) = \frac{2aV^2}{(2\pi\hbar)^6}\int \delta(\vec{p}_1+\vec{p}_2-\vec{p}_3-\vec{p}_4)\delta(p_1^2/2m+p_2^2/2m-p_3^2/2m-p_4^2/2m)\\ \times\theta(p_{F2}-|\vec{p}_2|)d^3p_2\theta(|\vec{p}_3|-p_{F1})d^3p_3\theta(|\vec{p}_4|-p_{F2})d^3p_4.\end{aligned} \tag{2.36}$$

For holes, it can be expressed in a similar way as

$$\Gamma^{\downarrow}_{1h}(\vec{p}_1) = 2\pi\langle|U|\rangle^2\rho_{1h\to 1p2h}(\vec{p}_1), \tag{2.37}$$

with

$$\begin{aligned}\rho_{1h\to 1p2h}(\vec{p}_1) = \frac{2aV^2}{(2\pi\hbar)^6}\int \delta(\vec{p}_1+\vec{p}_2-\vec{p}_3-\vec{p}_4)\delta(p_1^2/2m+p_2^2/2m-p_3^2/2m-p_4^2/2m)\\ \times\theta(|\vec{p}_2|-p_{F2})d^3p_2\theta(p_{F1}-|\vec{p}_3|)d^3p_3\theta(p_{F2}-|\vec{p}_4|)d^3p_4.\end{aligned} \tag{2.38}$$

The factor 2 in the definition of the densities is accounted by the sum over the spin value of particle 2. For particle 3 and 4, it is included in the average squared matrix element. By doing that, we ignore details of interaction, such as scattering with no exchange of spin, when calculating the density. It is also consistent with the convention normally adopted for unpolarized cross-sections.

When $p_1 \geq p_{F2}$, the transition density of $1p \to 2p1h$ yields

$$\begin{aligned}\rho_{1p\to 2p1h}(\vec{p}_1) = \frac{2aV^2}{(2\pi)^4\hbar^6}\frac{m}{p_1}\{(p_1^2-p_{F1}^2-2p_{F2}^2/5)p_{F2}^3/3+2p_{2\,\min}^5/15\\ -\theta(p_{F2}-p_{F1})(p_{F2}-p_{F1})^3(p_{F1}^2+3p_{F1}p_{F2}+p_{F2}^2)/15\},\end{aligned} \tag{2.39}$$

where $p_{2\,\min}^2 = \min(0, p_{F1}^2 + p_{F2}^2 - p_1^2)$. When $p_1 < p_{F2}$, in which case necessarily $p_{F1} < p_{F2}$, it yields

$$\rho_{1p\to 2p1h}(\vec{p}_1) = \frac{2aV^2}{(2\pi)^4\hbar^6}\frac{m}{p_1}(p_1 - p_{F1})^2(2p_1^3 + 4p_1p_{F1}^3 + 6p_1^2p_{F1}^2 + 3p_{F1}^5)/15. \tag{2.40}$$

For $1h \to 1p2h$, when $p_1 \leq p_{F2}$, we have

$$\begin{aligned}\rho_{1h\to 1p2h}(\vec{p}_1) = \frac{2aV^2m}{4(2\pi)^4(\hbar)^6}\Big\{&(p_{F1}^2 - p_1^2)^2 \\ &- \theta(p_{F1} - p_{F2})\Big[(p_{F1}^2 - p_{F2}^2)^2 - 4p_1^2(p_{F1}^2 - p_{F2}^2)/3 \\ &+ 8\Big(p_1^4 - (p_1^2 + p_{F2}^2 - p_{F1}^2)^{5/2}/p_1\Big)/15\Big]\Big\}.\end{aligned} \tag{2.41}$$

And, lastly, when $p_1 > p_{F2}$, in which case necessarily $p_{F1} > p_{F2}$, we have

$$\rho_{1h\to 1p2h}(\vec{p}_1) = \frac{2aV^2}{(2\pi)^4\hbar^6}\frac{m}{p_1}\Big\{p_{F2}^3(p_{F1}^2 - p_1^2)/3 - 2\Big[p_{F2}^5 - (p_1^2 + p_{F2}^2 - p_{F1}^2)^{5/2}\Big]/15\Big\}. \tag{2.42}$$

To establish a relation with the scattering width that Blann uses in (BLANN, 1996), we use the PWBA (Plane-Wave Born Approximation),

$$\frac{d\sigma_{NN}}{d\Omega} = \frac{m^2}{(2\pi\hbar)^2}|\omega|^2, \tag{2.43}$$

with ω as the matrix element of the interaction between plane wave states. It is used to associate the integrated cross-section with our average squared matrix element as,

$$\sigma_{NN} = 4\pi\frac{m^2V^2}{(2\pi\hbar^2)^2}a\langle|U|\rangle^2, \tag{2.44}$$

where it is assumed that the antisymmetrization factor is included in the cross-section. With that, the scattering width is given by

$$\Gamma_{1p}^{\downarrow}(\vec{p}) = \frac{(2\pi\hbar^2)^2}{2m^2V^2}\frac{\sigma_{NN}}{a}\rho_{1p\to 2p1h}(\vec{p}_1). \tag{2.45}$$

For the case of equal Fermi energy/momenta, we can write the scattering width as

$$\rho_{1p\to 2p1h}(\vec{p}_1) = \frac{2aV^2}{(2\pi)^4\hbar^6}mp_1\frac{p_F^3}{3}P_{p,Pauli}(p_1), \tag{2.46}$$

where the Pauli exclusion factor is

$$P_{p,Pauli}(p_1) = 1 - \frac{7}{5}\frac{p_F^2}{p_1^2} + \frac{2}{5}\frac{p_{2min}^5}{p_1^2 p_F^3}, \tag{2.47}$$

with $p_{2min}^2 = \max(0, 2p_F^2 - p_1^2)$. The particle scattering width is then

$$\begin{aligned}\Gamma_{1p}^{\downarrow}(\vec{p_1}) &= \frac{1}{3(2\pi\hbar)^2} p_F^3 \frac{p_1}{m} \sigma_{NN} P_{p,Pauli}(p_1) \\ &= \frac{1}{4}\hbar\frac{p_1}{m}\rho_0\sigma_{NN}P_{p,Pauli}(p_1),\end{aligned} \tag{2.48}$$

with ρ_0 as the neutron or proton density inside the nucleus. This must be summed over neutrons and protons to obtain the total scattering width. This is identical to the scattering width used by Blann, after he has taken into account the "medium correction".

In the same way, we can calculate the scattering width for holes,

$$\Gamma_{1h}^{\downarrow}(\vec{p_1}) = \frac{(2\pi\hbar^2)^2}{2m^2V^2}\frac{\sigma_{NN}}{a}\rho_{1h\to 1p2h}(\vec{p_1}), \tag{2.49}$$

which we can write as

$$\Gamma_{1h}^{\downarrow}(\vec{p_1}) = \frac{3}{16}\hbar\frac{p_F}{m}\rho_0\sigma_{NN}P_{p,Pauli}(p_1), \tag{2.50}$$

where

$$P_{p,Pauli}(p_1) = \left(1 - \frac{p_1^2}{p_F^2}\right)^2. \tag{2.51}$$

2.3 Unified model

Based on the ideas of the Exciton Model (EM), Cline and Blann proposed a pre-equilibrium master equation to quantitatively describe the reaction equilibration process, (CLINE; BLANN, 1971). The master equation describes the evolution of the exciton probability distribution, (KONING *et al.*, 1999). In summary, it accounts for the internal transition rates and the total emission rate as well as the probability that the system is in a certain exciton state in a certain time. The most important parameters for the master equation are the transition and emission rates.

In the Hybrid-Monte Carlo Simulation Model (HMS), the transition rates, as we have already seen in sec. 2.2, are calculated differently than in the exciton model. According to

Carlson *et al.* (2014), the HMS "is more consistent than the exciton and hybrid models and can describe pre-equilibrium spectra and double differential data at least as well as these".

To develop the HMS further, instead of just accounting for nucleon emissions, a model was necessary to combine the ideas of describing pre-equilibrium reactions with composite particle emissions, for example, deuterons, tritiums, and alpha particles.

In 1982, Iwamoto and Harada, (IWAMOTO; HARADA, 1982), proposed a unified model of light-composite particle emission based on the Exciton Model. This model, which we will call the Unified Model (UM), includes the effects of the emitted particle's intrinsic structure. To do that, it generalizes the exciton model.

In their first published paper on the model, Iwamoto and Harada, (IWAMOTO; HARADA, 1982), proposed a description of (p,α) reactions. One year later, K. Sato published a paper in collaboration with both authors, (SATO *et al.*, 1983), expanding their model for (p,d), (p,t), and (p,^{3}He) reactions.

In the Unified model, the formation factor, which we are going more about on the next topic, plays the most important role as it represents the composite particle formation probability. In (SATO *et al.*, 1983), the authors calculate the formation factor for (p,d), (p,t) and (p,^{3}He) reactions using a quasi-classical method following the Fermi-gas model described in (IWAMOTO; HARADA, 1982). The authors had used this method for the following reasons,

- Due to the interest in studying the formation factor properties;
- To obtain simple analytical expressions for the formation factors, which are very convenient for analyses of light-composite particle emission in an exciton model framework;
- Due to the plausibility of a quasi-classical calculation with an rms approximation.

As our aim is to develop a model to calculate deuteron emissions in pre-equilibrium nuclear reactions, we will focus on the related content from (SATO *et al.*, 1983) in the next subsections.

2.3.1 Definitions

In the Unified model, it is important to have an idea of how a deuteron can be formed from two incident particles. In Fig. 2.6, we illustrate the deuteron formation from two nucleons in momentum space. It can be interpreted as an integration in the momentum space of all deuteron formation factors. With that in mind, the proton and deuteron coordinates inside the nucleus are defined as $\vec{r}_1$ and $\vec{r}_2$, respectively. We will discuss the formation factors shortly.

The Unified model works with the following coordinate system

$$\vec{R}_d = \frac{1}{2}(\vec{r}_1 + \vec{r}_2) \quad \text{and} \quad \vec{P}_d = \vec{p}_1 + \vec{p}_2, \tag{2.52}$$

where $\vec{R}_d$ and $\vec{P}_d$ are the deuteron center of mass coordinate and momentum, respectively. The relative coordinates are given by

$$\vec{r} = \vec{r}_1 - \vec{r}_2 \quad \text{and} \quad \vec{p} = \frac{1}{2}(\vec{p}_1 - \vec{p}_2). \tag{2.53}$$

A deuteron can be emitted by different reaction mechanisms. However, as we will focus on emissions caused by a pickup type reaction, we will not discuss further any other mechanism at the moment. Deuteron formation by a pickup mechanism can be pictured as in Fig. 2.6, where we have an incident proton colliding with a target (Al, Ca, Fe..) and a neutron with momentum below the target Fermi momentum (p_F) to form a deuteron. We call this type of formation as $F_{1,1}$ (pickup).

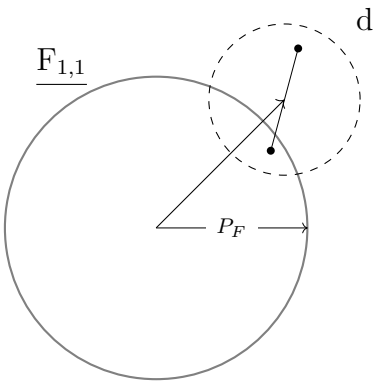

FIGURE 2.6 – Deuteron formation by a pickup type reaction mechanism.

To introduce the Unified model restrictions, we must define several parameters of the model. First, we take the hamiltonian of deuteron-bound state to be

$$h = \frac{p^2}{2\mu} + \frac{1}{2}\mu\omega^2 r^2, \quad \text{with } \mu = \frac{m}{2}, \tag{2.54}$$

where ω represents the oscillator parameter. The ground state of the hamiltonian is given by

$$\phi_d(\vec{r}) = \frac{1}{(\pi b^2)^{3/4}} \exp\Big[-\frac{1}{2}\Big(\frac{\vec{r}}{b}\Big)^2\Big], \quad \text{with } b = \sqrt{\frac{\hbar}{\mu\omega}}. \tag{2.55}$$

To obtain the formation factors for a composite particle with two nucleons, we calculate the following restricted integral

$$F_{lm}(\epsilon_d) = \frac{1}{(2\pi\hbar)^3} \int' d^3p d^3r, \tag{2.56}$$

with l and m being the number of nucleons above and below the Fermi energy ϵ_F, respectively. For the case of this work, for deuteron, we have that $l + m = 2$. We also have ϵ_d as the observed deuteron energy, which we take it to be

$$\epsilon_d = E_d - 2\epsilon_F + \frac{\varepsilon_0}{2} + Q, \tag{2.57}$$

with Q as the Q-value for deuteron emission, in other words, it is the energy released during the reaction that causes the deuteron to be emitted, and $\varepsilon_0 = \frac{3}{2}\hbar\omega$ the ground-state energy of the deuteron. The deuteron energy in the nucleus E_d and the Fermi energy ϵ_F, are given by

$$E_d = \frac{\vec{P}_d^2}{2(2m)} \quad \text{and} \quad \epsilon_F = \frac{p_F^2}{2m}, \tag{2.58}$$

with p_F being the Fermi momentum of the target nucleus.

2.3.1.1 Phase space restrictions

The restrictions on the integral defining the formation factor F_{lm}, eq. (2.56), can be easier to visualize with Fig. 2.6 in mind. They are the model phase space restrictions

governed by the following items:

1) $\dfrac{p^2}{2\mu} + \dfrac{1}{2}\mu\omega^2 r^2 \leq \varepsilon_0\,,$ fundamental oscillator energy;

2) $\left|\vec{R}_d\right| = R,$ the deuteron center of mass is fixed at the target radius;

3) $\vec{P}_d,$ the deuteron momentum in the nucleus is fixed;

4) The nucleon positions are limited by $|\vec{r}_i| \leq R_0 = R + \Delta R\,,\ i = 1, 2;$
where ΔR is a parameter to be adjusted;

5) The nucleons momenta are limited by $|\vec{p}_i| > p_F\,, \quad i = 1, \ldots, l\,,$
and $|\vec{p}_j| \leq p_F\,, \quad j = 1, \ldots, m\,.$

These restrictions are a classical version of the superposition of the neutron and proton wave functions with the deuteron wave function in the coalescence model. The first item defines the phase space ellipsoid, represented by Fig. 2.7, with r as the deuteron radius on x-axis and p the deuteron momentum on y-axis.

The second restriction limits the deuteron radius to be equal to the residual nucleus radius, consistent with the superficial nature expected of the reaction. The third one implies that the model uses a fixed momentum $\vec{P}_d$ for the emitted deuteron. This momentum will be used as an input in the simulation. The fourth restriction determines that the coordinate vector of each nucleon, proton and neutron, must be less or equal to R_0. R_0 is the target nucleus radius plus a parameter ΔR. The fifth and last restriction implies that the nucleon momentum i must be greater than the Fermi momentum p_F, with l nucleons with momentum higher than p_F. It also implies that the nucleon momentum j must be lower than p_F, with m nucleons below p_F. Note that, in our case, for pickup, l and m are equal to one.

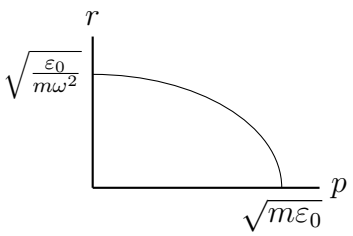

FIGURE 2.7 – Equivalent energy surface defined by the first restriction on eq. (2.56).

In (SATO *et al.*, 1983), the authors calculated the formation factors analytically. In this work, we calculate them numerically. For the pickup mechanism, for a reaction ^{40}Ca(p,d)^{39}Ca, with an incident proton with $E_p = 65$ MeV, $F_{1,1}$ is shown in Fig. 2.8. In (TEIXEIRA, 2018), the formation factors are discussed in great detail and including a generalization of the calculation to other emission mechanisms instead of just for the pickup one. One could also check Fig. **??** and Fig. **??** for an angle-integrated energy spectra using Sato, Iwamoto and Harada formation factor.

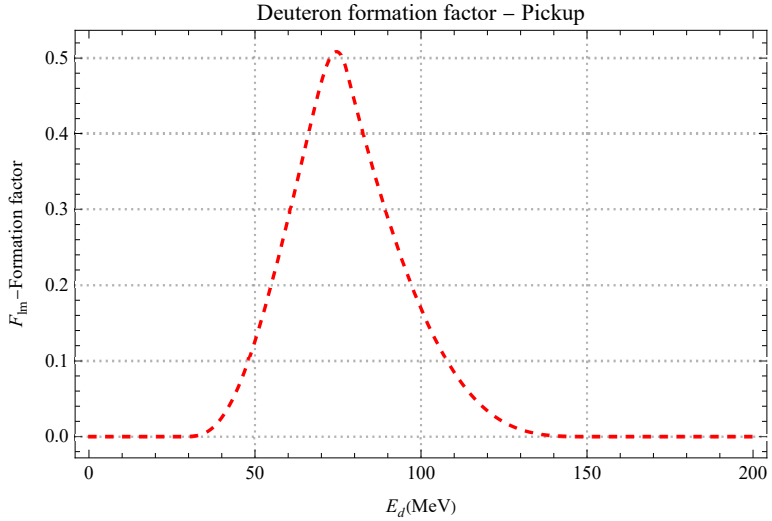

FIGURE 2.8 – Deuteron formation factor with $\Delta R = 2.1$ fm as function of deuteron energy E_d with ^{40}Ca as target with $E_p = 65$ MeV.

The formation factor gives us the probability of deuteron formation from nucleons with certain characteristics in an excited target nucleus. For the pickup case, an illustration of the process defined by the formation factor is shown in Fig. 2.9.

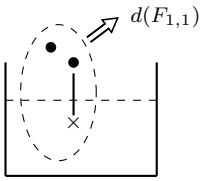

(pickup)

FIGURE 2.9 – Illustration for the pickup formation factor process ($F_{1,1}$).

2.3.1.2 Emission/decay rate

Now that we know how to calculate the deuteron formation probability, we must also determine its emission rate. The emission rate is important to relate the unified model

with the HMS. While the HMS calculates the emission of nucleons alone, the unified model emission rate will give us a way to insert a composite particle emission in our calculations using the HMS. So, instead of having just nucleon emissions, with the Unified model emission rate, we will be able to calculate proton, neutrons and deuteron emissions in a pre-equilibrium nuclear reaction.

The emission rate for the unified model involves the formation factors, F_{lm}. As we are calculating only the pickup-case, Iwamoto and Harada, (IWAMOTO; HARADA, 1982), consider that it occurs in a two-step process: the formation and the emission of the composite particle. We have already calculated the first step, the formation. It is given by eq. 2.56. The second step, the emission, will be discussed now.

Iwamoto and Harada treated the emitted particle as an elementary particle. From (IWAMOTO; HARADA, 1982), we have that

$$\frac{d\Gamma_{n(l,m)}}{d\epsilon} = \frac{1}{\pi^2\hbar^3}\mu\epsilon\sigma_{abs}F_{l,m}(\epsilon)\frac{\omega^*_{n(l,m)}(U)}{\omega(p,h,E)}, \tag{2.59}$$

for the emission rate per unit of energy from a n-exciton state. In our case, we will calculate just the F_{11} component. ϵ is the emitted particle energy, $\omega^*_{n(l,m)}(U)$ is the level density of the residual nucleus, and $\omega(p,h,E)$ is the level density of the nucleus before its decay. E is the nucleus excitation energy, and U is the residual nucleus energy. Both excitation and residual energy are related by

$$U = E - \epsilon - Q. \tag{2.60}$$

Iwamoto and Harada, (IWAMOTO; HARADA, 1982), state that if an initial p-particle h-hole exciton state (p,h) is defined, the final state given by F_{lm} will be equal to $(p{-}l, h{+}m)$. Thinking of the pickup case with a $2p1h$ state, we would have a F_{11} giving us a final $1p2h$ state. They also claim that the summation over particle configurations is already accounted for by the newly created freedom of m holes. With that, it is not necessary to include the change in m in $\omega^*_{n(l,m)}(U)$. Iwamoto and Harada assume that "the nucleons below the Fermi level, which emerge as constituents of the [emitted] particle, come out freely with no interaction with the remaining nucleons". With that, the following relation

is assumed

$$\omega^*_{n(l,m)}(U) = \omega(p-l, h, U), \tag{2.61}$$

with

$$\omega(p, h, E) = \frac{g[g(E-Y)]^{p+h-1}}{p!h!(p+h-1)!}, \tag{2.62}$$

where g is the single-particle level density of the target nucleus, and A is given by

$$Y = \frac{1}{4}(p^2 + h^2 - p - 3h). \tag{2.63}$$

Eq. (2.61) was postulated as an ansatz by Iwamoto and Harada, (IWAMOTO; HARADA, 1982).

The inverse cross-section is given by

$$\sigma_{abs} = \pi R^2 \left[1 - \frac{V_{\text{Coul}}}{\epsilon}\right], \tag{2.64}$$

with V_{Coul} being the Coulomb barrier. Finally, the cross-section is given by

$$\frac{d\sigma}{d\epsilon} = \hbar \sum_n \sigma_n \sum_{l+m} \frac{1}{\Gamma^{tot}_n} \frac{\Gamma_{n(l,m)}}{d\epsilon}, \tag{2.65}$$

where, in a general case, we would sum it over $n = 3, 5, 7, \ldots$ excitons. As Iwamoto and Harada state, "σ_n stands for the cross-section for the formation of the n-exciton state by the projectile nucleon". The last term, Γ^{tot}_n, is the total width of a n-exciton state. It means that Γ^{tot}_n represents the total value of the emission and scattering widths. Dividing $\hbar$ (reduced Planck constant) by the total width gives the mean life time of the system is in the n-exciton state. Another important thing to highlight is that eq. 2.65 is used by Iwamoto and Harada to perform their numerical calculations in (IWAMOTO; HARADA, 1982).

3 Discussion

In this chapter, we will discuss everything we have done and that we intended to accomplish with this work. To begin our discussion, it is important to note that we have used some results from our last study, (TEIXEIRA, 2018). One interesting result for pickup can be seen in Fig. 3.1. The deuteron and proton emission rate ratio for pickup decreases when the target mass increases. It gets even smaller for heavier nuclei as one can see when comparing the width values for ^{27}Al, ^{56}Fe, and ^{120}Sn.

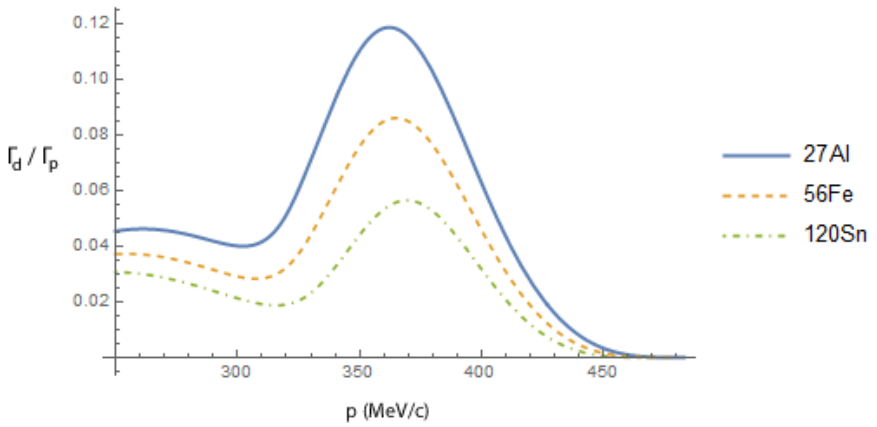

FIGURE 3.1 – Ratio between proton and deuteron emission rate by pickup for ^{27}Al, ^{56}Fe, and ^{120}Sn.

In the next section, we will discuss the steps that we have taken to understand why our results were not satisfactory, how we tried to improve the model formulation and some ideas that we have tried in order to link the unified model with a semi-classical approximation. Furthermore, we also discuss some ideas of how a new model could improve the Hybrid-Monte Carlo model to give better cross-section results using the ideas of multi-step direct pre-equilibrium nuclear reactions.

3.1 DWBA

In order to study the effects on an incident particle of the target potential while working in a nuclear reaction, calculations are usually performed in the framework of quantum mechanical scattering theory (SATCHLER, 1990).

The asymptotic wave function in the scattering theory is represented as

$$\underset{scatt,\beta}{\Psi(r,\theta,\phi)} \xrightarrow{large\ r} A_0 f_\beta(\theta,\phi)\frac{\exp(ik_\beta r\beta)}{r\beta}\psi_b\psi_B, \tag{3.1}$$

where r is the direction, θ and ϕ are the scattering angles, ψ_b and ψ_B represent the wave function for the internal states of the outgoing particle b and residual nucleus B. A_0 is the incident amplitude and f_β is a factor called the scattering amplitude in the β channel.

Solving the Schrodinger equation to obtain the scattering wave function, we can get the scattering amplitude f_β and the differential cross-section for a nuclear reaction,

$$\frac{d\sigma}{d\Omega} = \frac{v_\beta}{v_\alpha}\Big|f_\beta(\theta,\phi)\Big|^2, \tag{3.2}$$

where v_α and v_β are the incident particle and residual nucleus relative velocity, respectively.

In a collision with a neutral particle, we have an incident plane wave plus an outgoing spherical wave, given by

$$\Psi(k,r) \xrightarrow{large\ r} \exp(ik\cdot r) - \frac{\exp(ikr)}{4\pi r}\int \exp(-ik'\cdot r')U(r')\Psi(k,r')dr', \tag{3.3}$$

where we can identify the scattering amplitude as

$$f(\theta,\phi) = -\frac{1}{4\pi}\int \exp(-ik'\cdot r')U(r')\Psi(k,r')dr', \tag{3.4}$$

with U as the potential, k' the momentum of the outgoing particle.

3.1.1 Born Approximation

We can use the Born Approximation (BA) to calculate eq. 3.3. In the BA context, we say that if the potential is weak, we can approximate the incoming wave in the plane-wave Born approximation. With that, the scattering amplitude is given by

$$f_{BA}(\theta, \phi) = -\frac{1}{4\pi} \int \exp(iq \cdot r') U(r') dr', \tag{3.5}$$

where $q = k - k'$.

However, if we have a sum of potentials $U = U_1 + U_2$, we can say that the scattered wave is divided in two, as *incoming* scattered wave ($\psi^{(-)}$) and *outgoing* scattered wave ($\psi^{(+)}$). By doing that, we use a distorted-wave function with a first order Born approximation. We call it the Distorted-Wave Born Approximation (DWBA). Its general form is

$$f_{DWBA}(\theta, \phi) = -\frac{1}{4\pi} \int \psi^{(-)}(k', r')^* U_2(r') \psi^{(+)}(k, r') dr', \tag{3.6}$$

where U_1 is the elastic potential (used in f_1), and U_2 the interaction potential.

3.1.2 DWUCK4

To provide a numerical solution to DWBA problems, P. D. Kunz developed a FORTRAN code called DWUCK (Distorted-Wave University of Colorado Kunz). Although Kunz did not published an article discussing the code, one can find a description of its formulation and how to use the software on (KUNZ; ROST, 1993). DWUCK4 uses the DWBA to calculate the scattering amplitude for a binary nuclear reaction considering a zero-range interaction. He also developed another version of the code called DWUCK5. The DWUCK5 code does the same as DWUCK4 but for a finite-range interaction. In this work, we will discuss about DWUCK4 only, as we are working with a zero-range interaction. We will also call DWUCK4 simply DWUCK in the rest of this work.

Although we are developing our own code to perform calculations within the ideas of the unified model, DWUCK is an interesting tool to compare the results. It is also a well-known code which provides some useful information on calculations of interest to us.

The results obtained using DWUCK can be varied by adjusting our inputs. With that, we can relate these results from DWUCK to the calculations in our own code.

Kunz made documentation on DWUCK available to the user, (KUNZ; ROST, 1993), where one can see how DWUCK performs, its description, formulation, cases of use, and how to run the code. The documentation also has some examples of use.

3.1.2.1 Comparing results

While developing our model, we needed to compare our results with reliable data. We started by choosing experimental data for a reaction of interest to us, ^{40}Ca(p,d)^{39}Ca. With that, we started with the data from (MATOBA *et al.*, 1993).

In (MATOBA *et al.*, 1993), the differential cross-sections and analyzing power data were analyzed using DWUCK. The authors state that the conventional calculations with best-fit optical potential in the proton and deuteron channels did not reproduce the shape of differential cross-section data well for (p,d) reactions at medium energies. Because of that, they also used an adiabatic potential. They also state that the adiabatic potential for the deuteron channel considerably improves the overall fitting of the angular distribution.

They used a global optical potential (a Wood-Saxon potential) for the incident proton and an adiabatic potential for the emitted deuteron. As we were comparing models, we ignored the adiabatic potential in our calculations replacing it with the same Wood-Saxon potential used for the proton but keeping their deuteron parameters values. One can check the section B.2 on Appendix B for formulas and parameters values of the optical potential used here. The neutron bound-state wave function was calculated based on the separation energy or the effective binding energy method. They also modified several parameters to adjust the results from DWUCK to meet their experimental results, (MATOBA *et al.*, 1993).

Our first goal was to reproduce the results from (MATOBA *et al.*, 1993) using DWUCK (as they did). By doing that, we would be able to analyze its functionality.

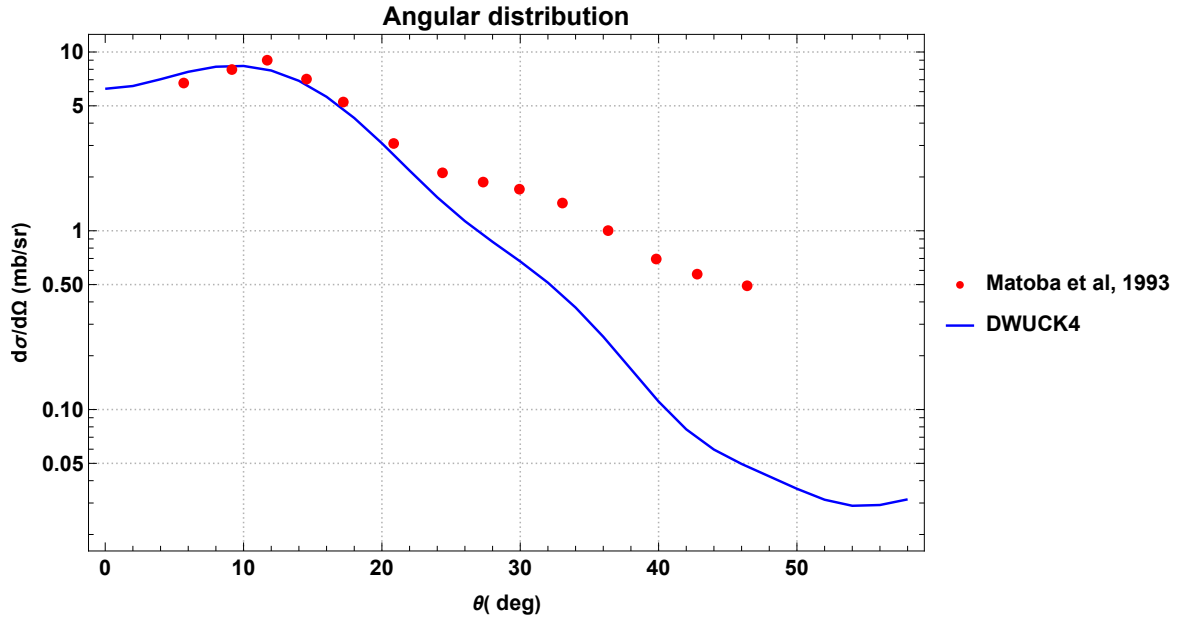

FIGURE 3.2 – Angular distribution comparison for ^{40}Ca(p,d)^{39}Ca for the experimental values and DWUCK4 results using the data input provided in (MATOBA *et al.*, 1993).

In Fig. 3.2, we compare our calculations using DWUCK to the experimental values of Matoba. One can see that the results for DWUCK are in good agreement at small angles but it begins to diverge after 20 degrees. This deviation was expected as it was said in (MATOBA *et al.*, 1993) that the authors used an adiabatic potential for the deuteron because it provides a better fit at medium energies. Due to this, we believe that our DWUCK input can reproduce the cross-section at low energies but that does not reproduce it well at medium energies because we used the same optical potential for all energy values. We could have used the adiabatic potential to try to get a better agreement with the results, however it was not our goal. This comparison was important to understand how DWUCK could help our model development. In the next sections, we will discuss several attempts that we have made to rewrite the unified model to reproduce the results given by DWUCK. The values used as input in DWUCK were taken from (MATOBA *et al.*, 1993). The input values will be the same as the ones used in Fig. 3.2, and will remain the same on the next calculations using DWUCK, unless otherwise noted.

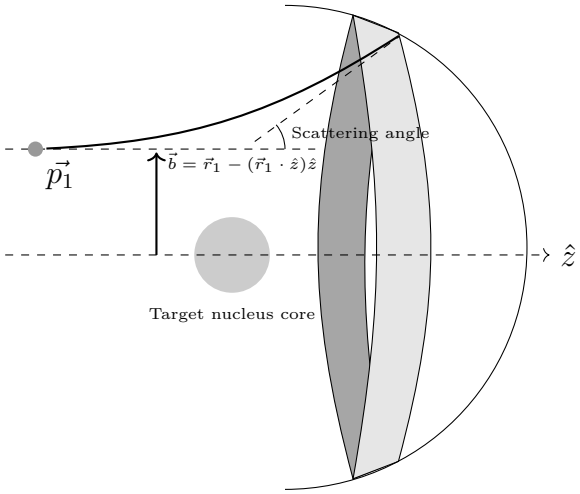

FIGURE 3.3 – Incident proton with moment $\vec{p_1}$ colliding with a target nucleus along the z axis with impact parameter $\vec{b}$.

3.2 Eikonal approximation

In this section, we will further discuss our attempt to obtain a semi-classical description of a pre-equilibrium nuclear reaction using an eikonal approximation. The reaction was idealized as in Fig. 3.3.

In order to improve the unified model, (SATO *et al.*, 1983), we had studied the phase space of their model. In our last work, (TEIXEIRA, 2018), we reached the conclusion that the simple model proposed by Sato *et al.* (1983) was not precise enough or that other deuteron production mechanisms were needed to be included in their calculations. These assumptions were made because their results were not satisfactory in comparison with experimental data.

The eikonal approximation is a good approximation for a short-range potential in scattering processes. It fits in our work as we are working with a proton colliding with a target, such as ^{40}Ca, having deuterons as the emitted composite particles. So, we hoped that the eikonal approximation could improve the unified model by redefining its phase space.

3.2.1 One-step DWBA Amplitude

We started with an one-step DWBA amplitude. We expected to calculate the scattering amplitude and the differential cross-section from it. Starting from a simpler version of our problem and complementing Fig. 3.3, one could idealize the scattering region as in Fig. 3.4.

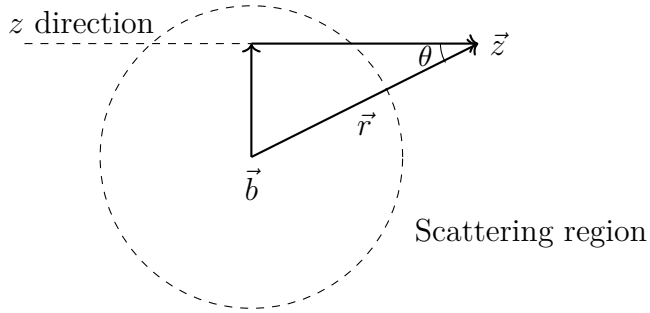

FIGURE 3.4 – Scattering region for a one-step DWBA calculation.

To calculate the angular distribution, we start by calculating the transition amplitude. For the incident proton and the emitted deuteron, the transition amplitude was given by

$$\begin{aligned}\langle \vec{K}_d; h|T^{(1)}|\vec{K}_p\rangle &= \int d^3r_d \int d^3r_p \phi_d^* \psi_d^{*(-)} V(\vec{r}_d - \vec{r}_p)\psi_p \psi_p^{(+)}, \\ &= V_0 \int d^3r \exp(i\vec{q}\cdot\vec{r})\psi_n \exp\left[-\frac{i}{\hbar v_p}\int U_p(z',\vec{b})dz' - \frac{i}{\hbar v_d}\int U_d(z',\vec{b})dz' \right],\end{aligned} \tag{3.7}$$

with $\vec{q} = |\vec{k}_p - \vec{k}_d| = 2k\sin(\theta/2)$, $v = \hbar k/\mu$, $\psi_n = U_{nl}(r_n)Y_L^m(\theta_n, \phi_n)$, and $b = \sin(\theta/2)r$.

We tried two potentials for U. The potentials are introduced in appendix A, and more details are given in appendix B. We also discuss inelastic scattering with DWBA in appendix D.

3.2.2 Deuteron pickup

We start with the amplitude, which in the post form of the DWBA is given by

$$T\left(\vec{k}_d, \vec{k}_p\right) = \left\langle \tilde{\psi}_d^{(-)}(\vec{k}_d, \vec{r}_d)\phi_d(\vec{r})\Psi_B(\chi)\left|v_{pn}(\vec{r})\right|\Psi_A(\chi, \vec{r}_n)\,\psi_p^{(+)}(\vec{k}_p, \vec{r}_p)\right\rangle, \tag{3.8}$$

where Ψ_A and Ψ_B are the initial and final nuclear wave functions, respectively. Assuming that

$$\Psi_A(\chi, \vec{r}_n) \approx \Psi_B(\chi)\,\phi_n(\vec{r}_n)\,, \tag{3.9}$$

this reduces to

$$T\left(\vec{k}_d, \vec{k}_p\right) = \left\langle \tilde{\psi}_d^{(-)}(\vec{k}_d, \vec{r}_d)\phi_d(\vec{r})\,|v_{pn}(\vec{r})|\,\phi_n(\vec{r}_n)\,\psi_p^{(+)}(\vec{k}_p, \vec{r}_p)\right\rangle\,. \tag{3.10}$$

The eikonal approximation to this amplitude is

$$\begin{aligned} T\left(\vec{k}_d, \vec{k}_p\right) &= \int d^3r_p d^3r_n \exp\left[-i\vec{k}_d\cdot\vec{r}_d - \frac{i}{\hbar v_d}\int_{z_d}^{\infty} U_d\left(z',\,\vec{b}_d\right)dz'\right] \\ &\quad \times v_{pn}(\vec{r})\,\phi_d(\vec{r})\,\phi_n(\vec{r}_n)\exp\left[i\vec{k}_p\cdot\vec{r}_p - \frac{i}{\hbar v_p}\int_{-\infty}^{z_p} U_p\left(z',\,\vec{b}_p\right)dz'\right], \end{aligned}$$

with

$$\vec{r}_d = \frac{\vec{r}_p + \vec{r}_n}{2} \qquad \text{and} \qquad \vec{r} = \vec{r}_p - \vec{r}_n\,. \tag{3.11}$$

We rewrite this in terms of $\vec{r}_n$ and $\vec{r}$, substituting

$$\vec{r}_p = \vec{r}_n + \vec{r} \qquad \text{and} \qquad \vec{r}_d = \vec{r}_n + \frac{\vec{r}}{2}\,, \tag{3.12}$$

and use the zero range approximation ($\vec{r}_p = \vec{r}_n = \vec{r}_d$) in the the eikonal phases integrals. We find

$$\begin{aligned} T\left(\vec{k}_d, \vec{k}_p\right) &= \int d^3r\, v_{pn}(\vec{r})\,\phi_d(\vec{r})\exp\left[i\left(\vec{k}_p - \vec{k}_d/2\right)\cdot\vec{r}\right] \\ &\quad \times \int d^3r_n\,\phi_n(\vec{r}_n)\exp\left[i\left(\vec{k}_p - \vec{k}_d\right)\cdot\vec{r}_n\right] \\ &\quad \times \exp\left[-\frac{i}{\hbar v_d}\int_{z_n}^{\infty} U_d\left(z',\,\vec{b}_n\right)dz' - \frac{i}{\hbar v_p}\int_{-\infty}^{z_n} U_p\left(z',\,\vec{b}_n\right)dz'\right]. \end{aligned}$$

Since $v_{pn}(\vec{r})$ is of short range, the first integral modulates the amplitude slightly at large values of $\left|\vec{k}_p - \vec{k}_d/2\right|$. The second term is the most important one. It gives the amplitude as essentially the Fourier transform in $\vec{k}_p - \vec{k}_d$ of the neutron wave function, modulated by the eikonal integrals, which should lead to strong absorption in the nuclear interior. We thus expect the principal contribution to the integral to come from values of $\left|\vec{b}_n\right| \approx R$, where R is the nuclear radius.

3.2.3 Conclusions about the eikonal approximation

Although we had obtained the differential energy-angular distribution using the eikonal approximation, our results have not provided the improvement to the unified model we expected. In the next paragraphs, we discuss several results that we have obtained and compare them using the unified model and DWUCK.

Our first attempt was to use the eikonal approximation to obtain similar values as the unified model for the pickup mechanism. As the unified model and the eikonal approximation are semi-classical, we also studied the results from DWUCK to compare them with a quantum-mechanical result. We started by comparing the transition amplitude T. For the following discussion, we have defined the amplitude T as

$$T = \left| \langle \vec{K}_d; h | T^{(1)} | \vec{K}_p \rangle \right|^2. \tag{3.13}$$

One can see in Fig. 3.5 that the calculations show good agreement between the three amplitudes (including a normalization of the values). For this result, we have used the optical potential values obtained from (MATOBA *et al.*, 1993) and explained in appendix A.

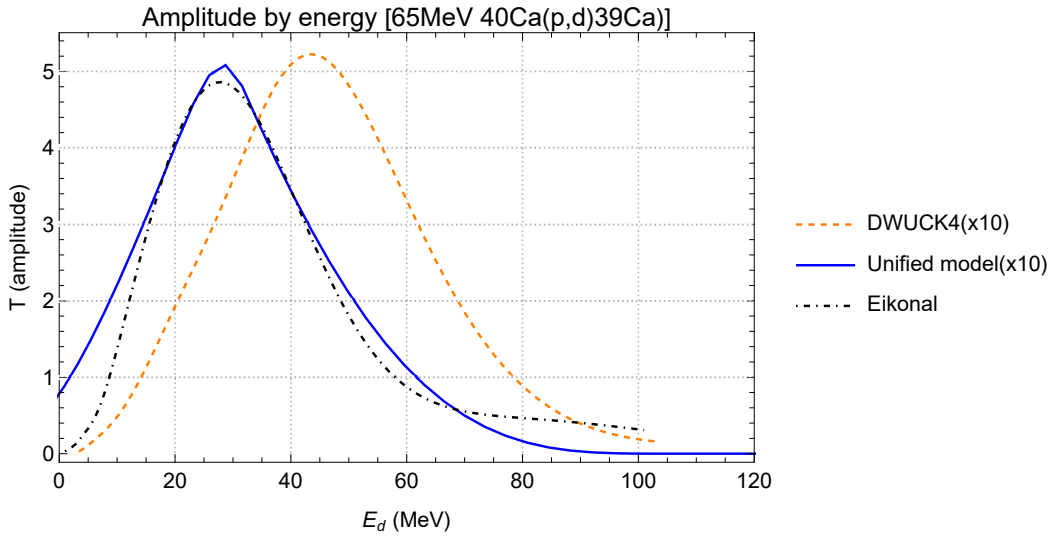

FIGURE 3.5 – Comparison between the transition amplitude for DWUCK (multiplied by 10), the unified model (multiplied by 10) and the eikonal approximation for ^{40}Ca(p,d)^{39}Ca with $E_p = 65$ MeV.

Continuing our studies, we tried to understand the behavior of the transition amplitude in terms of $l = k_p \times b$ (here we forget the last definition of l, from the exciton model,

and we are going to define it as the phase-space radius) and the deuteron energy (E_d). Besides comparing DWUCK with eikonal, DWUCK also gives us the transition amplitude by each orbit in the nuclear shell model. One can see in Fig. 3.6 the amplitude T for each orbit in a ^{40}Ca(p,d)^{39}Ca reaction with $E_p = 65$ MeV.

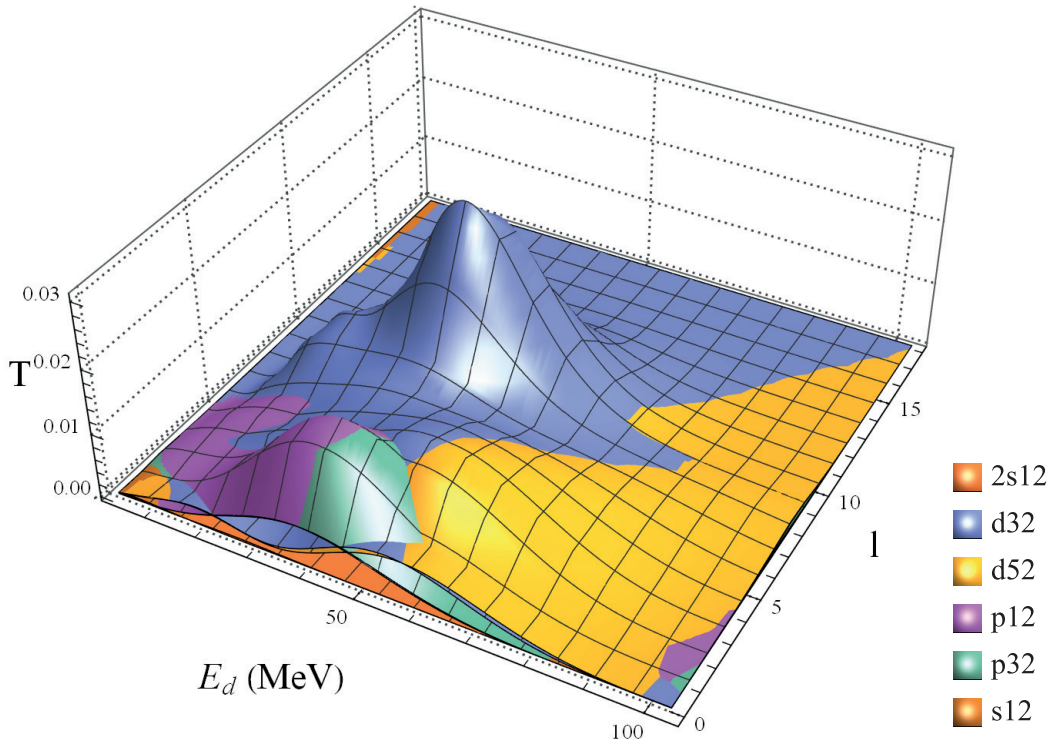

FIGURE 3.6 – Transition amplitude for ^{40}Ca(p,d)^{39}Ca with $E_p = 65$ MeV in terms of $l = k_p \times b$ (where b is the impact parameter) and E_d (deuteron energy). The legends represent each orbit in the nuclear shell model for this reaction. Results obtained using DWUCK.

In contrast to DWUCK, our calculation using the eikonal approximation does not give the amplitude orbit by orbit. However, we can obtain the total value of the amplitude as seen in Fig. 3.7 (A). For the sake of comparison, we have also included the summed amplitude from DWUCK in Fig. 3.7 (B). The results in Fig. 3.7 are similar to those in Fig. 3.5.

In conclusion, the results from the last figures show that the eikonal approximation provides good agreement with the unified model but it is slightly different than the results

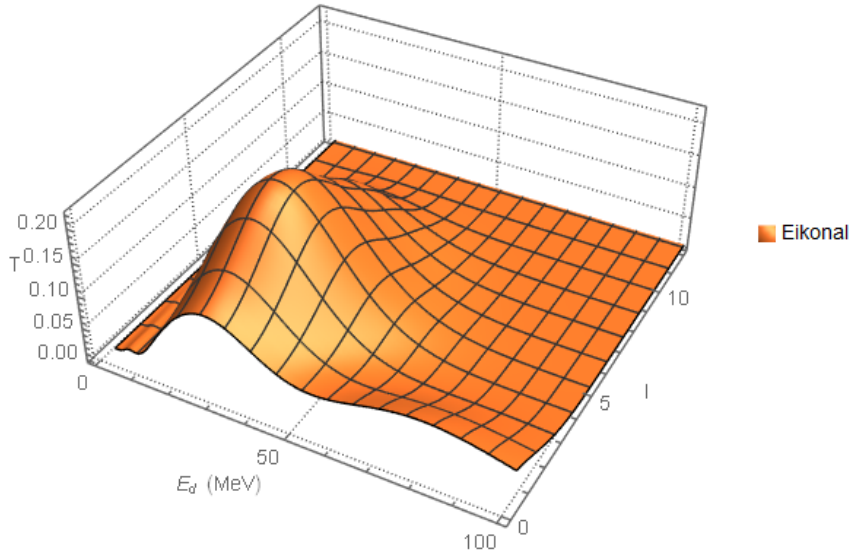

(A-Eikonal)

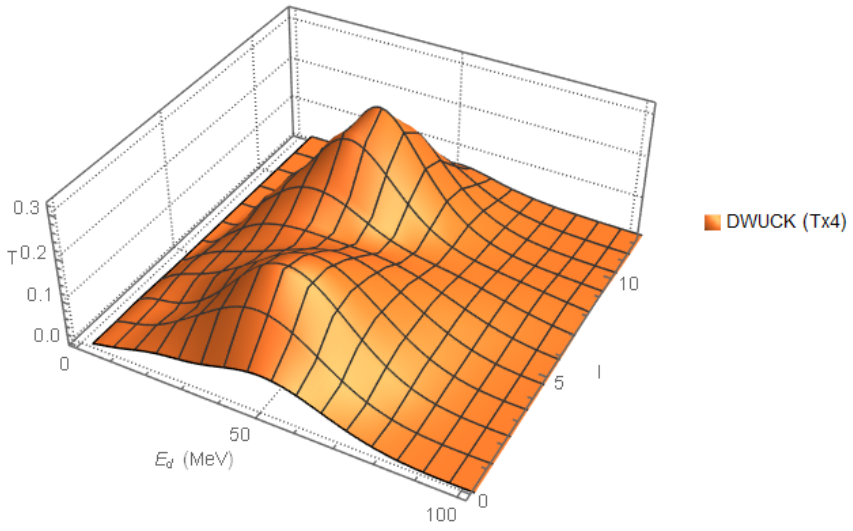

(B-DWUCK)

FIGURE 3.7 – Transition amplitude for ^{40}Ca(p,d)^{39}Ca with $E_p = 65$ MeV by $l = k_p \times b$ (where b is the impact parameter) and E_d (deuteron energy). The values on DWUCK were summed by each nuclear orbit. The amplitude for DWUCK is multiplied by 4.

provided by DWUCK. In Fig. 3.7 (A), apart from the difference in magnitude between both results, one can see that the eikonal amplitude is concentrated in the range from 0 to 45 MeV with low l values, while the results from DWUCK have two peaks at about 30 and 50 MeV spread in l values. Low l values means that the reaction occurs in the target core, and high l values means interactions near the target surface. The different

peaks in DWUCK are due to the nuclear orbits. The amplitude in the eikonal result has an oscillatory behavior with low l values, which is odd.

Our goal in this study was to obtain the deuteron formation factor, the differential cross-section and other data using this approximation. With that, we would be able to compare it with the experimental data. We would also compare it with the results found by Iwamoto and Harada in (SATO *et al.*, 1983).

By improving the unified model, we would be able to implement it in the Hybrid-Monte Carlo Model (HMS) (BLANN; CHADWICK, 1998). With this implementation, we would have a more physically-motivated description of deuteron emission in pre-equilibrium nuclear reactions.

One can read more about this study on Appendix C.

4 The semi-classical distorted-wave model

To advance our understanding of this line of research, we put the last study aside and we focused on a new phase space model for the unified model. Instead of calculating the amplitude using the eikonal approximation, we formulate a direct calculation of the transition rates. We also compare the results of this new model for the pickup reaction with those from DWUCK.

4.1 One-step DWBA excitation

The semi-classical distorted-wave model, (LUO; KAWAI, 1991; WEILI *et al.*, 1999), assumes the usual form for the one-step DWBA cross-section for the excitation of a mode α

$$\frac{d^3\sigma_\alpha}{dk_f^3} = \frac{2\pi}{hv_i}\frac{1}{(2\pi)^3}\left|\left\langle \vec{k}_f\left|T_\alpha\right|\vec{k}_i\right\rangle\right|^2 \delta\left(E_f - E_i - \epsilon_\alpha\right) , \tag{4.1}$$

where we have suppressed all spin indices. The excitation energy of the mode is given by ϵ_α, where α represents any and all quantum numbers needed to specify the excitation mode. We write the T-matrix element as

$$\left\langle \vec{k}_f\left|T_\alpha\right|\vec{k}_i\right\rangle = \int d^3r\, d^3r_0 \chi^{(-)\dagger}_{\vec{k}_f}\left(\vec{r}_0\right) V\left(\vec{r}_0 - \vec{r}\right) \rho_\alpha\left(\vec{r}\right) \chi^{(+)}_{\vec{k}_i}\left(\vec{r}_0\right) , \tag{4.2}$$

where we assume that the transition density $\rho_\alpha\left(\vec{r}\right)$ is given by some linear combination of nuclear states,

$$\rho_\alpha\left(\vec{r}\right) = \sum_{a,b} X^\alpha_{ab} \psi^\dagger_{b\mu_b}\left(\vec{r}\right) \psi_{a\mu_a}\left(\vec{r}\right) . \tag{4.3}$$

We wish to approximate the squared amplitude

$$\begin{aligned}\left|\left\langle \vec{k}_f \left| T_\alpha \right| \vec{k}_i \right\rangle\right|^2 = & \int d^3r\, d^3r_0 \chi^{(-)\dagger}_{\vec{k}_f}(\vec{r}_0)\, V(\vec{r}_0-\vec{r})\, \rho_\alpha(\vec{r})\, \chi^{(+)}_{\vec{k}_i}(\vec{r}_0) \\ & \times \int d^3r'\, d^3r'_0 \chi^{(+)\dagger}_{\vec{k}_i}(\vec{r}'_0)\, V^\dagger(\vec{r}'_0-\vec{r}')\, \rho^\dagger_\alpha(\vec{r}')\, \chi^{(-)}_{\vec{k}_f}(\vec{r}'_0) \\ = & \int d^3r_0\, d^3r'_0 \chi^{(-)\dagger}_{\vec{k}_f}(\vec{r}_0)\, \chi^{(-)}_{\vec{k}_f}(\vec{r}'_0)\, \chi^{(+)}_{\vec{k}_i}(\vec{r}_0)\, \chi^{(+)\dagger}_{\vec{k}_i}(\vec{r}'_0) \\ & \times \int d^3r\, d^3r' V(\vec{r}_0-\vec{r})\, V^\dagger(\vec{r}'_0-\vec{r}')\, \rho_\alpha(\vec{r})\, \rho^\dagger_\alpha(\vec{r}')\,. \end{aligned} \tag{4.4}$$

To proceed, we write

$$V(\vec{r}_0-\vec{r}) = \frac{1}{(2\pi)^3}\int d^3q e^{i\vec{q}\cdot(\vec{r}_0-\vec{r})} V(\vec{q}) \tag{4.5}$$

and

$$V^\dagger(\vec{r}_0-\vec{r}) = \frac{1}{(2\pi)^3}\int d^3q' e^{-i\vec{q}'\cdot\left(\vec{r}'_0-\vec{r}'\right)} V^\dagger(\vec{q}')\,, \tag{4.6}$$

and note that $V(\vec{q})$ is a smooth function of $\vec{q}$. When the interaction is a contact one, the transformed interaction is in fact a constant. We also write

$$\chi^{(+)}_{\vec{k}_i}(\vec{r}_0)\, \chi^{(+)\dagger}_{\vec{k}_i}(\vec{r}'_0) = \frac{1}{(2\pi)^3}\int d^3\kappa_i e^{i\vec{\kappa}_i\cdot\left(\vec{r}_0-\vec{r}'_0\right)} \Phi^{(+)}_{\vec{k}_i}\left(\vec{\kappa}_i, \frac{\vec{r}_0+\vec{r}'_0}{2}\right), \tag{4.7}$$

$$\chi^{(-)\dagger}_{\vec{k}_f}(\vec{r}_0)\, \chi^{(-)}_{\vec{k}_f}(\vec{r}'_0) = \frac{1}{(2\pi)^3}\int d^3\kappa_f e^{-i\vec{\kappa}_f\cdot\left(\vec{r}_0-\vec{r}'_0\right)} \Phi^{(-)\dagger}_{\vec{k}_f}\left(\vec{\kappa}_f, \frac{\vec{r}_0+\vec{r}'_0}{2}\right), \tag{4.8}$$

as well as

$$\rho_\alpha(\vec{r})\, \rho^\dagger_\alpha(\vec{r}') = \frac{1}{(2\pi)^3}\int d^3\kappa_\alpha e^{i\vec{\kappa}_\alpha\cdot(\vec{r}-\vec{r}')} K_\alpha\left(\vec{\kappa}_\alpha, \frac{\vec{r}+\vec{r}'}{2}\right). \tag{4.9}$$

We now substitute these expressions and transform the coordinate variables to

$$\begin{aligned} \vec{s}_0 &= \vec{r}_0-\vec{r}'_0 & \vec{s} &= \vec{r}-\vec{r}' \\ \vec{R}_0 &= \frac{1}{2}\left(\vec{r}_0+\vec{r}'_0\right) & \vec{R} &= \frac{1}{2}\left(\vec{r}+\vec{r}'\right). \end{aligned} \tag{4.10}$$

We have

$$\begin{aligned}\left|\left\langle \vec{k}_f\left|T_\alpha\right|\vec{k}_i\right\rangle\right|^2 = \int d^3R_0 d^3s_0 \frac{1}{(2\pi)^3}\int d^3\kappa_f e^{-i\vec{\kappa}_f\cdot\vec{s}_0}\Phi^{(-)\dagger}_{\vec{k}_f}\left(\vec{\kappa}_f,\vec{R}_0\right)\\ \times\frac{1}{(2\pi)^3}\int d^3\kappa_i e^{i\vec{\kappa}_i\cdot\vec{s}_0}\Phi^{(+)}_{\vec{k}_i}\left(\vec{\kappa}_i,\vec{R}_0\right)\\ \times\int d^3R\, d^3s\,\frac{1}{(2\pi)^3}\int d^3\kappa_\alpha e^{i\vec{\kappa}_\alpha\cdot\vec{s}}K_\alpha\left(\vec{\kappa}_\alpha,\vec{R}\right)\\ \times\frac{1}{(2\pi)^6}\int d^3q\, d^3q' e^{i(\vec{q}-\vec{q}')\cdot\left(\vec{R}_0-\vec{R}\right)+i(\vec{q}+\vec{q}')\cdot(\vec{s}_0-\vec{s})/2}\\ \times V\left(\vec{q}\right)V^\dagger\left(\vec{q}'\right)\,.\end{aligned} \tag{4.11}$$

We can perform the same transformation of the momenta $\vec{q}$ and $\vec{q}'$, writing

$$\vec{p}=\vec{q}-\vec{q}' \quad \text{and} \quad \vec{Q}=\frac{1}{2}\left(\vec{q}+\vec{q}'\right) \tag{4.12}$$

to obtain

$$\begin{aligned}\left|\left\langle \vec{k}_f\left|T_\alpha\right|\vec{k}_i\right\rangle\right|^2 = \int d^3R_0 d^3s_0 \frac{1}{(2\pi)^3}\int d^3\kappa_f e^{-i\vec{\kappa}_f\cdot\vec{s}_0}\Phi^{(-)\dagger}_{\vec{k}_f}\left(\vec{\kappa}_f,\vec{R}_0\right)\\ \times\frac{1}{(2\pi)^3}\int d^3\kappa_i e^{i\vec{\kappa}_i\cdot\vec{s}_0}\Phi^{(+)}_{\vec{k}_i}\left(\vec{\kappa}_i,\vec{R}_0\right)\\ \times\int d^3R\, d^3s\,\frac{1}{(2\pi)^3}\int d^3\kappa_\alpha e^{i\vec{\kappa}_\alpha\cdot\vec{s}}K_\alpha\left(\vec{\kappa}_\alpha,\vec{R}\right)\\ \times\frac{1}{(2\pi)^6}\int d^3p\, d^3Q e^{i\vec{p}\cdot\left(\vec{R}_0-\vec{R}\right)+i\vec{Q}\cdot(\vec{s}_0-\vec{s})}\\ \times V\left(\vec{Q}+\vec{p}/2\right)V^\dagger\left(\vec{Q}-\vec{p}/2\right)\,.\end{aligned} \tag{4.13}$$

Performing the integrals over $\vec{s}$ and $\vec{s}_0$ and then over $\vec{\kappa}_\alpha$, we have

$$\begin{aligned}\left|\left\langle \vec{k}_f\left|T_\alpha\right|\vec{k}_i\right\rangle\right|^2 =&\frac{1}{(2\pi)^9}\int d^3R_0\int d^3\kappa_f\Phi^{(-)\dagger}_{\vec{k}_f}\left(\vec{\kappa}_f,\vec{R}_0\right)\int d^3\kappa_i\Phi^{(+)}_{\vec{k}_i}\left(\vec{\kappa}_i,\vec{R}_0\right)\\ &\times\int d^3R\, d^3p\, d^3Q\, e^{i\vec{p}\cdot\left(\vec{R}_0-\vec{R}\right)}K_\alpha\left(\vec{Q},\vec{R}\right)\delta\left(\vec{\kappa}_i-\vec{\kappa}_f+\vec{Q}\right)\\ &\times V\left(\vec{Q}+\vec{p}/2\right)V^\dagger\left(\vec{Q}-\vec{p}/2\right)\,.\end{aligned} \tag{4.14}$$

We note that this result is still exact. No approximations have been made.

If we now use the fact that the interaction V is of short-range in $\vec{r}$ and thus smooth

in $\vec{q}$, to approximate

$$V\left(\vec{Q}+\vec{p}/2\right)V^{\dagger}\left(\vec{Q}-\vec{p}/2\right)\approx\left|V\left(\vec{Q}\right)\right|^{2} \tag{4.15}$$

and perform the integrals over $\vec{p}$ and $\vec{R}_0$ (or $\vec{R}$), we obtain

$$\begin{aligned}\left|\left\langle \vec{k}_f\left|T_\alpha\right|\vec{k}_i\right\rangle\right|^2 \approx & \frac{1}{(2\pi)^6}\int d^3R\, d^3\kappa_f\, d^3\kappa_i\, d^3Q\, \Phi^{(-)\dagger}_{\vec{k}_f}\left(\vec{\kappa}_f,\vec{R}\right)\Phi^{(+)}_{\vec{k}_i}\left(\vec{\kappa}_i,\vec{R}\right) \\ & \times K_\alpha\left(\vec{Q},\vec{R}\right)\left|V\left(\vec{Q}\right)\right|^2\delta\left(\vec{\kappa}_i-\vec{\kappa}_f+\vec{Q}\right).\end{aligned} \tag{4.16}$$

If we take the transition density to be a pure particle-hole one,

$$\rho_\alpha\left(\vec{r}\right)\rightarrow\psi^{\dagger}_b\left(\vec{r}\right)\psi_a\left(\vec{r}\right), \tag{4.17}$$

then, after defining

$$\psi_a\left(\vec{R}+\vec{s}/2\right)\psi^{\dagger}_a\left(\vec{R}-\vec{s}/2\right)=\frac{1}{(2\pi)^3}\int d^3\kappa_a e^{i\vec{\kappa}_a\cdot\vec{s}}\Psi_a\left(\vec{\kappa}_a,\vec{R}\right) \tag{4.18}$$

and

$$\psi^{\dagger}_b\left(\vec{R}+\vec{s}/2\right)\psi_b\left(\vec{R}-\vec{s}/2\right)=\frac{1}{(2\pi)^3}\int d^3\kappa_b e^{-i\vec{\kappa}_b\cdot\vec{s}}\Psi^{\dagger}_b\left(\vec{\kappa}_b,\vec{R}\right), \tag{4.19}$$

we can write the squared transition amplitude as

$$\begin{aligned}\left|\left\langle \vec{k}_f\left|T_{ba}\right|\vec{k}_i\right\rangle\right|^2 \approx & \frac{1}{(2\pi)^6}\int d^3R\, d^3\kappa_f\, d^3\kappa_i\, d^3\kappa_a\, d^3\kappa_b\, d^3Q \\ & \times\Phi^{(-)\dagger}_{\vec{k}_f}\left(\vec{\kappa}_f,\vec{R}\right)\Psi^{\dagger}_b\left(\vec{\kappa}_b,\vec{R}\right)\Psi_a\left(\vec{\kappa}_a,\vec{R}\right)\Phi^{(+)}_{\vec{k}_i}\left(\vec{\kappa}_i,\vec{R}\right) \\ & \times\left|V\left(\vec{Q}\right)\right|^2\delta\left(\vec{\kappa}_i-\vec{\kappa}_f+\vec{Q}\right)\delta\left(\vec{\kappa}_a-\vec{\kappa}_b-\vec{Q}\right).\end{aligned} \tag{4.20}$$

For a general transition density,

$$\rho_\alpha\left(\vec{r}\right)=\sum_{a,b}X^{\alpha}_{ab}\psi^{\dagger}_b\left(\vec{r}\right)\psi_a\left(\vec{r}\right), \tag{4.21}$$

the squared matrix element takes the form

$$\begin{aligned}\left|\left\langle \vec{k}_f\left|T_\alpha\right|\vec{k}_i\right\rangle\right|^2 = & \sum_{a,b,a',b'}X^{\alpha}_{ab}X^{\alpha\dagger}_{a'b'}\int d^3r\, d^3r_0\chi^{(-)\dagger}_{\vec{k}_f}\left(\vec{r}_0\right)V\left(\vec{r}_0-\vec{r}\right)\psi^{\dagger}_b\left(\vec{r}\right)\psi_a\left(\vec{r}\right)\chi^{(+)}_{\vec{k}_i}\left(\vec{r}_0\right) \\ & \times\int d^3r'\, d^3r'_0\chi^{(+)\dagger}_{\vec{k}_i}\left(\vec{r}'_0\right)V^{\dagger}\left(\vec{r}'_0-\vec{r}'\right)\psi^{\dagger}_{a'}\left(\vec{r}'\right)\psi_{b'}\left(\vec{r}'\right)\chi^{(-)}_{\vec{k}_f}\left(\vec{r}'_0\right).\end{aligned} \tag{4.22}$$

It can be shown that the expansion coefficients X_{ab}^{α} become random already at reasonably low excitation energy, having the property that

$$\sum_{\epsilon_\alpha \in \Delta E} X_{ab}^{\alpha} X_{a'b'}^{\alpha\dagger} \approx \sum_{\epsilon_\alpha \in \Delta E} \left| X_{ab}^{\alpha} \right|^2 \delta_{aa'} \delta_{bb'} \,, \tag{4.23}$$

where the squared coefficients $\left|X_{ab}^{\alpha}\right|^2$ are approximately distributed as a Breit-Wigner function in the energy ϵ_α centered at the energy of the ab particle-hole state. We then have

$$\begin{aligned}
\sum_{\epsilon_\alpha \in \Delta E} \left| \left\langle \vec{k}_f \left| T_\alpha \right| \vec{k}_i \right\rangle \right|^2 \approx & \sum_{\epsilon_\alpha \in \Delta E} \sum_{a,b} \left| X_{ab}^{\alpha} \right|^2 \int d^3r \, d^3r_0 \chi_{\vec{k}_f}^{(-)\dagger} \left(\vec{r}_0 \right) V \left(\vec{r}_0 - \vec{r} \right) \psi_b^\dagger \left(\vec{r} \right) \psi_a \left(\vec{r} \right) \chi_{\vec{k}_i}^{(+)} \left(\vec{r}_0 \right) \\
& \times \int d^3r' \, d^3r'_0 \chi_{\vec{k}_i}^{(+)\dagger} \left(\vec{r}'_0 \right) V^\dagger \left(\vec{r}'_0 - \vec{r}' \right) \psi_a^\dagger \left(\vec{r}' \right) \psi_b \left(\vec{r}' \right) \chi_{\vec{k}_f}^{(-)} \left(\vec{r}'_0 \right) , \\
\approx & \frac{1}{(2\pi)^6} \sum_{\epsilon_\alpha \in \Delta E} \int d^3R \, d^3\kappa_f \, d^3\kappa_i \, d^3\kappa_a \, d^3\kappa_b \, d^3Q \\
& \times \Phi_{\vec{k}_f}^{(-)\dagger} \left(\vec{\kappa}_f, \vec{R} \right) \left[\sum_{a,b} \left| X_{ab}^{\alpha} \right|^2 \Psi_b^\dagger \left(\vec{\kappa}_b, \vec{R} \right) \Psi_a \left(\vec{\kappa}_a, \vec{R} \right) \right] \Phi_{\vec{k}_i}^{(+)} \left(\vec{\kappa}_i, \vec{R} \right) \\
& \times \left| V \left(\vec{Q} \right) \right|^2 \delta \left(\vec{\kappa}_i - \vec{\kappa}_f + \vec{Q} \right) \delta \left(\vec{\kappa}_a - \vec{\kappa}_b - \vec{Q} \right) .
\end{aligned} \tag{4.24}$$

4.1.1 Excitation to the continuum (Knockout)

In the case of excitation to the continuum, (a knockout reaction), we have

$$\rho_\alpha \left(\vec{r} \right) = \sum_{a,b} X_{ab}^{\alpha} \psi_b^\dagger \left(\vec{r} \right) \psi_a \left(\vec{r} \right) \to \chi_{f_2}^{(-)\dagger} \left(\vec{r} \right) \psi_a \left(\vec{r} \right) , \tag{4.25}$$

and

$$\frac{1}{(2\pi)^3} \int d^3\kappa_\alpha e^{i\vec{\kappa}_\alpha \cdot \vec{s}} K_\alpha \left(\vec{\kappa}_\alpha, \vec{R} \right) \to \frac{1}{(2\pi)^6} \int d^3\kappa_a e^{i\vec{\kappa}_a \cdot \vec{s}} \Psi_a \left(\vec{\kappa}_a, \vec{R} \right) \int d^3\kappa_{f_2} e^{-i\vec{\kappa}_{f_2} \cdot \vec{s}} \Phi_{\vec{k}_{f_2}}^{(-)\dagger} \left(\vec{\kappa}_{f_2}, \vec{R} \right) , \tag{4.26}$$

where

$$\psi_a \left(\vec{R} + \vec{s}/2 \right) \psi_a^\dagger \left(\vec{R} - \vec{s}/2 \right) = \frac{1}{(2\pi)^3} \int d^3\kappa_a e^{i\vec{\kappa}_a \cdot \vec{s}} \Psi_a \left(\vec{\kappa}_a, \vec{R} \right) , \tag{4.27}$$

while the expression for the second outgoing particle is similar to that of the first.

The squared matrix element is then

$$\left|\left\langle \vec{k}_{f_1}\vec{k}_{f_2}\left|T_\alpha\right|\vec{k}_i\right\rangle\right|^2 \approx \frac{1}{(2\pi)^9}\int d^3R\, d^3\kappa_{f_1}\, d^3\kappa_{f_2}\, d^3\kappa_a\, d^3\kappa_i\, d^3Q \times \Phi^{(-)\dagger}_{\vec{k}_{f_1}}\left(\vec{\kappa}_{f_1},\vec{R}\right)\Phi^{(-)\dagger}_{\vec{k}_{f_2}}\left(\vec{\kappa}_{f_2},\vec{R}\right)\Psi_a\left(\vec{\kappa}_a,\vec{R}\right)\Phi^{(+)}_{\vec{k}_i}\left(\vec{\kappa}_i,\vec{R}\right) \times \left|V\left(\vec{Q}\right)\right|^2\delta\left(\vec{\kappa}_i-\vec{\kappa}_{f_1}+\vec{Q}\right)\delta\left(\vec{\kappa}_a-\vec{\kappa}_{f_2}-\vec{Q}\right). \tag{4.28}$$

4.2 Wigner functions in the eikonal approximation

The Wigner transforms of the wave functions play an essential role in the semi-classical distorted-wave model. We investigate them here in the eikonal approximation. The Wigner transforms of the wave functions are given by

$$\Phi^{(\pm)}_{\vec{k}}\left(\vec{\kappa},\vec{R}\right) = \int d^3s\, e^{-i\vec{\kappa}\cdot\vec{s}}\chi^{(\pm)}_{\vec{k}}\left(\vec{R}+\vec{s}/2\right)\chi^{(\pm)\dagger}_{\vec{k}}\left(\vec{R}-\vec{s}/2\right). \tag{4.29}$$

4.2.1 The incoming wave function

Following Goldberger-Watson, (GOLDBERGER *et al.*, 1964), the eikonal approximation to the wave functions is given by

$$\chi^{(+)}_{\vec{k}}\left(\vec{r}\right) = \exp\left[i\int_{-\infty}^{z} p\left(z',\vec{b}\right)dz' - \frac{1}{2}\ln\left(p\left(z,\vec{b}\right)/k\right)\right] \tag{4.30}$$

and

$$\chi^{(-)}_{\vec{k}}\left(\vec{r}\right) = \exp\left[-i\int_{z}^{\infty} p^*\left(z',\vec{b}\right)dz' - \frac{1}{2}\ln\left(p^*\left(z,\vec{b}\right)/k\right)\right], \tag{4.31}$$

where

$$p\left(\vec{r}\right) = \sqrt{k^2-\frac{2\mu}{\hbar^2}U\left(\vec{r}\right)} = \sqrt{k^2-\frac{2\mu}{\hbar^2}\left(V\left(\vec{r}\right)-iW\left(\vec{r}\right)\right)} \tag{4.32}$$

with

$$z = \hat{k}\cdot\vec{r} \qquad \text{and} \qquad \vec{b} = \vec{r}-z\hat{k} = -\hat{k}\times\left(\hat{k}\times\vec{r}\right). \tag{4.33}$$

Denoting $\vec{R} = \vec{B} + Z\hat{k}$ and $\vec{s} = \vec{s}_b + s_z\hat{k}$, we write the incoming wave product as

$$\chi^{(+)}_{\vec{k}}\left(\vec{R}+\vec{s}/2\right)\chi^{(+)\dagger}_{\vec{k}}\left(\vec{R}-\vec{s}/2\right) = \exp\left[i\phi_+\left(\vec{R}+\vec{s}/2,\vec{k}\right)-i\phi^*_+\left(\vec{R}-\vec{s}/2,\vec{k}\right)\right] \tag{4.34}$$

where

$$\phi_+\left(\vec{r},\vec{k}\right)=\int_{-\infty}^{z}p\left(z',\vec{b}\right)dz'+\frac{i}{2}\ln\left(p\left(z,\vec{b}\right)/k\right)\,, \tag{4.35}$$

and expand to first order in $\vec{s}$,

$$\begin{aligned}\phi_+\left(\vec{R}+\vec{s}/2,\vec{k}\right)-\phi_+^*\left(\vec{R}-\vec{s}/2,\vec{k}\right)&=\phi_+\left(\vec{R},\vec{k}\right)-\phi_+^*\left(\vec{R},\vec{k}\right)+\frac{\vec{s}}{2}\cdot\left(\overrightarrow{\nabla}\phi_+\left(\vec{R},\vec{k}\right)+\overrightarrow{\nabla}\phi_+^*\left(\vec{R},\vec{k}\right)\right)\\&=2i\int_{-\infty}^{Z}\text{Im }p\left(z',\vec{B}\right)dz'+i\ln\left(p\left(Z,\vec{B}\right)/k\right)+\text{Re }p\left(Z,\vec{B}\right)s_z\\&\qquad+\int_{-\infty}^{Z}\overrightarrow{\nabla}_{\vec{B}}\text{Re }p\left(z',\vec{B}\right)dz'\cdot\vec{s}_b\,,\\&=2i\int_{-\infty}^{Z}\text{Im }p\left(z',\vec{B}\right)dz'+i\ln\left(p\left(Z,\vec{B}\right)/k\right)\\&\qquad+\vec{s}\cdot\int_{-\infty}^{Z}\text{Re }\overrightarrow{\nabla}p\left(z',\vec{B}\right)dz'+ks_z\,.\end{aligned} \tag{4.36}$$

Substituting, we have

$$\chi_{\vec{k}}^{(+)}\left(\vec{R}+\vec{s}/2\right)\chi_{\vec{k}}^{(+)\dagger}\left(\vec{R}-\vec{s}/2\right)\approx\exp\left[i\vec{p}_+\left(\vec{R},\vec{k}\right)\cdot\vec{s}\right]\left|\chi_{\vec{k}}^{(+)}\left(\vec{R}\right)\right|^2\,, \tag{4.37}$$

where

$$\left|\chi_{\vec{k}}^{(+)}\left(\vec{R}\right)\right|^2=\exp\left[-2\int_{-\infty}^{Z}\text{Im }p\left(z',\vec{B}\right)dz'-\ln\left(\text{Re }p\left(Z,\vec{B}\right)/k\right)\right] \tag{4.38}$$

and

$$\vec{p}_+\left(\vec{R},\vec{k}\right)=\vec{k}+\int_{-\infty}^{Z}\text{Re}\overrightarrow{\nabla}p\left(z',\vec{B}\right)dz' \tag{4.39}$$

Note that

$$p\left(\vec{r}\right)=\sqrt{k^2-\frac{2m}{\hbar^2}U\left(\vec{r}\right)}\approx k-\frac{1}{\hbar v}\left(V\left(\vec{r}\right)-iW\left(\vec{r}\right)\right)\,, \tag{4.40}$$

so that we can interpret

$$\int_{-\infty}^{Z}\text{Re}\overrightarrow{\nabla}p\left(z',\vec{B}\right)dz'\approx-\frac{1}{\hbar v}\int_{-\infty}^{Z}\overrightarrow{\nabla}'V\left(z',\vec{B}\right)dz'\approx\frac{1}{\hbar}\int_{-\infty}^{t}\vec{F}\left(t'\right)dt'=\frac{\Delta\vec{p}}{\hbar}=\Delta\vec{k} \tag{4.41}$$

as the change in wave number along the trajectory, where we interpret

$$\vec{F}\left(t'\right)=-\overrightarrow{\nabla}'V\left(\vec{r}'\right)\qquad\text{and}\qquad dt'=\frac{1}{v}dz'\,. \tag{4.42}$$

The Wigner transform of the incoming wave function is then

$$\begin{aligned}\Phi_{\vec{k}}^{(+)}\left(\vec{\kappa},\vec{R}\right) &= \int d^3s\, e^{-i\vec{\kappa}\cdot\vec{s}}\chi_{\vec{k}}^{(+)}\left(\vec{R}+\vec{s}/2\right)\chi_{\vec{k}}^{(+)\dagger}\left(\vec{R}-\vec{s}/2\right)\\ &\approx (2\pi)^3\,\delta\left(\vec{\kappa}-\vec{p}_+\left(\vec{R},\vec{k}\right)\right)\left|\chi_{\vec{k}}^{(+)}\left(\vec{R}\right)\right|^2 .\end{aligned} \tag{4.43}$$

4.2.2 The outgoing wave function

The outgoing wave product of interest to us is

$$\chi_{\vec{k}}^{(-)\dagger}\left(\vec{R}+\vec{s}/2\right)\chi_{\vec{k}}^{(-)}\left(\vec{R}-\vec{s}/2\right) = \exp\left[i\phi_-\left(\vec{R}+\vec{s}/2,\vec{k}\right)-i\phi_-^*\left(\vec{R}-\vec{s}/2,\vec{k}\right)\right] \tag{4.44}$$

where

$$\phi_-\left(\vec{r},\vec{k}\right) = \int_z^\infty p\left(z',\vec{b}\right)dz' + \frac{i}{2}\ln\left(p\left(\vec{r}\right)/k\right) . \tag{4.45}$$

Expanding to first order in $\vec{s}$, as before, we find

$$\begin{aligned}\phi_-\left(\vec{R}+\vec{s}/2,\vec{k}\right)-\phi_-^*\left(\vec{R}-\vec{s}/2,\vec{k}\right) &= \phi_-\left(\vec{R},\vec{k}\right)-\phi_-^*\left(\vec{R},\vec{k}\right)+\frac{\vec{s}}{2}\cdot\left(\overrightarrow{\nabla}\phi_-\left(\vec{R},\vec{k}\right)+\overrightarrow{\nabla}\phi_-^*\left(\vec{R},\vec{k}\right)\right)\\ &= 2i\int_Z^\infty \mathrm{Im}\; p\left(z',\vec{B}\right)dz' + i\ln\left(p\left(Z,\vec{B}\right)/k\right)+\mathrm{Re}\; p\left(Z,\vec{B}\right)s_z\\ &\qquad +\int_Z^\infty \overrightarrow{\nabla}_{\vec{B}}\mathrm{Re}\; p\left(z',\vec{B}\right)dz'\cdot\vec{s}_b\\ &= 2i\int_Z^\infty \mathrm{Im}\; p\left(z',\vec{B}\right)dz' + i\ln\left(p\left(Z,\vec{B}\right)/k\right)\\ &\qquad +\vec{s}\cdot\int_Z^\infty \mathrm{Re}\;\overrightarrow{\nabla}p\left(z',\vec{B}\right)dz' - ks_z .\end{aligned} \tag{4.46}$$

Substituting, we have

$$\chi_{\vec{k}}^{(-)\dagger}\left(\vec{R}+\vec{s}/2\right)\chi_{\vec{k}}^{(-)}\left(\vec{R}-\vec{s}/2\right) \approx \exp\left[-i\vec{p}_-\left(\vec{R},\vec{k}\right)\cdot\vec{s}\right]\left|\chi_{\vec{k}}^{(-)}\left(\vec{R}\right)\right|^2 , \tag{4.47}$$

where

$$\left|\chi_{\vec{k}}^{(-)}\left(\vec{R}\right)\right|^2 = \exp\left[-2\int_Z^\infty \mathrm{Im}\; p\left(z',\vec{B}\right)dz' - \ln\left(\mathrm{Re}p\left(Z,\vec{B}\right)/k\right)\right] \tag{4.48}$$

and

$$\vec{p}_-\left(\vec{R},\vec{k}\right) = \vec{k} - \int_Z^\infty \mathrm{Re}\overrightarrow{\nabla}p\left(z',\vec{B}\right)dz' . \tag{4.49}$$

We then find for the Wigner transform

$$\begin{aligned}\Phi_{\vec{k}}^{(-)\dagger}\left(\vec{\kappa},\vec{R}\right) &= \int d^3s\, e^{i\vec{\kappa}\cdot\vec{s}}\chi_{\vec{k}}^{(-)\dagger}\left(\vec{R}+\vec{s}/2\right)\chi_{\vec{k}}^{(-)}\left(\vec{R}-\vec{s}/2\right) \\ &\approx (2\pi)^3\,\delta\left(\vec{\kappa}-\vec{p}_-\left(\vec{R},\vec{k}\right)\right)\left|\chi_{\vec{k}}^{(-)}\left(\vec{R}\right)\right|^2 .\end{aligned} \tag{4.50}$$

4.2.3 The propagator

The eikonal approximation to the propagator can be written as

$$G^{(+)}\left(\vec{r}_2,\vec{r}_1;E_m\right) = \frac{2\mu}{4\pi}\frac{\exp\left[i\int_{z_1}^{z_2} p\left(z',\vec{b}_1\right)dz' - \frac{1}{2}\ln\left(p\left(\vec{r}_2\right)p\left(\vec{r}_1\right)/k_m^2\right)\right]}{|\vec{r}_2-\vec{r}_1|}\theta\left(z_2-z_1\right)\ , \tag{4.51}$$

where

$$p\left(z,\vec{b}\right) = \sqrt{\frac{2\mu}{\hbar^2}\left(E_m - U\left(\vec{r}\right)\right)} = \sqrt{k_m^2 - \frac{2\mu}{\hbar^2}U\left(\vec{r}\right)}, \tag{4.52}$$

and the integral is along the direction

$$\hat{k} = \frac{\vec{r}_2-\vec{r}_1}{|\vec{r}_2-\vec{r}_1|}\,, \tag{4.53}$$

with

$$\begin{aligned} z_1 &= \hat{k}\cdot\vec{r}_1 \qquad & \vec{b}_1 &= \vec{r}_1 - \left(\hat{k}\cdot\vec{r}_1\right)\hat{k} \\ z_2 &= \hat{k}\cdot\vec{r}_2 \qquad & \vec{b}_2 &= \vec{r}_2 - \left(\hat{k}\cdot\vec{r}_2\right)\hat{k}\,. \end{aligned} \tag{4.54}$$

One can easily show that

$$z_2 - z_1 = |\vec{r}_2-\vec{r}_1| \qquad \text{and} \qquad \vec{b}_1 = \vec{b}_2\,. \tag{4.55}$$

After a fairly extensive calculation, the Wigner transform of the propagator can be

put into the form

$$\begin{aligned}\Gamma^{(+)}\left(\vec{\kappa}_2,\vec{R}_2;\vec{\kappa}_1,\vec{R}_1;E_m\right) &= \left(\frac{2\mu}{4\pi}\right)^2\int d^3s_2\,d^3s_1 e^{-i\vec{\kappa}_2\cdot\vec{s}_2+i\vec{\kappa}_1\cdot\vec{s}_1}G^{(+)}\left(\vec{R}_2+\vec{s}_2/2,\vec{R}_1+\vec{s}_1/2;E_m\right)\\ &\qquad\times G^{(+)\dagger}\left(\vec{R}_2-\vec{s}_2/2,\vec{R}_1-\vec{s}_1/2;E_m\right)\\ &= \left(\frac{2\mu}{4\pi}\right)^2(2\pi)^6\,\delta\left(\vec{\kappa}_2-\vec{p}_+\left(\vec{R}_2,\vec{k}_m\right)\right)\\ &\qquad\times\delta\left(\vec{\kappa}_1-\vec{p}_+\left(\vec{R}_1,\vec{k}_m\right)\right)\frac{\left|G\left(\vec{R}_2,\vec{R}_1;E_m\right)\right|^2}{\left|\vec{R}_2-\vec{R}_1\right|^2},\end{aligned} \tag{4.56}$$

where

$$\left|G\left(\vec{R}_2,\vec{R}_1;E_m\right)\right|^2=\exp\left[-2\int_{Z_1}^{Z_2}\mathrm{Im}\;p\left(z',\vec{B}\right)dz'-\ln\left(\mathrm{Re}p\left(Z_1,\vec{B}_1\right)\mathrm{Re}p\left(Z_2,\vec{B}_2\right)/k_m^2\right)\right], \tag{4.57}$$

$$\vec{p}_+\left(\vec{R}_i,\vec{k}_m\right)=\vec{k}_m+\int_{-\infty}^{Z_i}\mathrm{Re}\overrightarrow{\nabla}p\left(z',\vec{B}\right)dz', \tag{4.58}$$

with

$$\vec{k}_m=k_m\hat{k}_m,\qquad \hat{k}_m=\frac{\vec{R}_2-\vec{R}_1}{\left|\vec{R}_2-\vec{R}_1\right|},\qquad E_m=\frac{\hbar^2}{2\mu}k_m^2, \tag{4.59}$$

and

$$Z_i=\vec{k}_m\cdot\vec{R}_i\quad\text{and}\quad\vec{B}=\vec{B}_i=\vec{R}_i-Z_i\hat{k}_m. \tag{4.60}$$

4.2.4 Asymptotic limit of the propagator

Here we analyze the propagator in the limit $\left|\vec{R}_2\right|\to\infty$. For the values $\vec{\kappa}_1$ and $\vec{\kappa}_2$ of the local momentum satisfying the momentum conservation δ functions, we have

$$\begin{aligned}\vec{\kappa}_2&=\vec{k}_m+\int_{-\infty}^{Z_2}\mathrm{Re}\overrightarrow{\nabla}p\left(z',\vec{B}\right)dz',\\ &=\vec{\kappa}_1+\int_{Z_1}^{Z_2}\mathrm{Re}\overrightarrow{\nabla}p\left(z',\vec{B}\right)dz'.\end{aligned} \tag{4.61}$$

When $\left|\vec{R}_2\right|\to\infty$, due to the geometry of the problem, we have $\vec{\kappa}_2\to\kappa_2\hat{k}_m$. But to the extent to which the momentum integral is energy conserving, we should also have

$\kappa_2 \to k_m$. We can thus write, in the limit,

$$\begin{aligned}\vec{\kappa}_1 &= \lim_{|\vec{R}_2|\to\infty}\left(\vec{\kappa}_2 - \int_{Z_1}^{Z_2} \mathrm{Re}\overrightarrow{\nabla} p\left(z', \vec{B}\right) dz'\right) \\ &= \vec{k}_m - \int_{Z_1}^{\infty} \mathrm{Re}\overrightarrow{\nabla} p\left(z', \vec{B}\right) dz' \\ &= \vec{p}_-\left(\vec{R}_1, \vec{k}_m\right) .\end{aligned} \tag{4.62}$$

Noting that

$$\lim_{|\vec{R}_2|\to\infty}\left|G\left(\vec{R}_2, \vec{R}_1; E_m\right)\right|^2 = \exp\left[-2\int_{Z_1}^{\infty} \mathrm{Im}\ p\left(z', \vec{B}\right) dz' - \ln\left(\mathrm{Re}p\left(Z_1, \vec{B}_1\right)/k_m\right)\right], \tag{4.63}$$

and that in the eikonal approximation,

$$\Phi^{(-)\dagger}_{\vec{k}}\left(\vec{\kappa}, \vec{R}\right) \approx (2\pi)^3\,\delta\left(\vec{\kappa} - \vec{p}_-\left(\vec{R}, \vec{k}\right)\right)\exp\left[-2\int_{Z}^{\infty} \mathrm{Im}\ p\left(z', \vec{B}\right) dz' - \ln\left(\mathrm{Re}p\left(Z_1, \vec{B}_1\right)/k_m\right)\right], \tag{4.64}$$

we can write

$$\lim_{|\vec{R}_2|\to\infty} (2\pi)^3\,\delta\left(\vec{\kappa}_2 - \vec{p}_+\left(\vec{R}_2, \vec{k}_m\right)\right)\delta\left(\vec{\kappa}_1 - \vec{p}_+\left(\vec{R}_1, \vec{k}_m\right)\right) \tag{4.65}$$

$$\times\left|G\left(\vec{R}_2, \vec{R}_1; E_m\right)\right|^2 = \frac{1}{k_m}\Phi^{(-)\dagger}_{\vec{k}_m}\left(\vec{\kappa}_1, \vec{R}_1\right)\delta\left(\vec{\kappa}_2 - \vec{k}_m\right) . \tag{4.66}$$

We thus have

$$\begin{aligned}\lim_{|\vec{R}_2|\to\infty} \Gamma^{(+)}\left(\vec{\kappa}_2, \vec{R}_2; \vec{\kappa}_1, \vec{R}_1; E_m\right) d^3\kappa_2\, d^3R_2 \to \left(\frac{2\mu}{4\pi}\right)^2 \frac{(2\pi)^3}{k_m}\Phi^{(-)\dagger}_{\vec{k}_m}\left(\vec{\kappa}_1, \vec{R}_1\right) \\ \times\,\delta\left(\vec{\kappa}_2 - \vec{k}_m\right) d^3\kappa_2\, dR_2 d\Omega_m .\end{aligned} \tag{4.67}$$

4.3 Monte Carlo evaluation of the scattering series

When the eikonal form of the wave functions is substituted in the one-step excitation squared matrix element, we find

$$\begin{aligned}\left|\left\langle \vec{k}_f \left| T_\alpha \right| \vec{k}_i \right\rangle\right|^2 \approx \frac{1}{(2\pi)^6} \int & d^3R\, d^3\kappa_f\, d^3\kappa_i\, d^3\kappa_a\, d^3\kappa_b\, d^3Q \\ & \times \Phi^{(-)\dagger}_{\vec{k}_f}\left(\vec{\kappa}_f, \vec{R}\right) \left[\sum_{a,b} \left|X^\alpha_{ab}\right|^2 \Psi^\dagger_b\left(\vec{\kappa}_b, \vec{R}\right) \Psi_a\left(\vec{\kappa}_a, \vec{R}\right)\right] \Phi^{(+)}_{\vec{k}_i}\left(\vec{\kappa}_i, \vec{R}\right) \\ & \times \left|V\left(\vec{Q}\right)\right|^2 \delta\left(\vec{\kappa}_i - \vec{\kappa}_f + \vec{Q}\right) \delta\left(\vec{\kappa}_a - \vec{\kappa}_b - \vec{Q}\right) . \\ = \int & d^3R\, d^3\kappa_a\, d^3\kappa_b\, d^3Q \left|\phi^{(-)}_{\vec{k}_f}\left(\vec{R}\right)\right|^2 \left|\phi^{(+)}_{\vec{k}_i}\left(\vec{R}\right)\right|^2 \\ & \times \left|V\left(\vec{Q}\right)\right|^2 \delta\left(\vec{\kappa}_a - \vec{\kappa}_b - \vec{Q}\right) \left[\sum_{a,b} \left|X^\alpha_{ab}\right|^2 \Psi^\dagger_b\left(\vec{\kappa}_b, \vec{R}\right) \Psi_a\left(\vec{\kappa}_a, \vec{R}\right)\right] \\ & \times \delta\left(\vec{p}_+\left(\vec{R}, \vec{k}_i\right) + \vec{\kappa}_a - \vec{p}_-\left(\vec{R}, \vec{k}_f\right) - \vec{\kappa}_b\right) .\end{aligned} \tag{4.68}$$

We can interpret the integrand as propagation along an absorptive eikonal trajectory defined by $\vec{k}_i$ with the absorption factor $\left|\phi^{(+)}_{\vec{k}_i}\left(\vec{R}\right)\right|^2$, followed by a momentum and energy conserving collision at $\vec{R}$ and subsequent propagation along the final absorptive eikonal trajectory defined by $\vec{k}_f$. The momentum and energy conservation at the collision coordinate $\vec{R}$ are determined by the local values of the momenta, $\vec{\kappa}_i + \vec{\kappa}_a = \vec{\kappa}_f + \vec{\kappa}_b$. For fixed values of the initial and final momenta, one must integrate over all values of the internal momenta $\vec{\kappa}_a$ and $\vec{\kappa}_b$ consistent with momentum conservation at the collision coordinate $\vec{R}$.

Considering now the propagation of the Wigner function after the collision in an one-step process, we have

$$\begin{aligned}\Phi^{(+)}_{\vec{k}}\left(\vec{\kappa}_2, \vec{R}_2\right) = \frac{1}{(2\pi)^9} \frac{1}{k_m} \delta\left(\vec{\kappa}_2 - \vec{k}_m\right) \int & d^3R_1\, d^3\kappa_1\, d^3\kappa_b\, d^3\kappa_a\, d^3\kappa_i\, d^3Q \\ & \times \Gamma^{(+)}\left(\vec{\kappa}_2, \vec{R}_2; \vec{\kappa}_1, \vec{R}_1; E_m\right) \\ & \times \left|V\left(\vec{Q}\right)\right| \delta\left(\vec{\kappa_i} + \vec{Q} - \vec{\kappa_1}\right) \delta\left(\vec{\kappa_a} - \vec{Q} - \vec{\kappa_b}\right) \\ & \times \left[\sum_{a,b} \left|X^\alpha_{ab}\right|^2 \Psi^\dagger_b\left(\vec{\kappa}_b, \vec{R}_1\right) \Psi_a\left(\vec{\kappa}_a, \vec{R}_1\right)\right] \Phi^{(+)}_{\vec{k}_i}\left(\vec{\kappa}_i, \vec{R}_1\right) .\end{aligned} \tag{4.69}$$

If no further collisions occur, we can calculate the asymptotic behavior of the Wigner function using the asymptotic behavior of the wave function in the eikonal approximation.

We recover the one-step amplitude squared, up to factor of the final momentum,

$$\begin{aligned}\lim_{|\vec{R}_2|\to\infty} \Phi^{(+)}_{\vec{k}}\left(\vec{\kappa}_2,\vec{R}_2\right) \to \frac{1}{k_m}\delta\left(\vec{\kappa}_2-\vec{k}_m\right)\frac{1}{(2\pi)^6}\int d^3R_1\, d^3\kappa_1\, d^3\kappa_b\, d^3\kappa_a\, d^3\kappa_i\, d^3Q \\ \times \Phi^{(-)\dagger}_{\vec{k}_m}\left(\vec{\kappa}_1,\vec{R}_1\right)\left[\sum_{a,b}\left|X^{\alpha}_{ab}\right|^2\Psi^{\dagger}_b\left(\vec{\kappa}_b,\vec{R}_1\right)\Psi_a\left(\vec{\kappa}_a,\vec{R}_1\right)\right]\Phi^{(+)}_{\vec{k}_i}\left(\vec{\kappa}_i,\vec{R}_1\right) \\ \times\left|V\left(\vec{Q}\right)\right|\delta\left(\vec{\kappa_i}+\vec{Q}-\vec{\kappa_1}\right)\delta\left(\vec{\kappa_a}-\vec{Q}-\vec{\kappa}_b\right), \\ = \frac{1}{k_m}\delta\left(\vec{\kappa}_2-\vec{k}_m\right)\int d^3R\, d^3\kappa_a\, d^3\kappa_b\, d^3Q\left|\phi^{(-)}_{\vec{k}_f}\left(\vec{R}\right)\right|^2\left|\phi^{(+)}_{\vec{k}_m}\left(\vec{R}\right)\right|^2 \\ \times\left|V\left(\vec{Q}\right)\right|^2\delta\left(\vec{\kappa}_a-\vec{\kappa}_b-\vec{Q}\right)\left[\sum_{a,b}\left|X^{\alpha}_{ab}\right|^2\Psi^{\dagger}_b\left(\vec{\kappa}_b,\vec{R}\right)\Psi_a\left(\vec{\kappa}_a,\vec{R}\right)\right] \\ \times\delta\left(\vec{p}_+\left(\vec{R},\vec{k}_i\right)+\vec{\kappa}_a-\vec{p}_-\left(\vec{R},\vec{k}_m\right)-\vec{\kappa}_b\right).\end{aligned} \tag{4.70}$$

If we were to consider the asymptotic wave function after two collisions, we would obtain the two step amplitude squared times the same factor of the final momentum. The entire scattering series could be calculated by considering the asymptotic limits of a series of Wigner functions with an increasing number of collisions. However, this sum quickly becomes numerically prohibitive.

Instead, we can use a Monte Carlo method similar to the HMS one, but now better founded in theory, to estimate all terms in the scattering series simultaneously. To do so, we use the absorption factor $\left|\phi^{(+)}_{\vec{k}}\left(\vec{R}\right)\right|^2$as a measure of the distance propagated between collisions. When compared to a random number, its value determines the position of the first collision. The momenta of the two particles and hole that result from the collision can be chosen randomly according to the phase space distribution of the collision term, just as is done in the HMS model. The subsequent propagation will take place according to the absorption factors of the two particles and the hole produced in the collision, just as in the HMS calculation. These can collide again or escape, in accord with the Monte Carlo evaluation of the absorption factors. By following a series of initial collisions until all particles escape or are bound, the entire scattering series can be evaluated, just as in the HMS calculation. The advantage here is that this Monte Carlo evaluation has as its basis a well-defined theoretical foundation.

The goal of this thesis is to insert the deuteron production into a Monte Carlo evaluation in a pre-equilibrium reaction. Although several paths to this goal have been studied,

none of them have been found successful until now. By offering a clear theoretical basis for the calculation of scattering cross-sections, the semi-classical distorted-wave model gives us hope that it will provide a framework for the systematic inclusion of deuteron production as well as other processes.

4.4 Deuteron pickup

We expect the deuteron pickup process to be fairly easy to be included in the Monte Carlo evaluation. In a collision, the phase space volume for deuteron pickup would be compared to that of a simple nucleon-nucleon collision to determine the relative frequency of each. A subsequent collision of the deuteron with a nucleon would require the comparison of the phase space volume for its scattering relative to that for its breakup into a pair of nucleons. The formalism provides a clear prescription for the calculation of these volumes, however.

In the case of a deuteron pickup reaction, we write the matrix element as

$$\left\langle \vec{k}_d \left| T_d \right| \vec{k}_p \right\rangle = \int d^3r\, d^3r_d \chi^{(-)\dagger}_{\vec{k}_d}\left(\vec{r}_d\right) \psi_d\left(\vec{r}\right) V\left(\vec{r}\right) \psi_a\left(\vec{r}_{nA}\right) \chi^{(+)}_{\vec{k}_p}\left(\vec{r}_{pB}\right) , \tag{4.71}$$

where ψ_a denotes the single particle state of the neutron in the nucleus, ψ_d the deuteron wave function and B denotes the nucleus $A+1$. With the coordinates defined as

$$\begin{aligned} \vec{r} &= \vec{r}_p - \vec{r}_n \\ \vec{r}_d &= \frac{\vec{r}_p + \vec{r}_n}{2} - \vec{r}_A \\ \vec{r}_{nA} &= \vec{r}_n - \vec{r}_A = \vec{r}_d - \frac{\vec{r}}{2} \\ \vec{r}_{pB} &= \vec{r}_p - \frac{A\vec{r}_A + \vec{r}_n}{A+1} = \frac{A}{A+1}\vec{r}_d + \frac{A+2}{2A+2}\vec{r} \equiv \alpha\vec{r}_d + \beta\vec{r}, \end{aligned} \tag{4.72}$$

with

$$\alpha = \frac{A}{A+1} \qquad \text{and} \qquad \beta = \frac{A+2}{2A+2}\,, \tag{4.73}$$

we have

$$\left\langle \vec{k}_d \left| T_d \right| \vec{k}_p \right\rangle = \int d^3r\, d^3r_d \chi^{(-)\dagger}_{\vec{k}_d}\left(\vec{r}_d\right) \psi_d\left(\vec{r}\right) V\left(\vec{r}\right) \psi_a\left(\vec{r}_d - \vec{r}/2\right) \chi^{(+)}_{\vec{k}_p}\left(\alpha\vec{r}_d + \beta\vec{r}\right) . \tag{4.74}$$

We now define the variables

$$\vec{s}_d = \vec{r}_d - \vec{r}'_d \qquad \vec{s} = \vec{r} - \vec{r}' \tag{4.75}$$

$$\vec{R}_d = \frac{\vec{r}_d + \vec{r}'_d}{2} \qquad \vec{R} = \frac{\vec{r} + \vec{r}'}{2}\,, \tag{4.76}$$

to simplify the expressions of the Wigner transforms,

$$\chi^{(+)}_{\vec{k}_p}\left(\alpha\vec{r}_d + \beta\vec{r}/2\right)\chi^{(+)\dagger}_{\vec{k}_p}\left(\alpha\vec{r}'_d + \beta\vec{r}'/2\right) = \frac{1}{(2\pi)^3}\int d^3\kappa_p e^{i\vec{k}_p\cdot(\alpha\vec{s}_d+\beta\vec{s}/2)}\Phi^{(+)}_{\vec{k}_p}\left(\vec{\kappa}_p, \alpha\vec{R}_d + \beta\vec{R}/2\right)\,, \tag{4.77}$$

$$\psi_a\left(\vec{r}_d - \vec{r}/2\right)\psi^\dagger_a\left(\vec{r}'_d - \vec{r}'/2\right) = \frac{1}{(2\pi)^3}\int d^3\kappa_n e^{i\vec{k}_n\cdot(\vec{s}_d-\vec{s}/2)}\Psi_a\left(\vec{\kappa}_n, \vec{R}_d - \vec{R}/2\right)\,, \tag{4.78}$$

$$\chi^{(-)\dagger}_{\vec{k}_d}\left(\vec{r}_d\right)\chi^{(-)}_{\vec{k}_d}\left(\vec{r}'_d\right) = \frac{1}{(2\pi)^3}\int d^3\kappa_d e^{-i\vec{\kappa}_d\cdot\vec{s}_d}\Phi^{(-)\dagger}_{\vec{k}_d}\left(\vec{\kappa}_d, \vec{R}_d\right)\,, \tag{4.79}$$

as well as

$$\psi_d\left(\vec{r}\right)\psi^\dagger_d\left(\vec{r}'\right) = \frac{1}{(2\pi)^3}\int d^3\kappa e^{i\vec{\kappa}\cdot\vec{s}}\Psi_d\left(\vec{\kappa}, \vec{R}\right)\,. \tag{4.80}$$

Here, we have

$$V\left(\vec{r}\right) = \frac{1}{(2\pi)^3}\int d^3q e^{i\vec{q}\cdot\vec{r}}V\left(\vec{q}\right) \tag{4.81}$$

and

$$V^\dagger\left(\vec{r}'\right) = \frac{1}{(2\pi)^3}\int d^3q' e^{-i\vec{q}'\cdot\vec{r}'}V^\dagger\left(\vec{q}'\right)\,. \tag{4.82}$$

Putting all the pieces together, we have

$$\begin{aligned}
\left|\left\langle \vec{k}_d\left|T_d\right|\vec{k}_p\right\rangle\right|^2 &= \int d^3r\, d^3r_d \chi^{(-)\dagger}_{\vec{k}_d}\left(\vec{r}_d\right)\psi_d\left(\vec{r}\right)V\left(\vec{r}\right)\psi_a\left(\vec{r}_d - \vec{r}/2\right)\chi^{(+)}_{\vec{k}_p}\left(\alpha\vec{r}_d + \beta\vec{r}\right) \\
&\quad\times\int d^3r'\, d^3r'_d \chi^{(+)\dagger}_{\vec{k}_p}\left(\alpha\vec{r}'_d + \beta\vec{r}'\right)\psi^\dagger_a\left(\vec{r}'_d - \vec{r}'/2\right)V^\dagger\left(\vec{r}'\right)\psi^\dagger_d\left(\vec{r}'\right)\chi^{(-)}_{\vec{k}_d}\left(\vec{r}'_d\right) \\
&= \int d^3R_d\, d^3s_d\, d^3R\, d^3s\, \frac{1}{(2\pi)^3}\int d^3\kappa_d e^{-i\vec{\kappa}_d\cdot\vec{s}_d}\Phi^{(-)\dagger}_{\vec{k}_d}\left(\vec{\kappa}_d, \vec{R}_d\right) \\
&\quad\times\frac{1}{(2\pi)^3}\int d^3\kappa e^{i\vec{\kappa}\cdot\vec{s}}\Psi_d\left(\vec{\kappa}, \vec{R}\right)\times\frac{1}{(2\pi)^3}\int d^3q e^{i\vec{q}\cdot\vec{r}}V\left(\vec{q}\right) \\
&\quad\times\frac{1}{(2\pi)^3}\int d^3q' e^{-i\vec{q}'\cdot\vec{r}'}V^\dagger\left(\vec{q}'\right)\times\frac{1}{(2\pi)^3}\int d^3\kappa_n e^{i\vec{\kappa}_n\cdot(\vec{s}_d-\vec{s}/2)}\Psi_a\left(\vec{\kappa}_n, \vec{R}_d - \vec{R}/2\right) \\
&\quad\times\frac{1}{(2\pi)^3}\int d^3\kappa_p e^{i\vec{\kappa}_p\cdot(\alpha\vec{s}_d+\beta\vec{s})}\Phi^{(+)}_{\vec{k}_p}\left(\vec{\kappa}_p, \alpha\vec{R}_d + \beta\vec{R}\right)\,.
\end{aligned} \tag{4.83}$$

Defining

$$\vec{Q} = \frac{\vec{q} + \vec{q}'}{2} \qquad \text{and} \qquad \vec{p} = \vec{q} - \vec{q}', \tag{4.84}$$

and noting that

$$\vec{q} \cdot \vec{r} - \vec{q}' \cdot \vec{r}' = \vec{Q} \cdot \vec{s} + \vec{p} \cdot \vec{R} \tag{4.85}$$

we can rearrange the integrals above to

$$\begin{aligned} \left|\left\langle \vec{k}_d \left| T_d \right| \vec{k}_p \right\rangle\right|^2 = & \frac{1}{(2\pi)^{18}} \int d^3R_d \, d^3s_d \, d^3R \, d^3s \, d^3\kappa_d \, d^3\kappa \, d^3\kappa_n \, d^3\kappa_p \, d^3Q \, d^3p \\ & \times e^{i(\alpha\vec{\kappa}_p + \vec{\kappa}_n - \vec{\kappa}_d)\cdot\vec{s}_d} e^{i\left(\vec{\kappa} + \vec{Q} + \beta\vec{\kappa}_p - \vec{\kappa}_n/2\right)\cdot\vec{s}} e^{i\vec{p}\cdot\vec{R}} \\ & \times \Phi^{(-)\dagger}_{\vec{k}_d}\left(\vec{\kappa}_d, \vec{R}_d\right) \Psi_d\left(\vec{\kappa}, \vec{R}\right) V\left(\vec{Q} + \vec{p}/2\right) V^\dagger\left(\vec{Q} - \vec{p}/2\right) \\ & \times \Psi_a\left(\vec{\kappa}_n, \vec{R}_d - \vec{R}/2\right) \Phi^{(+)}_{\vec{k}_p}\left(\vec{\kappa}_p, \alpha\vec{R}_d + \beta\vec{R}\right) . \end{aligned} \tag{4.86}$$

Integrating over $\vec{s}_d$ and $\vec{s}$, we find

$$\begin{aligned} \left|\left\langle \vec{k}_d \left| T_d \right| \vec{k}_p \right\rangle\right|^2 = & \frac{1}{(2\pi)^{12}} \int d^3R_d \, d^3R \, d^3\kappa_d \, d^3\kappa \, d^3\kappa_n \, d^3\kappa_p \, d^3Q \, d^3p \\ & \times \delta\left(\alpha\vec{\kappa}_p + \vec{\kappa}_n - \vec{\kappa}_d\right) \delta\left(\vec{\kappa} + \vec{Q} + \beta\vec{\kappa}_p - \vec{\kappa}_n/2\right) e^{i\vec{p}\cdot\vec{R}} \\ & \times \Phi^{(-)\dagger}_{\vec{k}_d}\left(\vec{\kappa}_d, \vec{R}_d\right) \Psi_d\left(\vec{\kappa}, \vec{R}\right) V\left(\vec{Q} + \vec{p}/2\right) V^\dagger\left(\vec{Q} - \vec{p}/2\right) \\ & \times \Psi_a\left(\vec{\kappa}_n, \vec{R}_d - \vec{R}/2\right) \Phi^{(+)}_{\vec{k}_p}\left(\vec{\kappa}_p, \alpha\vec{R}_d + \beta\vec{R}\right) . \end{aligned} \tag{4.87}$$

This result is still exact. If we assume that the interactions is a slowly-varying function of $\vec{Q}$, as before, so that

$$V\left(\vec{Q} + \vec{p}/2\right) V^\dagger\left(\vec{Q} - \vec{p}/2\right) \approx \left|V\left(\vec{Q}\right)\right|^2 , \tag{4.88}$$

we can perform the integrals in $\vec{p}$ and $\vec{R}$ to obtain

$$\begin{aligned} \left|\left\langle \vec{k}_d \left| T_d \right| \vec{k}_p \right\rangle\right|^2 = & \frac{1}{(2\pi)^9} \int d^3R_d \, d^3\kappa_d \, d^3\kappa \, d^3\kappa_n \, d^3\kappa_p \, d^3Q \\ & \times \Phi^{(-)\dagger}_{\vec{k}_d}\left(\vec{\kappa}_d, \vec{R}_d\right) \Psi_d\left(\vec{\kappa}, \vec{R} = 0\right) \Psi_a\left(\vec{\kappa}_n, \vec{R}_d\right) \Phi^{(+)}_{\vec{k}_p}\left(\vec{\kappa}_p, \alpha\vec{R}_d\right) \\ & \times \left|V\left(\vec{Q}\right)\right|^2 \delta\left(\alpha\vec{\kappa}_p + \vec{\kappa}_n - \vec{\kappa}_d\right) \delta\left(\vec{\kappa} + \vec{Q} + \beta\vec{\kappa}_p - \vec{\kappa}_n/2\right) . \end{aligned} \tag{4.89}$$

When the interaction $V(\vec{r})$ is of short range, as it is here, a zero-range approximation can

be useful. In the case of deuteron stripping and pickup reactions, one defines

$$D_0 = \int d^3r\, \psi_d\left(\vec{r}\right) V\left(\vec{r}\right) . \tag{4.90}$$

We then find

$$\begin{aligned} D_0^2 &= \int d^3r\, d^3r' \psi_d\left(\vec{r}\right) \psi_d\left(\vec{r}'\right) V\left(\vec{r}\right) V\left(\vec{r}'\right) \\ &= \frac{1}{(2\pi)^9} \int d^3R d^3s d^3\kappa d^3Q d^3p e^{i\vec{\kappa}\cdot\vec{s}} \Psi_d\left(\vec{\kappa},\vec{R}\right) \\ &\quad \times e^{i\left(\vec{Q}+\vec{p}/2\right)\cdot\left(\vec{R}+\vec{s}/2\right)} V\left(\vec{Q}+\vec{p}/2\right) e^{i\left(\vec{Q}-\vec{p}/2\right)\cdot\left(\vec{R}-\vec{s}/2\right)} V^\dagger\left(\vec{Q}-\vec{p}/2\right) \\ &= \frac{1}{(2\pi)^9} \int d^3R d^3s d^3\kappa d^3Q d^3p e^{i\left(\vec{\kappa}+\vec{Q}\right)\cdot\vec{s}} e^{i\vec{p}\cdot\vec{R}} \\ &\quad \times \Psi_d\left(\vec{\kappa},\vec{R}\right) V\left(\vec{Q}+\vec{p}/2\right) V^\dagger\left(\vec{Q}-\vec{p}/2\right) . \end{aligned} \tag{4.91}$$

Neglecting the $\vec{p}$ dependence in $V\left(\vec{Q}\right)$, we have

$$\begin{aligned} D_0^2 &= \frac{1}{(2\pi)^9} \int d^3R d^3s d^3\kappa d^3Q d^3p e^{i\left(\vec{\kappa}+\vec{Q}\right)\cdot\vec{s}} e^{i\vec{p}\cdot\vec{R}} \Psi_d\left(\vec{\kappa},\vec{R}\right) \left|V\left(\vec{Q}\right)\right|^2 \\ &= \frac{1}{(2\pi)^3} \int d^3\kappa d^3Q\, \delta\left(\vec{\kappa}+\vec{Q}\right) \Psi_d\left(\vec{\kappa},\vec{R}=0\right) \left|V\left(\vec{Q}\right)\right|^2 . \end{aligned} \tag{4.92}$$

Equivalently, in the expression for the squared scattering amplitude, we take

$$\frac{1}{(2\pi)^3} \int d^3\kappa\, d^3Q\, \Psi_d\left(\vec{\kappa},\vec{R}=0\right) \left|V\left(\vec{Q}\right)\right|^2 \delta\left(\vec{\kappa}+\vec{Q}+\beta\vec{\kappa}_p-\vec{\kappa}_n/2\right) = D_0^2 . \tag{4.93}$$

We then have (after eliminating the subscript on the remaining position vector)

$$\begin{aligned} \left|\left\langle \vec{k}_d \left|T_d\right| \vec{k}_p \right\rangle\right|^2 &= \frac{D_0^2}{(2\pi)^6} \int d^3R\, d^3\kappa_d\, d^3\kappa_n\, d^3\kappa_p \\ &\quad \times \Phi^{(-)\dagger}_{\vec{k}_d}\left(\vec{\kappa}_d,\vec{R}\right) \Psi_a\left(\vec{\kappa}_n,\vec{R}\right) \Phi^{(+)}_{\vec{k}_p}\left(\vec{\kappa}_p,\vec{R}\right) \delta\left(\alpha\vec{\kappa}_p+\vec{\kappa}_n-\vec{\kappa}_d\right) \\ &= \frac{D_0^2}{(2\pi)^6} \int d^3R\, d^3\kappa_d\, d^3\kappa_p \\ &\quad \times \Phi^{(-)\dagger}_{\vec{k}_d}\left(\vec{\kappa}_d,\vec{R}\right) \Psi_a\left(\vec{\kappa}_d-\alpha\vec{\kappa}_p,\vec{R}\right) \Phi^{(+)}_{\vec{k}_p}\left(\vec{\kappa}_p,\alpha\vec{R}\right) . \end{aligned} \tag{4.94}$$

If we now substitute the Wigner eikonal approximations to the incoming and outgoing

waves, we have

$$\begin{aligned}\left|\left\langle \vec{k}_d \left| T_d \right| \vec{k}_p \right\rangle\right|^2 &= D_0^2 \int d^3R_/\, d^3\kappa_d\, d^3\kappa_p \left|\chi^{(-)}_{\vec{k}_d}\left(\vec{R}\right)\right|^2 \left|\chi^{(+)}_{\vec{k}_p}\left(\alpha\vec{R}\right)\right|^2 \\ &\qquad \times \delta\left(\vec{\kappa}_d - \vec{p}_-\left(\vec{R},\vec{k}_d\right)\right) \Psi_a\left(\vec{\kappa}_d - \alpha\vec{\kappa}_p, \vec{R}\right) \delta\left(\vec{\kappa}_p - \vec{p}_+\left(\alpha\vec{R},\vec{k}_p\right)\right) , \\ &= D_0^2 \int d^3R \left|\chi^{(-)}_{\vec{k}_d}\left(\vec{R}\right)\right|^2 \left|\chi^{(+)}_{\vec{k}_p}\left(\alpha\vec{R}\right)\right|^2 \\ &\qquad \times \Psi_a\left(\vec{p}_-\left(\vec{R},\vec{k}_d\right) - \alpha\vec{p}_+\left(\alpha\vec{R},\vec{k}_p\right), \vec{R}\right) .\end{aligned} \tag{4.95}$$

The remaining integral must be performed numerically.

Assuming that the initial proton momentum is in the z direction, $\vec{k}_p = k_p\hat{z}$, we write the integral as

$$\begin{aligned}\left|\left\langle \vec{k}_d \left| T_d \right| \vec{k}_p \right\rangle\right|^2 &= D_0^2 \int b db\, d\phi_b\, dz \left|\chi^{(-)}_{\vec{k}_d}\left(\vec{R}\right)\right|^2 \left|\chi^{(+)}_{\vec{k}_p}\left(\alpha\vec{R}\right)\right|^2 \\ &\qquad \times \Psi_a\left(\vec{p}_-\left(\vec{R},\vec{k}_d\right) - \alpha\vec{p}_+\left(\alpha\vec{R},\vec{k}_p\right), \vec{R}\right) ,\end{aligned} \tag{4.96}$$

with

$$\vec{R} = b\cos\phi_b\,\hat{x} + b\sin\phi_b\,\hat{y} + z\,\hat{z}. \tag{4.97}$$

For a fixed transition, with

$$k_d = \left|\vec{k}_d\right| = \text{constant}\,, \tag{4.98}$$

we must calculate the scattering for all values of the direction of the deuteron momentum,

$$\hat{k}_d = \sin\theta_d\cos\phi_d\,\hat{x} + \sin\theta_d\sin\phi_d\,\hat{y} + \cos\theta_d\,\hat{z}. \tag{4.99}$$

However, the angular distribution will be azimuthally symmetric, if the potential depends only on $R = \left|\vec{R}\right|$. We will assume this to be the case. We can then calculate the angular distribution using the momentum vector $\vec{k}_d$ with $\phi_d = 0$. Equivalently, we can set the impact parameter angle $\phi_b = 0$ and integrate over the angle ϕ_d. Since the momenta $\vec{p}_\pm$ remain in the plane defined by the corresponding b and z, it is convenient to do the latter.

Taking

$$\vec{R} = b\,\hat{x} + z\,\hat{z}\,, \tag{4.100}$$

we find for the local proton momentum

$$\vec{p}_{+}\left(\vec{R},\vec{k}_{p}\right)=\hat{x}\int_{-\infty}^{z}\mathrm{Re}\frac{\partial}{\partial b}p_{p}\left(z',b\right)dz'+\hat{z}\,p_{p}\left(z,b\right) \tag{4.101}$$

with

$$p_{p}\left(z,b\right)=\sqrt{k_{p}^{2}-\frac{2m}{\hbar^{2}}V_{p}\left(z,b\right)}\,. \tag{4.102}$$

The equivalent coordinates for the deuteron with momentum in the $\hat{k}_d$ direction are

$$z_{d}=\hat{k}_{d}\cdot\vec{R}=b\sin\theta_{d}\cos\phi_{d}+z\cos\theta_{d} \tag{4.103}$$

and

$$b_{d}=\left|\vec{R}-z_{d}\,\hat{k}_{d}\right|=\sqrt{R^{2}-z_{d}^{2}}\,. \tag{4.104}$$

The deuteron scattering plane is defined by the two unit vectors, $\hat{k}_d$ and

$$\hat{b}_{d}=\left(\vec{R}-z_{d}\,\hat{k}_{d}\right)/b_{d,.} \tag{4.105}$$

Note that

$$\vec{R}=b\,\hat{x}+z\,\hat{z}=b_{d}\,\hat{b}_{d}+z_{d}\,\hat{k_{d}}\,. \tag{4.106}$$

For the local deuteron momentum, we find

$$\vec{p}_{-}\left(\vec{R},\vec{k}_{d}\right)=-\hat{b}_{d}\int_{z_{d}}^{\infty}\mathrm{Re}\frac{\partial p_{d}}{\partial b}\left(z',b_{d}\right)dz'+\hat{k}_{d}\,p_{d}\left(z_{d},b_{d}\right) \tag{4.107}$$

with

$$p_{d}\left(z_{d},b_{d}\right)=\sqrt{k_{d}^{2}-\frac{2m}{\hbar^{2}}V_{d}\left(z_{d},b_{d}\right)}\,. \tag{4.108}$$

The matrix element can now be calculated as

$$\begin{aligned}\left|\left\langle\vec{k}_{d}\left|T_{d}\right|\vec{k}_{p}\right\rangle\right|^{2}=&D_{0}^{2}\int bdb\,dz\,d\phi_{d}\left|\chi_{\vec{k}_{d}}^{(-)}\left(\vec{R}\right)\right|^{2}\left|\chi_{\vec{k}_{p}}^{(+)}\left(\alpha\vec{R}\right)\right|^{2}\\&\times\Psi_{a}\left(\vec{p}_{-}\left(\vec{R},\vec{k}_{d}\right)-\alpha\vec{p}_{+}\left(\alpha\vec{R},\vec{k}_{p}\right),\vec{R}\right)\,.\end{aligned} \tag{4.109}$$

The differential cross-section is given by

$$\begin{aligned} d\sigma &= \frac{2\pi}{\hbar v_p}\frac{d^3k_d}{(2\pi)^3}\left|\left\langle \vec{k}_d\left|T_d\right|\vec{k}_p\right\rangle\right|^2\delta\left(E_d-E_p-Q\right), \\ &= \frac{\mu_d\mu_p}{\left(2\pi\hbar^2\right)^2}\frac{k_d}{k_p}\left|\left\langle \vec{k}_d\left|T_d\right|\vec{k}_p\right\rangle\right|^2 d\Omega_d\,\delta\left(E_d-E_p-Q\right)dE_d\,, \end{aligned} \tag{4.110}$$

so that

$$\frac{d\sigma}{d\Omega_d} = \frac{\mu_d\mu_p}{\left(2\pi\hbar^2\right)^2}\frac{k_d}{k_p}\left|\left\langle \vec{k}_d\left|T_d\right|\vec{k}_p\right\rangle\right|^2 . \tag{4.111}$$

4.5 Comparison of semi-classical calculations of deuteron pickup with DWUCK

Here we compare cross-sections and angular distributions obtained with the semi-classical expressions of the preceding section with quantum mechanical calculations using the code DWUCK4.

The deuteron pickup reaction requires that a bound state neutron orbital be given. DWUCK calculates the wave function for the orbital, given the n, l and j quantum numbers of the orbital, as well as its binding energy. We use harmonic oscillator orbitals in the semi-classical calculations. Their Wigner functions can be calculated directly, using the expressions derived in the work of Martorell and Moya de Guerra (MARTORELL; Moya de Guerra, 1984).

Our calculations were developed using FORTRAN (as was DWUCK), Python and the Wolfram Language. For the cases discussed below, our code took just few minutes to run in a personal computer. Python and the Wolfram Language were used mostly to run and parse the data from the FORTRAN calculations. They were also used to improve the automation process of the numerical calculations, and to make the plots. As stated before in the subsection 3.1.2, all instances of DWUCK means DWUCK4.

We have performed calculations for two cases: (p,d) and (n,d). For (p,d), the reactions are: ^{40}Ca(p,d)^{39}Ca, ^{120}Sn(p,d)^{119}Sn, and ^{208}Pb(p,d)^{207}Pb. For (n,d), we have the following reactions: ^{40}Ca(n,d)^{39}K, ^{120}Sn(n,d)^{119}In, and ^{208}Pb(n,d)^{207}Tl. We start by looking at the (p,d) cases. In all cases, our results are denoted by Pickup (solid lines).

4.5.1 The (p,d) reaction

4.5.1.1 Ground state to ground-state cross-section

We begin our study by considering the ground state to ground-state (p,d) reaction.

In Figs. 4.1, 4.2 and 4.3, we compare the cross-section results from our code (Pickup) and DWUCK for pickup from the (1d3/2) orbital in the reaction ^{40}Ca(p,d)^{39}Ca, from the (2d3/2) orbital in the reaction ^{120}Sn(p,d)^{119}Sn to the ground-state, and from the (3p1/2) orbital in the reaction ^{208}Pb(p,d)^{207}Pb.

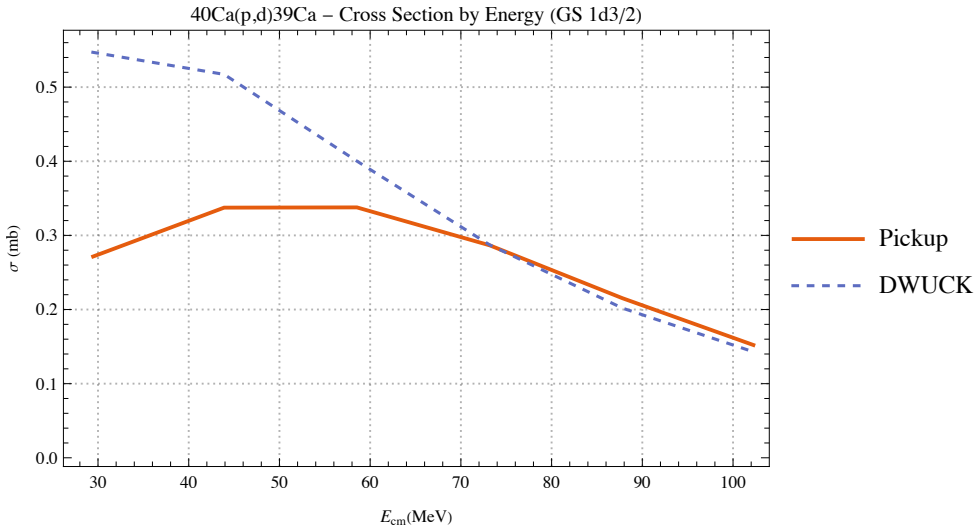

FIGURE 4.1 – Comparison of the cross-sections for the ^{40}Ca(p,d)^{39}Ca ground state to ground-state reaction as a function of proton incident energy.

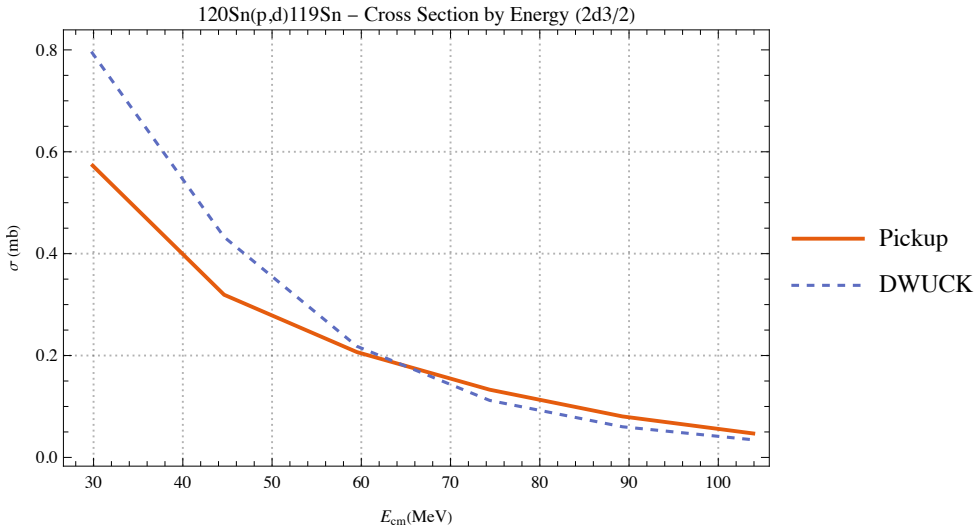

FIGURE 4.2 – Comparison of the cross-sections for the ^{120}Sn(p,d)^{119}Sn ground state to ground-state reaction as a function of proton incident energy.

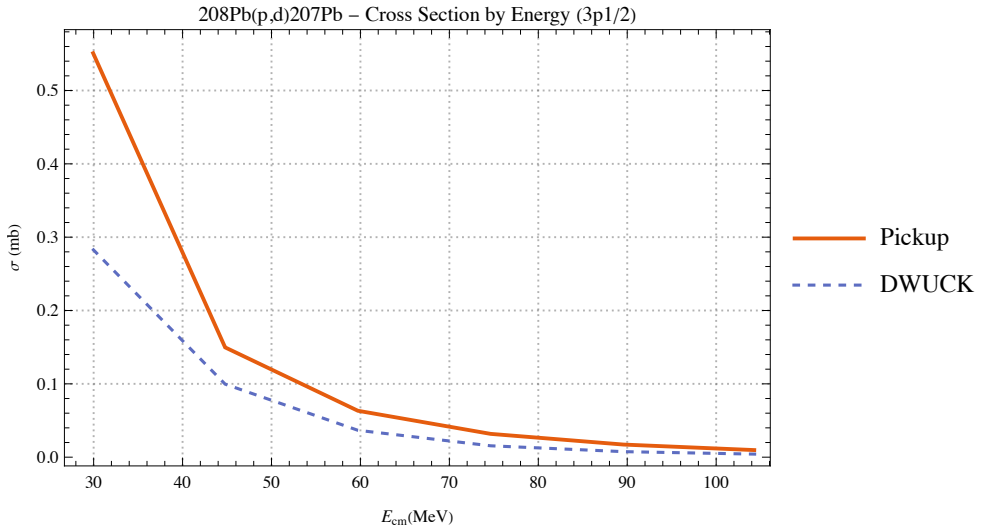

FIGURE 4.3 – Comparison of the cross-sections for the ^{208}Pb(p,d)^{207}Pb ground state to ground-state reaction as a function of proton incident energy.

One can observe that for high energies, above 60 MeV, our results are very close to the ones from DWUCK, while for lower energies, at 30 MeV for example, we have a difference of about 1/2 of the DWUCK result for the first case and about 1/4 for the second case. However, for the last case, ^{208}Pb(p,d)^{207}Pb, the largest mass, our result for 30 MeV is almost 2 times the result from DWUCK. So, as the mass of the target increases, our cross-section also increases at low energies, while the results tend to agree with DWUCK at higher energies.

To investigate the sensitivity to a variation of the level energy, we have applied a change of $\pm 10\%$ of the ground-state level energy in DWUCK and $\pm 5\%$ in Pickup. These variations are shown in Figs. 4.7, 4.8, and 4.9, for ^{40}Ca(p,d)^{39}Ca, ^{120}Sn(p,d)^{119}Sn, and ^{208}Pb(p,d)^{207}Pb, respectively. The results of the calculations are also given on Table 4.1

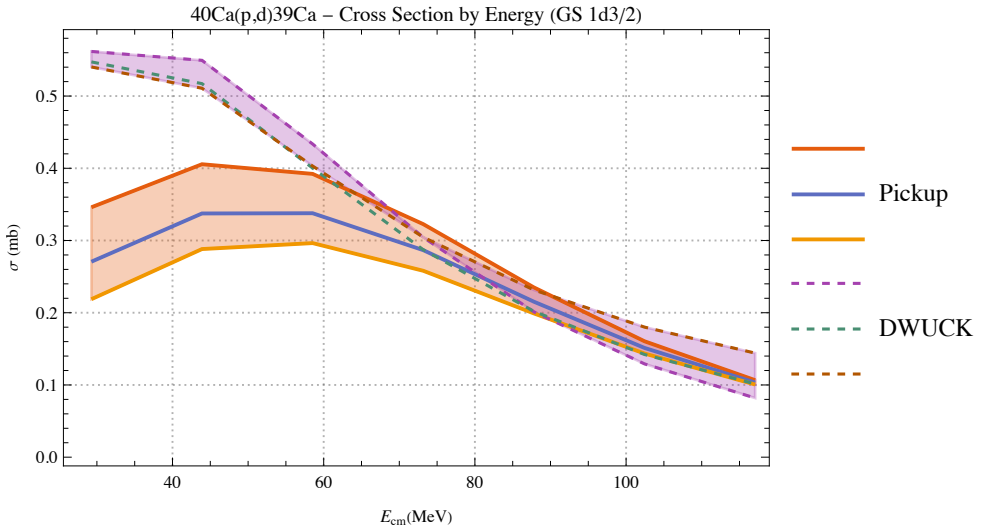

FIGURE 4.4 – Comparison of the cross-sections for the ^{40}Ca(p,d)^{39}Ca ground state to ground-state reaction as a function of proton incident energy, including sensitivity bands.

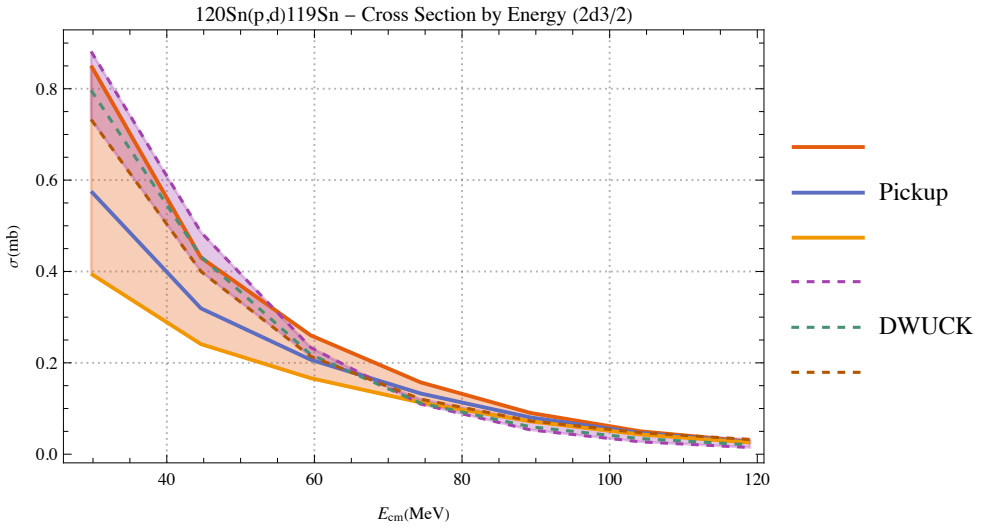

FIGURE 4.5 – Comparison of the cross-sections for the ^{120}Sn(p,d)^{119}Sn ground state to ground-state reaction as a function of proton incident energy, including sensitivity bands.

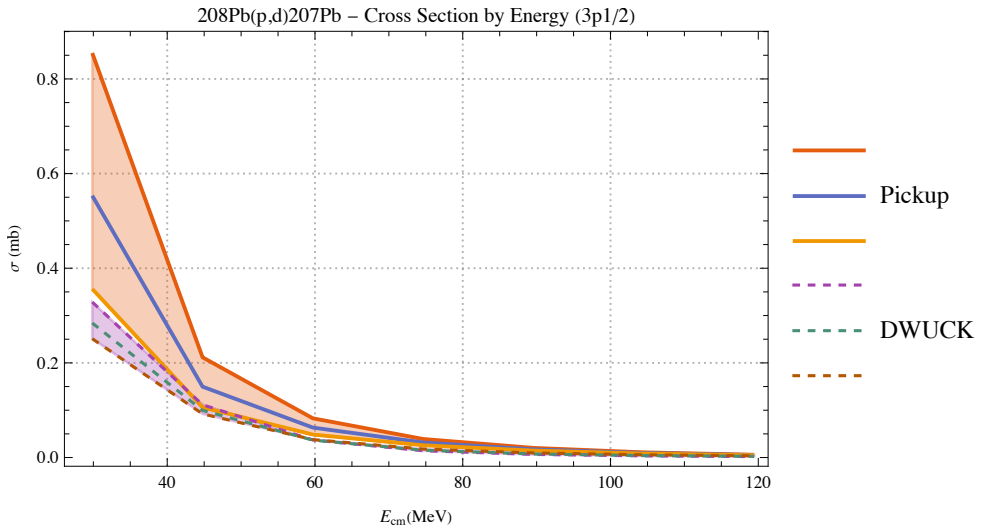

FIGURE 4.6 – Comparison of the cross-sections for the ^{208}Pb(p,d)^{207}Pb ground state to ground-state reaction as a function of proton incident energy, including sensitivity bands.

	rms radii (fm)		Cross-section (mb)			
	Pickup	DWUCK	$E_p = 30$MeV		$E_p = 120$MeV	
			Pickup	DWUCK	Pickup	DWUCK
^{40}Ca	3.5244 ± 0.0882	3.4579 ± 0.0434	0.2706 ± 0.0647	0.5473 ± 0.0114	0.1034 ± 0.0030	0.1013 ± 0.0043
^{120}Sn	5.3058 ± 0.1329	5.1235 ± 0.0598	0.5754 ± 0.2327	0.7965 ± 0.0752	0.0267 ± 0.0011	0.0205 ± 0.0012
^{208}Pb	6.3218 ± 0.1584	5.9730 ± 0.0780	0.5533 ± 0.2546	0.2842 ± 0.0391	0.0053 ± 0.0005	0.0025 ± 0.0001

TABLE 4.1 – Rms radii and cross-sections for Pickup and DWUCK with $E_p = 30$ MeV and $E_p = 120$ MeV for ^{40}Ca(p,d)^{39}Ca, ^{120}Sn(p,d)^{119}Sn, and ^{208}Pb(p,d)^{207}Pb. The values with $\pm$ represent the standard deviation of the changes due to the sensitivity analysis.

	Radii of the potentials (fm)				
	Incident nucleon		Deuteron		
	Volume	Surface	Volume		Surface
	Re/Im	Im	Re	Im	Im
^{40}Ca	4.0540	4.4056	3.8989	4.5246	4.6744
^{120}Sn	6.0259	6.0259	5.6585	6.5182	6.7130
^{208}Pb	7.3203	7.3974	6.8069	7.8191	8.0433

TABLE 4.2 – Potential radii used for (p,d) reactions: ^{40}Ca(p,d)^{39}Ca, ^{120}Sn(p,d)^{119}Sn, and ^{208}Pb(p,d)^{207}Pb, and also for (n,d) reactions: ^{40}Ca(n,d)^{39}K, ^{120}Sn(n,d)^{119}In, and ^{208}Pb(n,d)^{207}Tl.

One can see that for all cases the variation of the cross-sections from Pickup change much more than the ones from DWUCK for $E_p = 30$ MeV. We also note that the change

for $E_p = 30$ MeV increase with the increase of the target mass. For DWUCK, the deviations are relatively small but we also note that they are slightly bigger for ^{120}Sn with $E_p = 30$ MeV. We have used the following formula to calculate the standard deviation: $\sqrt{([\Sigma_{i=1,2}(x_i - x_0)^2]/2)}$, where x_0 is the value without any change. We made three calculations, one without changing the factors, and one with an increased factor and another one with a decreased factor (total of three values). Although we see that the Pickup calculation is much more sensitive than DWUCK to variations of the level energy, we do not understand the reason for this heightened sensitivity.

As we expect the (p,d) reaction to be predominantly a peripheral one, due to the absorption of the proton and deuteron in the interior region of the nucleus, we have looked for correlations between the rms radii of the neutron orbital of the pickup reaction and the resulting cross-section. We can also compare these and their variations with the radii of the potentials used in the calculations, given Table 4.2, which are the same at all energies. Note that the potentials values also apply for the (n,d) reactions that we will discuss after this subsection.

A comparison of the radii in the two tables shows that the neutron orbital involved in the pickup reactions is always well within the radii of the optical potentials. However, in each case, the orbital involved is the one with the largest rms radius and the closest to the nuclear surface. If we compare the orbital radii with the pickup cross-sections, we see some correlation between the Sn and Pb results. The rms radius of the Pb orbital in Pickup is about 10% larger than the one for DWUCK, which could explain the much larger cross-section obtained in this case. In the case of Sn, on the other hand, the rms radii of the two orbitals are similar, as are the cross-sections. The Ca results seem to contradict this line of reasoning, however, where similar radii result in very different cross-sections, at least at low energy. Here, the fact that the high energy cross-sections are quite similar could lead us to conclude that the limitations of the eikonal approximation should also be taken into account when making this comparison.

To perform a more complete analysis, this study should be extended to other levels beyond the ground-state. It will then be possible to have a better idea of the general sensitivity of the model to the other parameters. Before turning to these calculations, we analyze the ground state to ground-state angular distributions.

4.5.1.2 Angular distributions

We next compare the angular distributions from Pickup and DWUCK. We discuss the same reactions as in the previous section: the ground state to ground-state transitions for ^{40}Ca(p,d)^{39}Ca, ^{120}Sn(p,d)^{119}Sn, and ^{208}Pb(p,d)^{207}Pb.

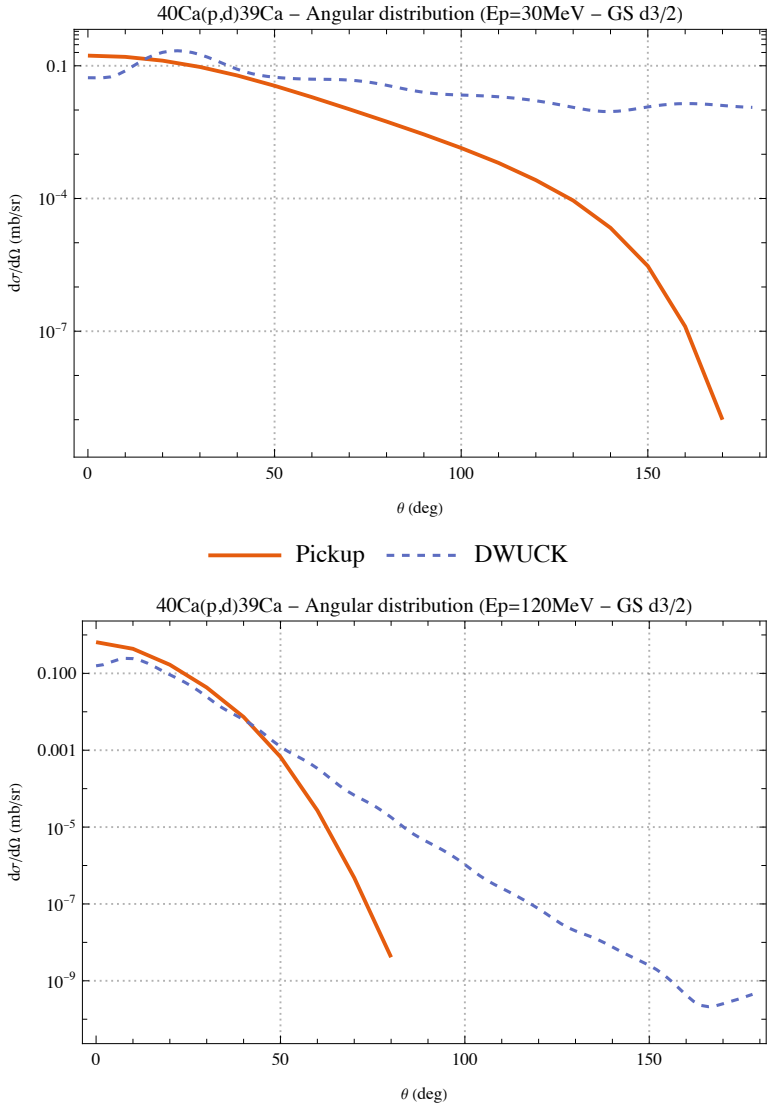

FIGURE 4.7 – Comparison of the angular distributions for the ground state to ground-state ^{40}Ca(p,d)^{39}Ca reaction with E_p equal to 30 MeV (top) and 120 MeV (bottom).

One can see that for all cases with $E_p = 30$ MeV, DWUCK gives results with an oscillatory behavior while Pickup does not. For ^{40}Ca, the results are quite good for low angles. For ^{120}Sn, both results are reasonable with the results for low angles (except for the oscillatory behavior). In the last case, ^{208}Pb, we can see almost the same pattern for the Pickup results. However, the oscillatory behavior for DWUCK is more present for this case.

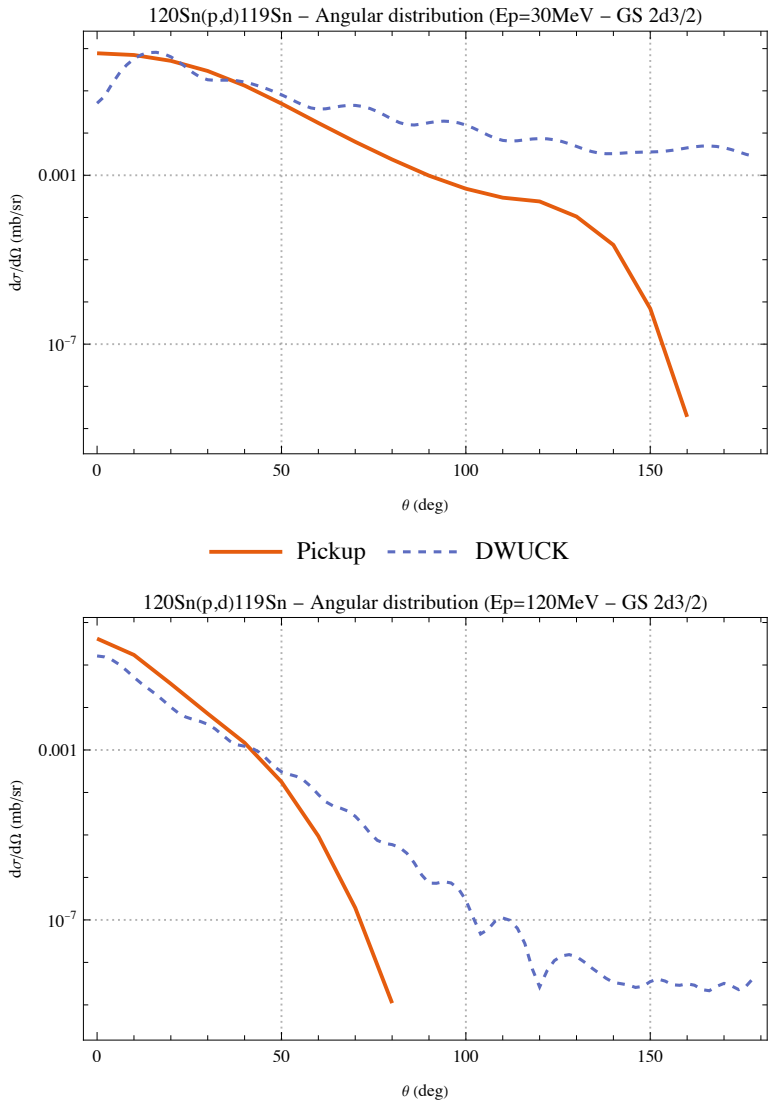

FIGURE 4.8 – Comparison of the angular distributions for the ground state to ground-state ^{120}Sn(p,d)^{119}Sn reaction with E_p equal to 30 MeV (top) and 120 MeV (bottom).

For angles greater than 120 degrees, our angular distributions tend to zero while DWUCK gives low but nonzero values. The discrepancies between the two calculations at back angles is larger at 30 MeV than at 120 MeV. This is in great part due to the eikonal approximation that we use to calculate the proton and deuteron Wigner functions. The eikonal approximation assumes straight line trajectories and systematically underestimates the angular distributions at back angles. We also note that the results for the angular distribution improve with increasing target mass.

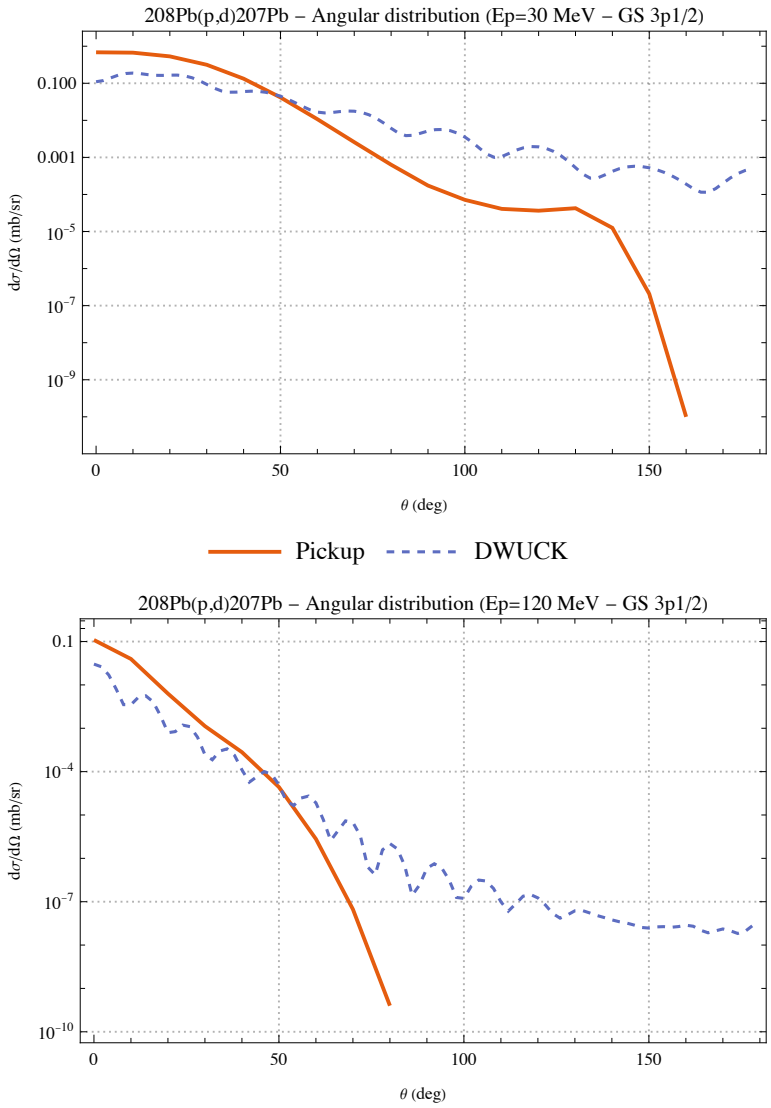

FIGURE 4.9 – Comparison of the angular distributions for the ground state to ground-state ^{208}Pb(p,d)^{207}Pb reaction with E_p equal to 30 MeV (top) and 120 MeV (bottom).

4.5.1.3 Cross-section summed over the orbitals

In order to extend our study to have a more physical idea of each reaction, we have calculated the cross-section for all orbitals for each case. For example, for the ^{40}Ca(p,d)^{39}Ca reaction, we were calculating the cross-section just for the ground-state (GS), the 1d3/2 orbit. Now, we calculate the cross-section for each orbital, starting from the 1s1/2, up to the 1d3/2 (for this case), and we sum over the values. The energy levels needed for the DWUCK calculation can be found on the Appendix E.

One can see the results for each reaction: ^{40}Ca(p,d)^{39}Ca, ^{120}Sn(p,d)^{119}Sn, and ^{208}Pb(p,d)^{207}Pb, in Figs. 4.10, 4.11, and 4.12, respectively.

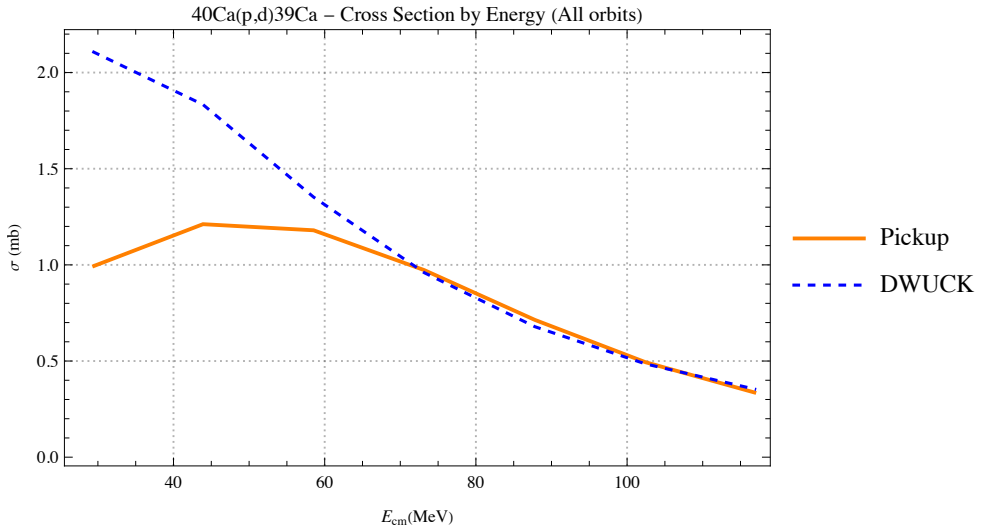

FIGURE 4.10 – Comparison of the cross-sections summed for all orbitals of the ^{40}Ca(p,d)^{39}Ca reaction as a function of the proton incident energy.

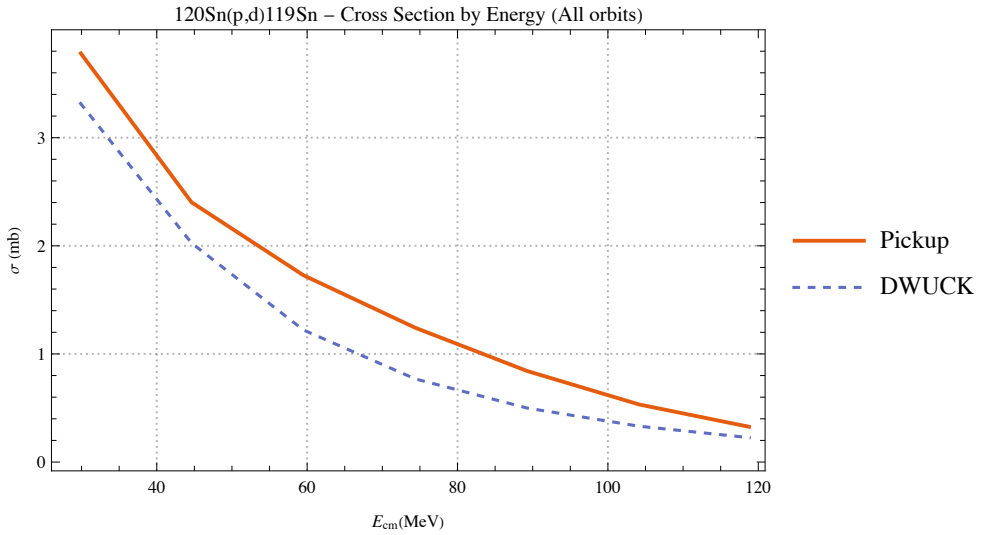

FIGURE 4.11 – Comparison of the cross-sections summed for all orbitals of the ^{120}Sn(p,d)^{119}Sn reaction as a function of the proton incident energy.

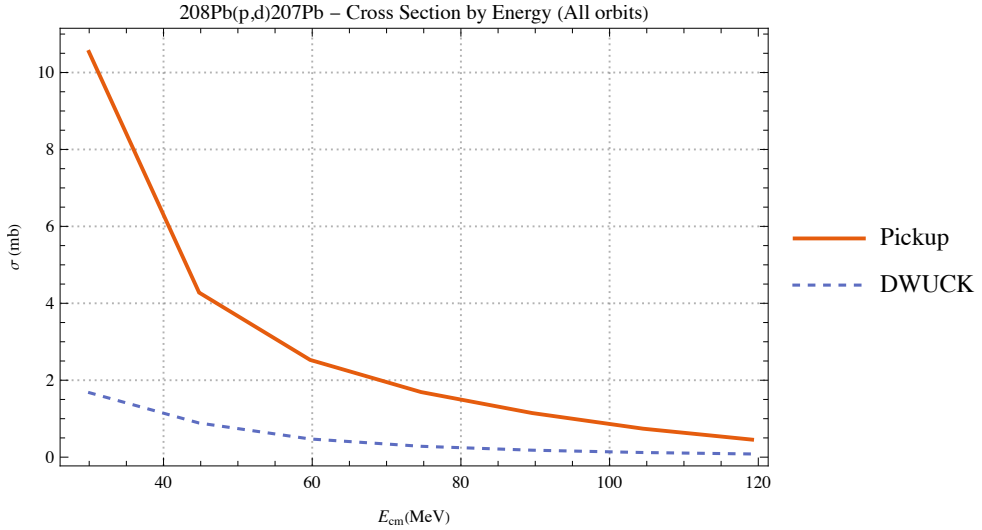

FIGURE 4.12 – Comparison of the cross-sections summed for all orbitals of the ^{208}Pb(p,d)^{207}Pb reaction as a function of the proton incident energy.

We found all results from Figs. 4.10, 4.11, and 4.12, to behave like the ones for the ground state to ground-state reaction. Nevertheless, we would like to point it out that as the target mass increased, the total cross-section for Pickup increased compared to the one for the ground state. Another point is that the results for ^{208}Pb cross-section are more discrepant than for the ground state.

A complete analysis for all orbitals should be made in order to have a deep understanding of these reactions and their differences.

4.5.1.4 Angular distributions summed over the orbitals

As we did for the cross-sections, we have extended our study to include all orbitals. One can see the results for each reaction: ^{40}Ca(p,d)^{39}Ca, ^{120}Sn(p,d)^{119}Sn, and ^{208}Pb(p,d)^{207}Pb, in Figs. 4.13, 4.14, and 4.15, respectively.

Except for ^{208}Pb, the results show good agreement for low angles (below 100 degrees). One should note that the oscillatory behavior in DWUCK has almost disappeared when we sum all the contributions from all orbitals. As for the ground state to ground-state reactions, the values for Pickup tend to zero for high angles while DWUCK has nonzero values.

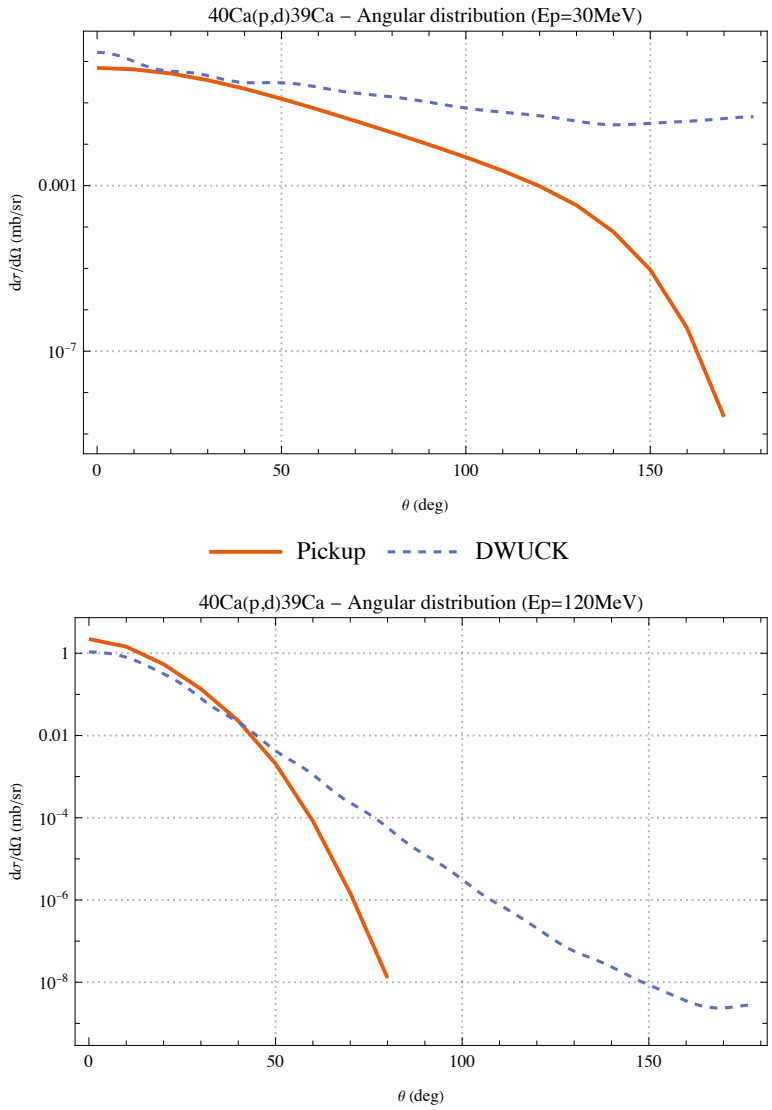

FIGURE 4.13 – Comparison of the angular distributions summed for all orbitals of the ^{40}Ca(p,d)^{39}Ca reaction with E_p equal to 30 MeV (top) and 120 MeV (bottom).

4.5.2 The (n,d) reaction

4.5.2.1 Ground state to ground-state cross-section

Now, we discuss the (n,d) cases. As we did for incident protons, we start discussing the ground state to ground-state reactions. The ground-state orbitals have changed (for ^{120}Sn and ^{208}Pb) since we are working with an incident neutron instead of a proton one. The neutron now pickups up a proton from the target. With that, we compare the cross-section results from our code (Pickup) and DWUCK for pickup from the (1d3/2) orbital in the reaction ^{40}Ca(n,d)^{39}K, from the (1g9/2) orbital in the reaction ^{120}Sn(n,d)^{119}In, and from the (3s1/2) orbital in the reaction ^{208}Pb(n,d)^{207}Tl.

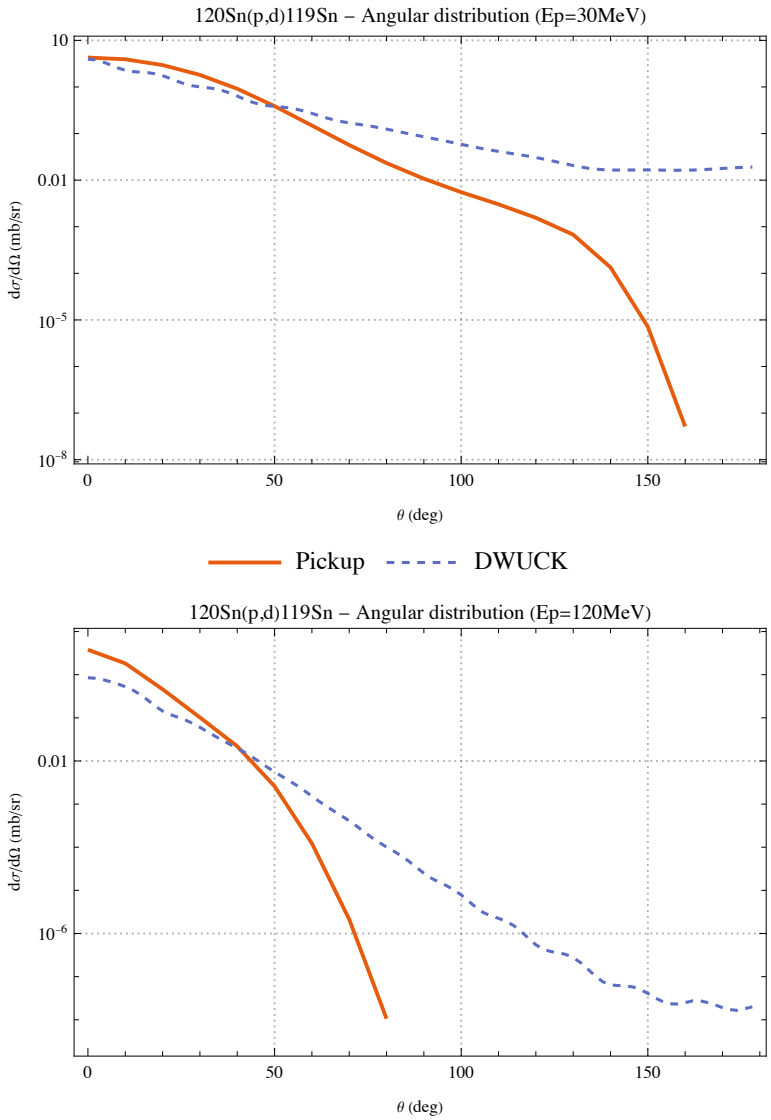

FIGURE 4.14 – Comparison of the angular distributions summed for all orbitals of the ^{120}Sn(p,d)^{119}Sn reaction with E_p equal to 30 MeV (top) and 120 MeV (bottom).

in Figs. 4.16, 4.17 and 4.18, we compiled the cross-sections and their deviations for a change of $\pm 10\%/\pm 5\%$ of the ground-state level energy in DWUCK/pickup for ^{40}Ca(n,d)^{39}K, ^{120}Sn(n,d)^{119}In, and ^{208}Pb(n,d)^{207}Tl, respectively. One can also see the data for the rms radii and for the cross-sections for $E_n = 30$ MeV and $E_n = 120$ MeV on Table 4.3.

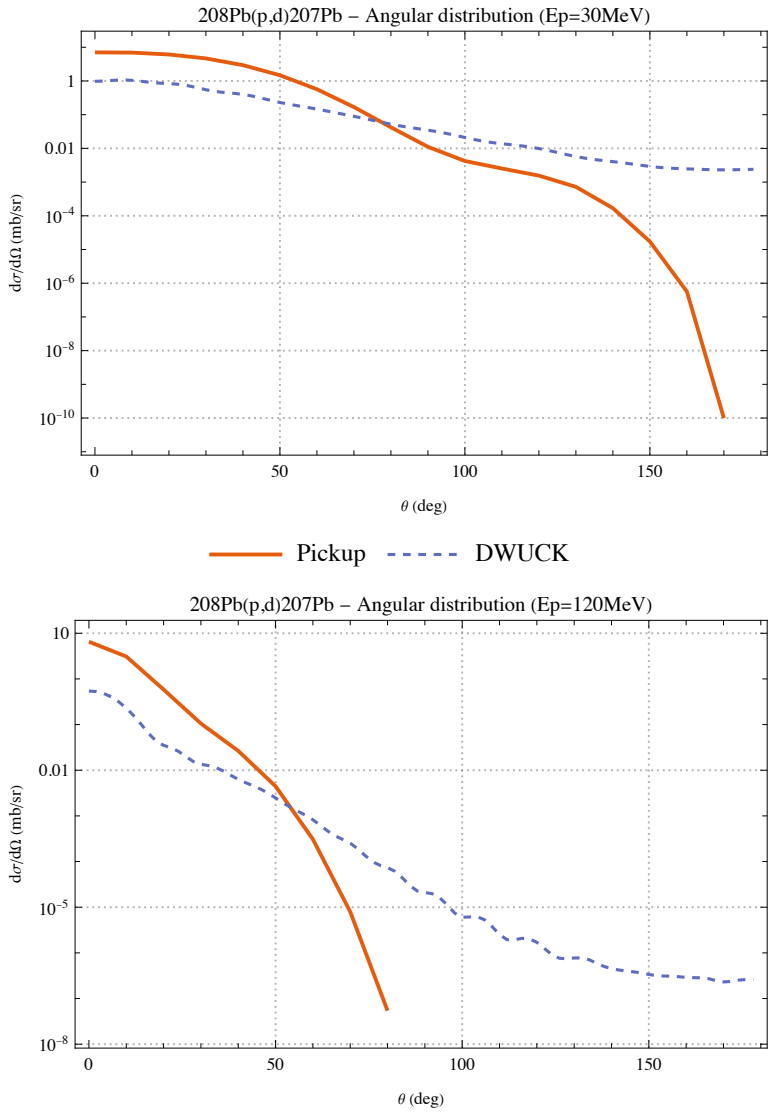

FIGURE 4.15 – Comparison of the angular distributions summed for all orbitals of the ^{208}Pb(p,d)^{207}Pb reaction with E_p equal to 30 MeV (top) and 120 MeV (bottom).

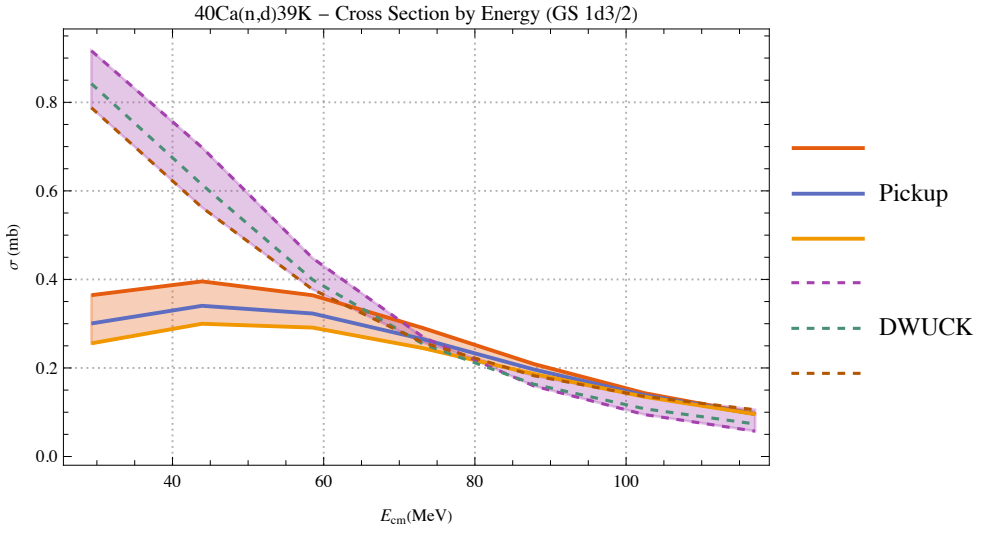

FIGURE 4.16 – Comparison of the cross-sections for the ^{40}Ca(n,d)^{39}K ground state to ground-state reaction as a function of proton incident energy, including sensitivity bands.

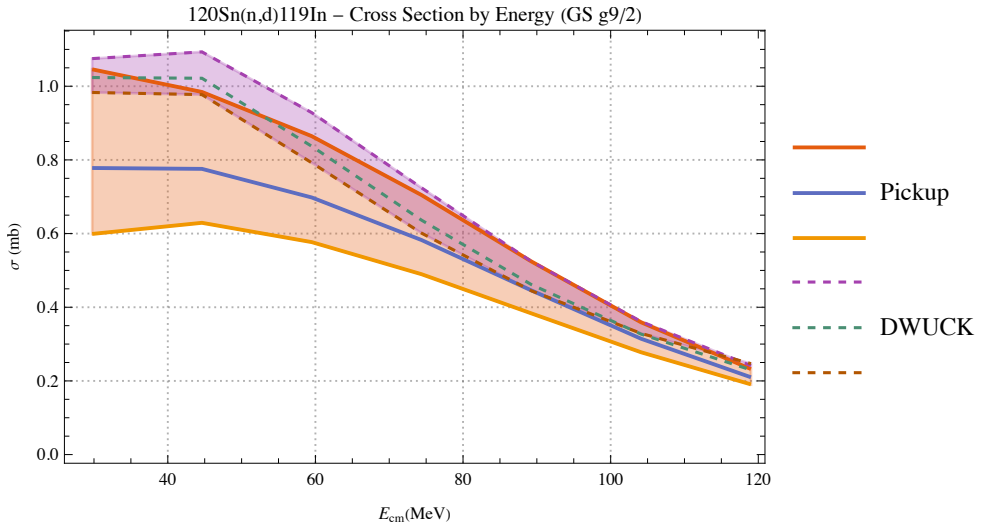

FIGURE 4.17 – Comparison of the cross-sections for the ^{120}Sn(n,d)^{119}In ground state to ground-state reaction as a function of proton incident energy, including sensitivity bands.

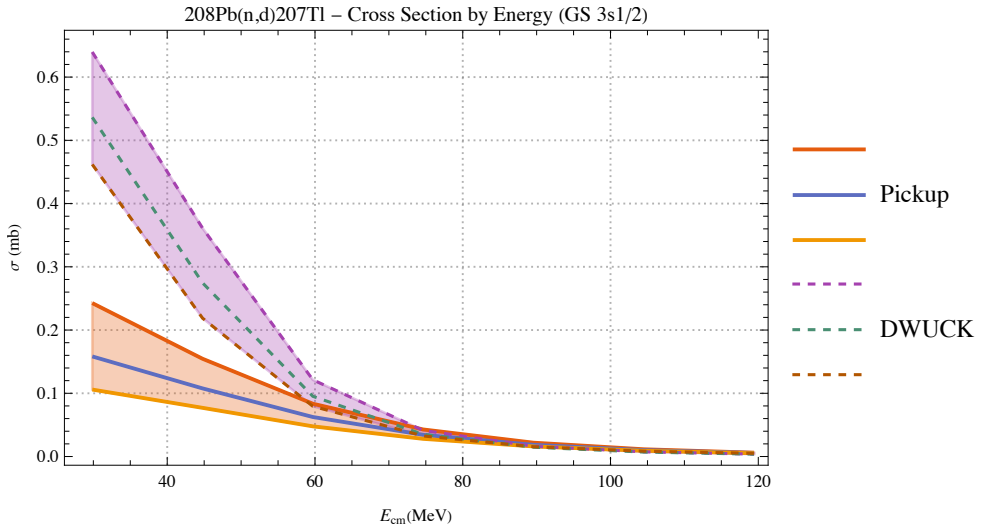

FIGURE 4.18 – Comparison of the cross-sections for the ^{208}Pb(n,d)^{207}Tl ground state to ground-state reaction as a function of proton incident energy, including sensitivity bands.

Before we discuss the Figs., one should note that for (n,d) reactions, the target loses one proton, resulting in a different element in the end of the reaction. While, for (p,d), the target loses one neutron, yielding a different isotope of the same element.

The results for all three cases of (n,d) look quite good. If we compare them with the (p,d) reactions, we see almost the same pattern for all cases. We can see that the (n,d) reactions contribute with a slightly larger cross-section than the (p,d) for the emission of deuterons in pre-equilibrium reactions.

A point to observe, while we compare (p,d) with (n,d), is that for ^{208}Pb(n,d)^{207}Tl, we

have an inversion of results (with DWUCK being larger than Pickup) for $E_{cm} = 30$ MeV. As ^{208}Pb has 82 protons and 126 neutrons, we note that for (n,d) the GS orbital (3s1/2) is than the GS orbital (3p1/2) for the (p,d) reaction.

All results tend to converge for $E_{cm} > 60$ MeV. We suspect the differences between the results and the large deviation for low energy in all reactions is related to the use of the eikonal approximation, as in the (p,d) reactions.

Looking at the the data on Table 4.3, we must observe that they are not equal to the one discussed for (p,d) reactions. First, one sees that the rms radii for Pickup are similar, except for ^{208}Pb (which is lower than the rms radius for an incident proton). For DWUCK, all values has changed. The rms radii decrease for ^{40}Ca and ^{208}Pb, and increases for ^{120}Sn. These changes are due to the differences on the potential used for each case (proton or neutron). The cross-section values were seen at the figures and have been discussed before.

	rms radii (fm)		Cross-section (mb)			
	Pickup	DWUCK	$E_n = 30$MeV		$E_n = 120$MeV	
			Pickup	DWUCK	Pickup	DWUCK
^{40}Ca	3.5244 ± 0.0883	3.7280 ± 0.0448	0.3005 ± 0.0552	0.8422 ± 0.0651	0.0958 ± 0.0004	0.0734 ± 0.0254
^{120}Sn	5.3058 ± 0.1329	5.0424 ± 0.0354	0.7780 ± 0.2278	1.0236 ± 0.0463	0.2099 ± 0.0209	0.2297 ± 0.0146
^{208}Pb	5.8152 ± 0.1457	5.7278 ± 0.0785	0.1583 ± 0.0702	0.5364 ± 0.0900	0.0056 ± 0.0004	0.0038 ± 0.0009

TABLE 4.3 – Rms radii and cross-sections for Pickup and DWUCK with $E_n = 30$ MeV and $E_n = 120$ MeV for ^{40}Ca(n,d)^{39}K, ^{120}Sn(n,d)^{119}In, and ^{208}Pb(n,d)^{207}Tl. The values with $\pm$ represent the standard deviation of the changes due to the sensitivity analysis.

4.5.2.2 Ground state to Ground-state Angular distribution

As we did for the (p,d) case, we next compare the angular distribution for (n,d) reactions. We discuss the same reactions as in the previous section: the ground state to ground-state transitions for ^{40}Ca(n,d)^{39}K, ^{120}Sn(n,d)^{119}In, and ^{208}Pb(n,d)^{207}Tl. One can observe the angular distributions for these reactions in Figs. 4.19, 4.20 and 4.21, respectively.

The (n,d) angular distributions show similar results to the (p,d) ones. The results show good agreement for back angles but they diverge for high angles. We note the high oscillatory behavior for the ^{208}Pb(n,d)^{207}Tl reaction for DWUCK.

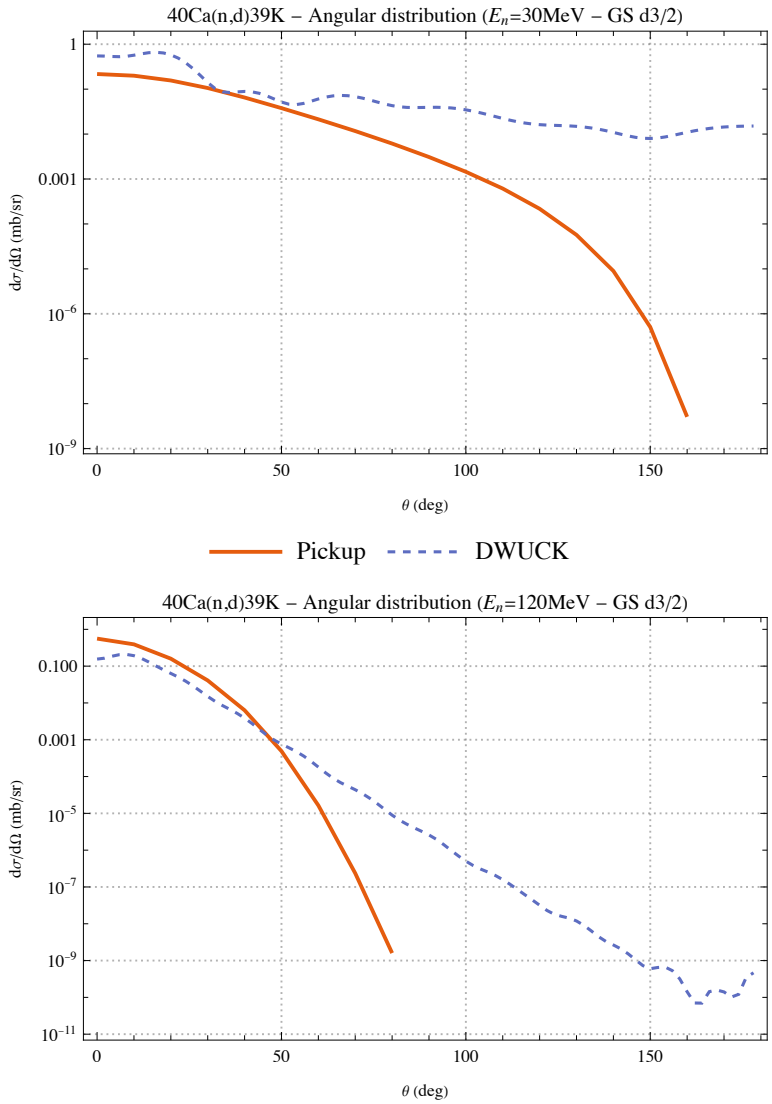

FIGURE 4.19 – Comparison of the angular distributions for the ground state to ground-state ^{40}Ca(n,d)^{39}K reaction with E_n equal to 30 MeV (top) and 120 MeV (bottom).

4.5.2.3 Cross-section summed over the orbitals

As we did before for the (p,d) case, we have also calculated the total cross-section for the (n,d) case.

One can see the results for each reaction: ^{40}Ca(n,d)^{39}K, ^{120}Sn(n,d)^{119}In, and ^{208}Pb(n,d)^{207}Tl, in Figs. 4.22, 4.23, and 4.24, respectively.

As before, for the (p,d) case, the results from Figs. 4.22, 4.23, and 4.24, behave like the ones for the ground state to ground-state reaction. Here, we highlight the differences for the total cross-section for ^{208}Pb(n,d)^{207}Tl. The Pickup-total cross-section surpassed the value from DWUCK. Even with this behavior, we can conclude that both values are

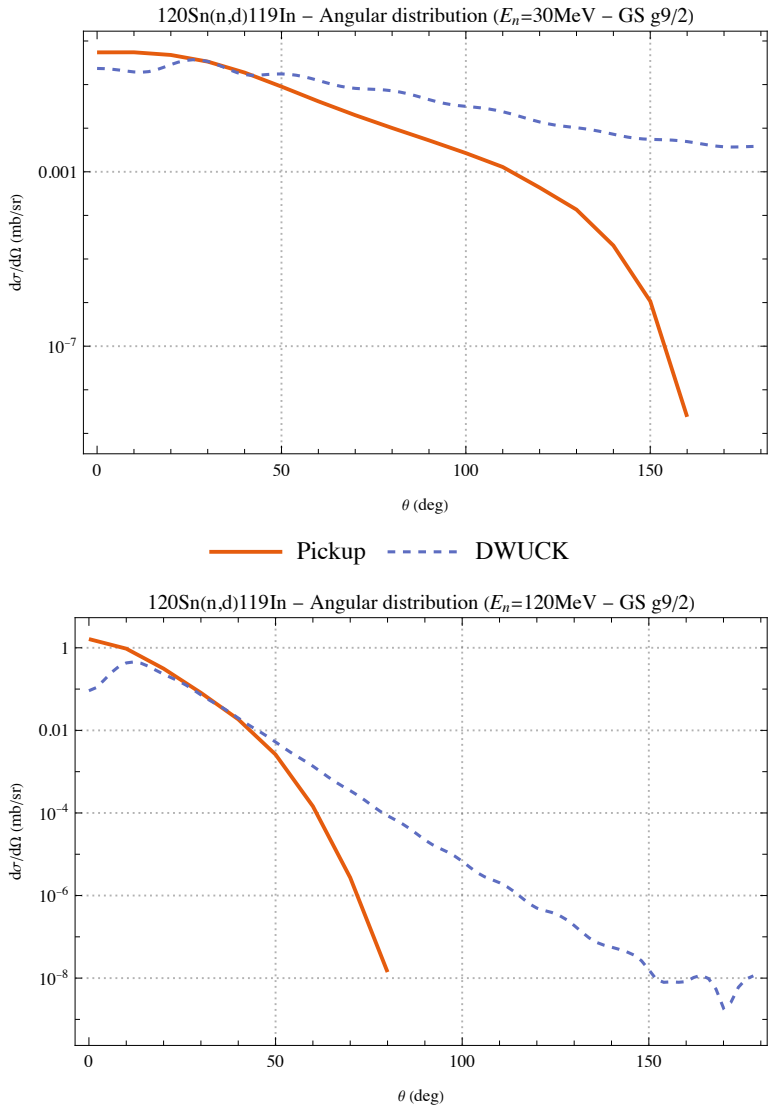

FIGURE 4.20 – Comparison of the angular distributions for the ground state to ground-state ^{120}Sn(n,d)^{119}In reaction with E_n equal to 30 MeV (top) and 120 MeV (bottom).

similar.

As stated before, a complete analysis for all orbitals should be made in order to have a deep understanding of these reactions and their differences.

4.5.2.4 Angular distribution summed over the orbitals

We have also extended our study for all orbitals of the (n,d) reactions. One can see the results for each reaction: ^{40}Ca(n,d)^{39}K, ^{120}Sn(n,d)^{119}In, and ^{208}Pb(n,d)^{207}Tl, in Figs. 4.25, 4.26, and 4.27, respectively.

All total angular distributions have good agreement between Pickup and DWUCK.

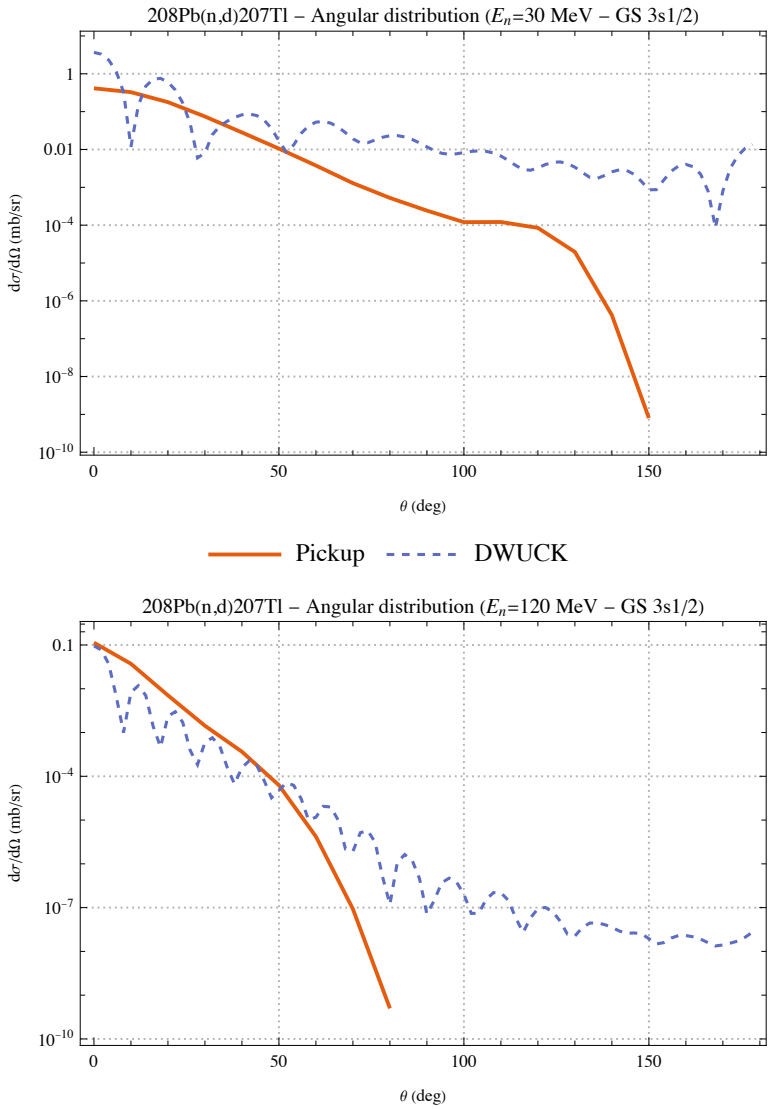

FIGURE 4.21 – Comparison of the angular distributions for the ground state to ground-state ^{208}Pb(n,d)^{207}Tl reaction with E_n equal to 30 MeV (top) and 120 MeV (bottom).

We can say that the results are even better than the ones obtained for the ground state to ground-state reactions. Except for ^{40}Ca, which the Pickup result diverges from DWUCK for angles greater than 100 degrees, the other results are similar up to 150 degrees. We also note that the oscillatory behavior for DWUCK is almost vanished for the total angular distribution. And again, as for the ground state to ground-state reactions, the values for Pickup tend to zero for high angles while DWUCK has nonzero values.

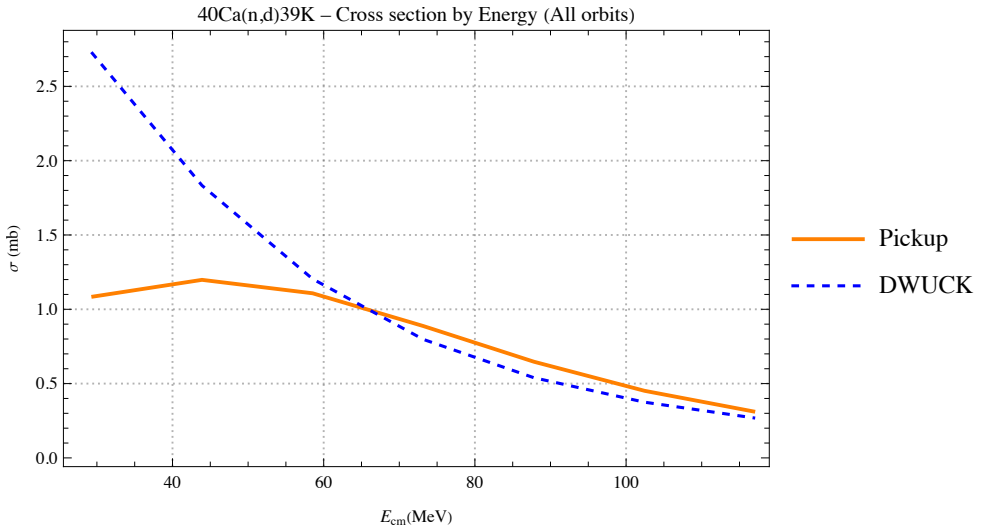

FIGURE 4.22 – Comparison of the cross-sections summed for all orbitals of the ^{40}Ca(n,d)^{39}K reaction as a function of the neutron incident energy.

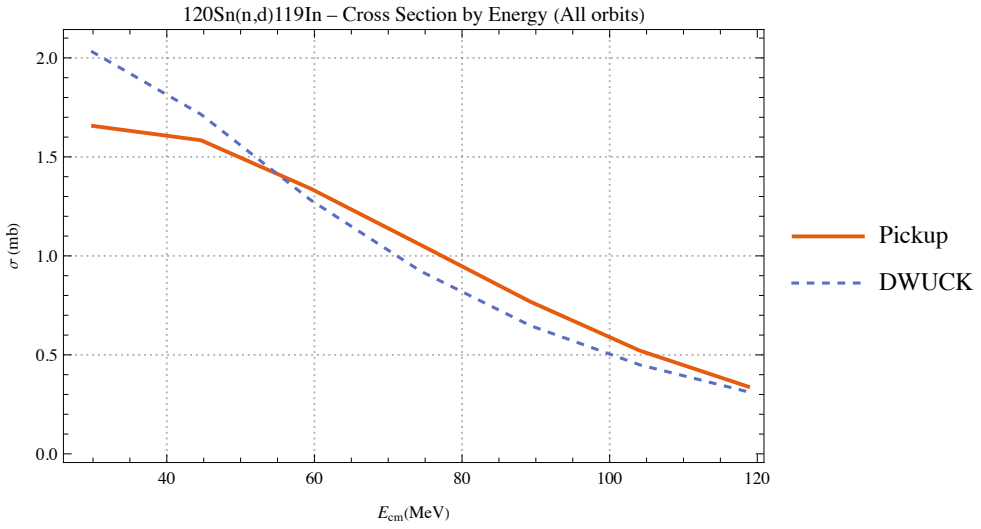

FIGURE 4.23 – Comparison of the cross-sections summed for all orbitals of the ^{120}Sn(n,d)^{119}In reaction as a function of the neutron incident energy.

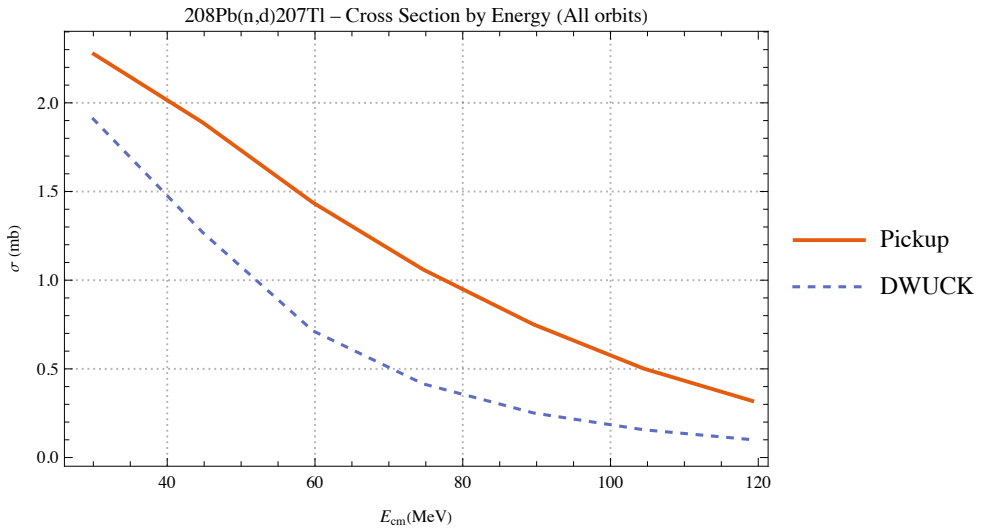

FIGURE 4.24 – Comparison of the cross-sections summed for all orbitals of the ^{208}Pb(n,d)^{207}Tl reaction as a function of the neutron incident energy.

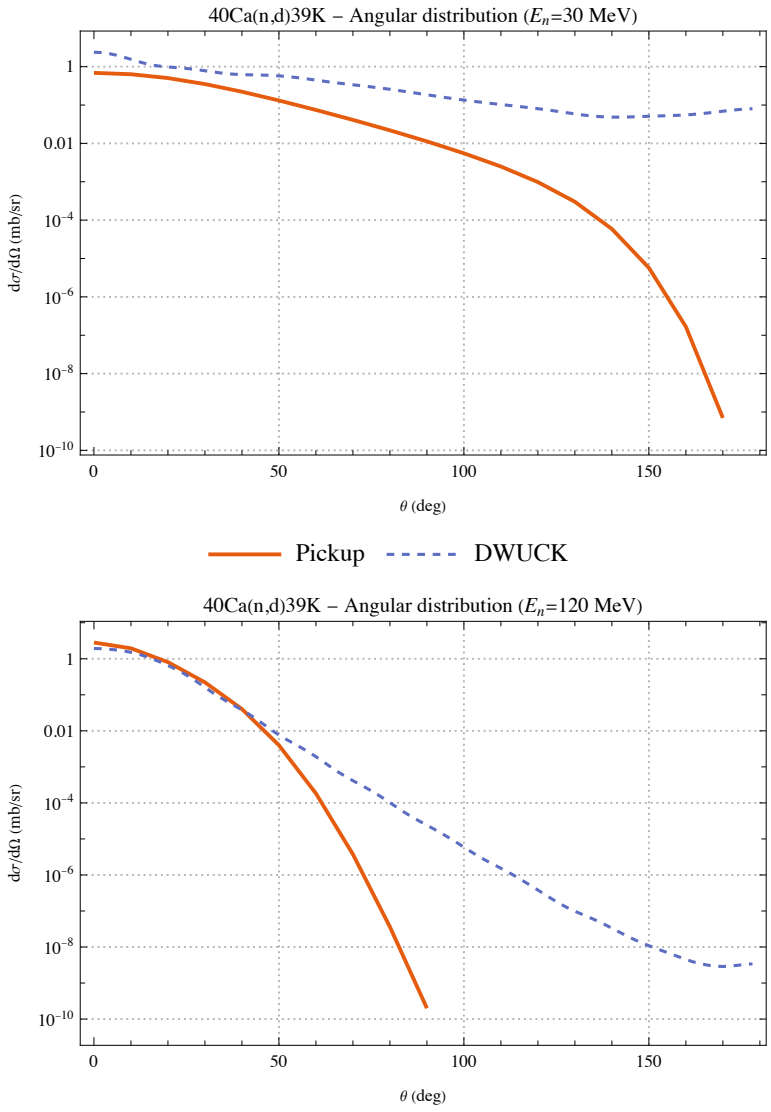

FIGURE 4.25 – Comparison of the angular distributions summed for all orbitals of the ^{40}Ca(n,d)^{39}K reaction with E_n equal to 30 MeV (top) and 120 MeV (bottom).

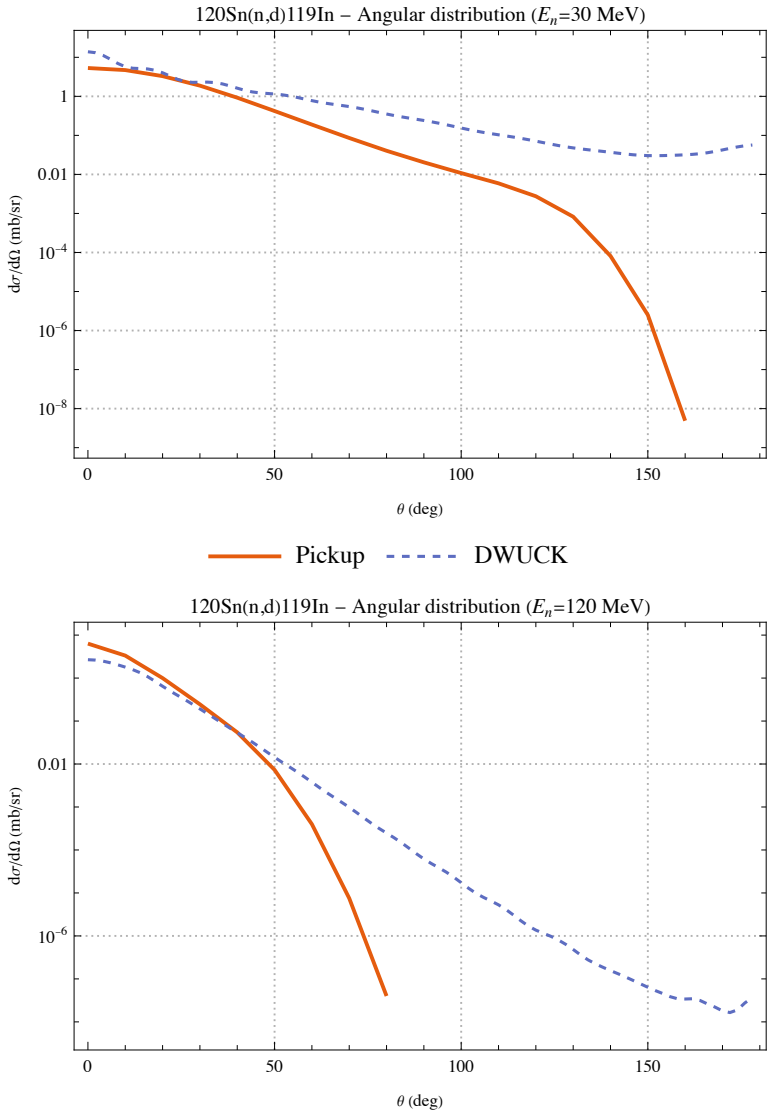

FIGURE 4.26 – Comparison of the angular distributions summed for all orbitals of the ^{120}Sn(n,d)^{119}In reaction with E_n equal to 30 MeV (top) and 120 MeV (bottom).

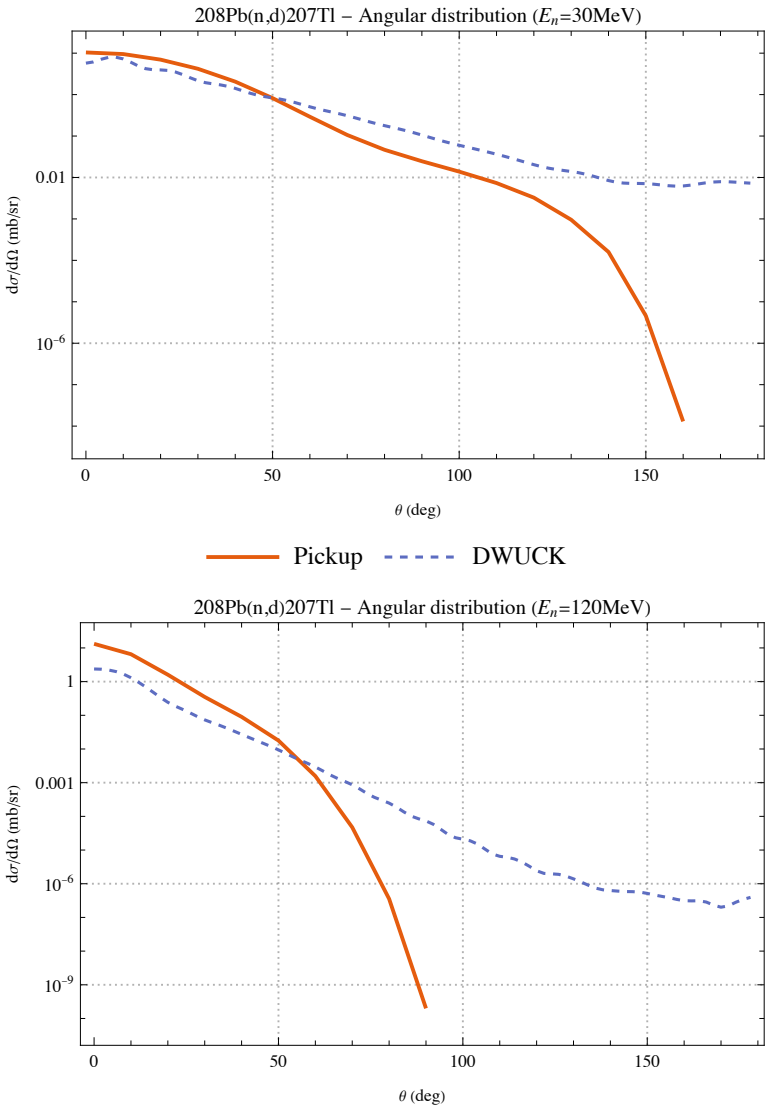

FIGURE 4.27 – Comparison of the angular distributions summed for all orbitals of the ^{208}Pb(n,d)^{207}Tl reaction with E_n equal to 30 MeV (top) and 120 MeV (bottom).

5 Conclusions

EMPIRE, (HERMAN *et al.*, 2007), is a well-known software used for theoretical investigations of nuclear reactions and for nuclear data evaluation. EMPIRE is constituted of several modules, two of which are the PCROSS module (based on the exciton model), and the DDHMS module (based on the Hybrid-Monte Carlo model). As already discussed in this work, both models are used for pre-equilibrium nuclear reactions.

The unified model of Iwamoto and Harada is implemented in PCROSS, which has been discussed extensively in this work. The unified model in the PCROSS module is used for cluster emission. On the other hand, in the DDHMS, the Hybrid-Monte Carlo model (HMS) furnishes a more precise approach to pre-equilibrium nuclear emission. In numerical calculations, the "HMS and PCROSS mutually exclude each other", (HERMAN *et al.*, 2007). To avoid errors while combining models, EMPIRE applies some priorities. In the case of pre-equilibrium, EMPIRE uses the HMS and suppresses the PCROSS results for particle emission, when it is used.

Apart from this, the HMS also has a limitation of calculating nucleon emission only. Due to this limitation, we started this work in (TEIXEIRA, 2018) to extend the HMS to calculate emission of composite particles, such as deuteron, tritium, and alpha particles.

The unified model, (IWAMOTO; HARADA, 1982), is already included in PCROSS. As stated, the DDHMS has priority over the results from PCROSS. In consideration of that, our intention is to combine the unified model ideas with those of the HMS. By combining these models, the HMS would be extended to include composite particle emissions. This extension is seen as an improvement in EMPIRE's features because one would be able to obtain a more physically-motivated description of pre-equilibrium nuclear reactions.

We started our research by studying the unified model. In (TEIXEIRA, 2018), we

concluded that more investigation is needed to understand the deuteron emission mechanisms. Broeders and Konobeyev, (BROEDERS; KONOBEYEV, 2005), had already discussed these different mechanisms and concluded that each of them contribute to the formation factor of the composite particle. As a result of that, we started to investigate the pickup reaction mechanism for deuterons.

As discussed earlier, we started with the unified model, and then used DWUCK calculations to compare them with our previous results. We also tried an eikonal approximation to improve the unified model. DWUCK was used in most of the steps of our investigations as it is a well-known software for differential cross-section calculations. It gave us important information while we were trying to obtain the angular distribution from the unified model.

Continuing our research, further investigations for the unified model phase space were needed. These investigations of the phase space are important for understanding the semi-classical limitations and restrictions of the unified model.

With the semi-classical distorted-wave model described in this work, we believe that we now have a theoretical basis that will permit the development of a more precise Monte Carlo model of nucleon and deuteron emission. We also hope this model can provide the framework for other composite particle production.

We have developed and discussed the calculations for the pickup mechanism for deuteron production from an incident proton and also from an incident neutron. Although we have not compared our data with experimental values, we have run the cross-section and angular distribution calculations using our code (Pickup) and compared with reference calculations from DWUCK4 for three different reactions for (p,d): ^{40}Ca(p,d)^{39}Ca, ^{120}Sn(p,d)^{119}Sn, and ^{208}Pb(p,d)^{207}Pb, and three different reactions for (n,d): ^{40}Ca(n,d)^{39}K, ^{120}Sn(n,d)^{119}In, and ^{208}Pb(n,d)^{207}Ti. We also compared the sensitivity of the cross-sections to a variation in the level energy for all cases.

We conclude from these calculations that our results are promising. For the (p,d) reactions, the cross-section results for Pickup increase compared to the reference calculations of DWUCK as the target mass increased for low energies. The results for DWUCK increase for ^{120}Sn but decrease considerably for ^{208}Pb, if one compare them with the results for ^{40}Ca. As for the (n,d) reactions, the Pickup results were lower than the results from

DWUCK for low energies. All results are promising, to the extent that they have quite similar behavior. For all cases in both (p,d) and (n,d) reactions, the results were quite similar for high energies.

We have also discussed the sensitivity to a variation of the level energy, and we concluded that these variations were more effective in Pickup than DWUCK for (p,d). For (n,d), we observe that both Pickup and DWUCK furnish similar variations except for the ^{120}Sn(n,d)^{119}In case. However, we still do not understand this sensitivity of the Pickup results.

By comparing the potential radii used for all reactions, we could conclude that the neutron orbital involved in the pickup reactions is always well within the radii of the optical potentials, as it should be. The comparisons show that the radii used could explain the results obtained for each reaction, if we have into account the limitations of the eikonal approximation. It is important to note that more studies should be done to get a broader idea of the general sensitivity of the model.

For the angular distribution, we have also made a comparison for the reactions discussed. DWUCK gives an oscillatory behavior for all cases at $E = 30$ MeV. For $E_n = 120$, the Pb case for the (n,d) reaction also oscillates (with a high frequency). However, the oscillatory behavior almost disappear for the total angular distributions. For all cases studied, the results were in good agreement for low angles. For angles greater than 120 degrees, our results tend to zero while DWUCK gave low but nonzero values. We also note that the eikonal approximation used to calculate the proton and deuteron Wigner functions can cause discrepancies in the angular distribution at low angles for low energies. But, one should note that more reactions need to be studied in order to confirm this conclusion.

Finally, we should say that this work was more difficult than expected. We had many results that were not promising, and we tried many different ways to reach our goal. It is clear that the physics involved in the process was the biggest challenge, but we can say we had promising results in the end. Even though the Monte Carlo part of this work is discussed, there was not enough time to develop this. We leave it to future research.

To conclude, we note that a substantial part of this work was performed during the pandemic of 2020–2021.

Bibliography

BERTRAND, F. E.; PEELLE, R. W. Complete hydrogen and helium particle spectra from 30- to 60-mev proton bombardment of nuclei with $a = 12$to209 and comparison with the intranuclear cascade model. **Phys. Rev. C**, American Physical Society, v. 8, p. 1045–1064, Sep 1973. Available from Internet: <https://link.aps.org/doi/10.1103/PhysRevC.8.1045>.

BERTULANI, C.; CAMPBELL, C.; GLASMACHER, T. A computer program for nuclear scattering at intermediate and high energies. **Computer Physics Communications**, v. 152, n. 3, p. 317 – 340, 2003. ISSN 0010-4655. Available from Internet: <http://www.sciencedirect.com/science/article/pii-/S001046550200824X>http://www.sciencedirect.com/science/article/pii/S001046550200824X.

BISPLINGHOFF, J. Configuration mixing in preequilibrium reactions: A new look at the hybrid-exciton controversy. **Phys. Rev. C**, American Physical Society, v. 33, p. 1569–1580, May 1986. Available from Internet: <https://link.aps.org/doi/10.1103/PhysRevC.33.1569>.

BLANN, M. Hybrid model for pre-equilibrium decay in nuclear reactions. **Phys. Rev. Lett.**, American Physical Society, v. 27, p. 337–340, Aug 1971. Available from Internet: <https://link.aps.org/doi/10.1103/PhysRevLett.27.337>.

BLANN, M. New precompound decay model. **Phys. Rev. C**, American Physical Society, v. 54, p. 1341–1349, Sep 1996. Available from Internet: <https://link.aps.org/doi/10.1103/PhysRevC.54.1341>.

BLANN, M.; CHADWICK, M. B. New precompound decay model: Angular distributions. **Phys. Rev. C**, American Physical Society, v. 57, p. 233–243, Jan 1998. Available from Internet: <https://link.aps.org/doi/10.1103/PhysRevC.57.233>.

BLANN, M.; VONACH, H. K. Global test of modified precompound decay models. **Phys. Rev. C**, American Physical Society, v. 28, p. 1475–1492, Oct 1983. Available from Internet: <https://link.aps.org/doi/10.1103/PhysRevC.28.1475>.

BROEDERS, C. H. M.; KONOBEYEV, A. Y. Phenomenological model for non-equilibrium deuteron emission in nucleon induced reactions. **Kerntechnik**, Hanser Verlag, v. 70, n. 5-6, p. 260–269, Nov 2005. ISSN 0932-3902. Available from Internet: <https://doi.org/10.3139/124.100254>.

BUTLER, S. T.; PEARSON, C. A. Deuterons from high-energy proton bombardment of matter. **Phys. Rev.**, American Physical Society, v. 129, p. 836–842, Jan 1963. Available from Internet: <https://link.aps.org/doi/10.1103/PhysRev.129.836>.

CARLSON, B. V.; ESCHER, J. E.; HUSSEIN, M. S. Theoretical descriptions of compound-nuclear reactions: open problems and challenges. **Journal of Physics G: Nuclear and Particle Physics**, IOP Publishing, v. 41, n. 9, p. 094003, jul 2014. Available from Internet: <https://doi.org/10.1088/0954-3899/41/9/094003>.

CLINE, C.; BLANN, M. The pre-equilibrium statistical model: Description of the nuclear equilibration process and parameterization of the model. **Nuclear Physics A**, v. 172, n. 2, p. 225 – 259, 1971. ISSN 0375-9474. Available from Internet: <http://www.sciencedirect.com/science/article/pii-/0375947471907135>http://www.sciencedirect.com/science/article/pii/0375947471907135.

GOLDBERGER, M.; WATSON, K.; WATSON, K. **Collision Theory**. Wiley, 1964. (Structure of matter series). ISBN 9780882753133. Available from Internet: <https://books.google.com.br/books?id=MR5RAAAAMAAJ>.

GRIFFIN, J. J. Statistical model of intermediate structure. **Phys. Rev. Lett.**, American Physical Society, v. 17, p. 478–481, Aug 1966. Available from Internet: <https://link.aps.org/doi/10.1103/PhysRevLett.17.478>.

HERMAN, M.; CAPOTE, R.; CARLSON, B. V.; OBLOŽINSKÝ, P.; SIN, M.; TRKOV, A.; WIENKE, H.; ZERKIN, V. EMPIRE: Nuclear Reaction Model Code System for Data Evaluation. **Nuclear Data Sheets**, v. 108, p. 2655–2715, dez. 2007.

IWAMOTO, A.; HARADA, K. Mechanism of cluster emission in nucleon-induced preequilibrium reactions. **Phys. Rev. C**, American Physical Society, v. 26, p. 1821–1834, Nov 1982. Available from Internet: <https://link.aps.org/doi/10.1103/PhysRevC.26.1821>.

KONING, A.; AKKERMANS, J.; GANDINI, A. Pre-equilibrium nuclear reactions: An introduction to classical and quantum-mechanical models. **Proceedings of the workshop on nuclear reaction data and nuclear reactors: Physics, design and safety**, World Scientific Publishing, p. 143–158, 1999. Available from Internet: <https://inis.iaea.org/search/search.aspx?orig_q=RN:31024058>.

KONING, A.; DUIJVESTIJN, M. A global pre-equilibrium analysis from 7 to 200 mev based on the optical model potential. **Nuclear Physics A**, v. 744, n. Supplement C, p. 15 – 76, 2004. ISSN 0375-9474. Available from Internet: <http://www.sciencedirect.com/science/article/pii-/S037594740400870X>http://www.sciencedirect.com/science/article/pii/S037594740400870X.

KONOBOEYEV, A. Y.; KOROVIN, Y. A. Calculation of deuteron spectra for nucleon induced reactions on the basis of the hybrid exciton model taking into account direct processes. **Kerntechnik**, v. 61, p. 45–49, 1996.

KUNZ, P. D.; ROST, E. The distorted-wave born approximation. In: _____. **Computational Nuclear Physics 2: Nuclear Reactions**. New York, NY: Springer New York, 1993. p. 88–107. ISBN 978-1-4613-9335-1. Available from Internet: <https://doi.org/10.1007/978-1-4613-9335-1_5>.

LUO, Y. L.; KAWAI, M. Semiclassical distorted wave model of nucleon inelastic scattering to continuum. **Phys. Rev. C**, American Physical Society, v. 43, p. 2367–2376, May 1991. Available from Internet: <https://link.aps.org/doi/10.1103/PhysRevC.43.2367>.

MARTORELL, J.; Moya de Guerra, E. Mean field approximation to the wigner distribution function of atomic nuclei. **Annals of Physics**, v. 158, n. 1, p. 1–30, 1984. ISSN 0003-4916. Available from Internet: <https://www.sciencedirect.com/science/article/pii/0003491684902379>.

MATOBA, M.; IWAMOTO, O.; UOZUMI, Y.; SAKAE, T.; KOORI, N.; FUJIKI, T.; OHGAKI, H.; IJIRI, H.; MAKI, T.; NAKANO, M. ^{40}Ca(p,d)^{39}ca reaction at 65 mev. **Phys. Rev. C**, American Physical Society, v. 48, p. 95–104, Jul 1993. Available from Internet: <https://link.aps.org/doi/10.1103/PhysRevC.48.95>.

NAGLE, J. L.; KUMAR, B. S.; KUSNEZOV, D.; SORGE, H.; MATTIELLO, R. Coalescence of deuterons in relativistic heavy ion collisions. **Phys. Rev. C**, American Physical Society, v. 53, p. 367–376, Jan 1996. Available from Internet: <https://link.aps.org/doi/10.1103/PhysRevC.53.367>.

SATCHLER, G. **Introduction to nuclear reactions 2 ed.** [S.l.]: United Kingdom: Macmillan Education Ltd., 1990.

SATO, K.; IWAMOTO, A.; HARADA, K. Pre-equilibrium emission of light composite particles in the framework of the exciton model. **Phys. Rev. C**, American Physical Society, v. 28, p. 1527–1537, Oct 1983. Available from Internet: <https://link.aps.org/doi/10.1103/PhysRevC.28.1527>.

SCHWARZSCHILD, A.; ZUPANCIC, C. Production of tritons, deuterons, nucleons, and mesons by 30-gev protons on a1, be, and fe targets. **Phys. Rev.**, American Physical Society, v. 129, p. 854–862, Jan 1963. Available from Internet: <https://link.aps.org/doi/10.1103/PhysRev.129.854>.

TEIXEIRA, E. A. **Modelo Monte Carlo para emissão de dêuterons em reações nucleares de pré-equilíbrio**. 93 p. Dissertation (Master) — Instituto Tecnológico de Aeronáutica - ITA, 2018. Available from Internet: <http://www.bdita.bibl.ita.br/tesesdigitais/lista_resumo-.php?num_tese=74158>http://www.bdita.bibl.ita.br/tesesdigitais/lista$_r esumo.php?num_t ese$ = 74158.

TEIXEIRA, E. A.; CARLSON, B. V. A monte carlo model of deuteron emission in pre-equilibrium nuclear reactions. **Journal of Physics: Conference Series**, IOP Publishing, v. 1291, p. 012036, jul 2019. Available from Internet: <https://doi.org/10.1088\%2F1742-6596\%2F1291\%2F1\%2F012036>.

WEILI, S.; WATANABE, Y.; KOHNO, M.; OGATA, K.; KAWAI, M. Semiclassical distorted wave model with wigner transform of one-body density matrix. **Phys. Rev. C**, American Physical Society, v. 60, p. 064605, Nov 1999. Available from Internet: <https://link.aps.org/doi/10.1103/PhysRevC.60.064605>.

Appendix A - Papers

We present a proceedings paper published in 2019, (TEIXEIRA; CARLSON, 2019), for your appreciation. The studies included in this paper were presented at the XLI Brazilian Meeting on Nuclear Physics, in Campos do Jordão, São Paulo, Brazil, in 2018.

We began the paper by introducing pre-equilibrium reactions, their importance, the exciton model, the HMS model, and the Iwamoto and Harada model. The second topic briefly describes the Iwamoto and Harada unified model. In the third topic, we give a brief description of our attempt to use an eikonal approximation with DWBA in order to have a better representation of the Iwamoto and Harada phase space. In the fourth topic, we discuss our preliminary results at that time, mentioning that we were using DWUCK4 code to analyze the differential cross section and comparing it with experimental data. In the final topic, we concluded that our results were yet not satisfactory and that we needed to investigate further to improve the unified model.

The proceedings paper follows on the next page.

IOP Conf. Series: Journal of Physics: Conf. Series **1291** (2019) 012036 doi:10.1088/1742-6596/1291/1/012036

A Monte Carlo model of deuteron emission in pre-equilibrium nuclear reactions

E A Teixeira and B V Carlson

Dep. de Física, Instituto Tecnológico de Aeronáutica, São José dos Campos, SP, Brazil

E-mail: estevao@ita.br

Abstract. Nucleon-induced pre-equilibrium reactions are important in many applications of nuclear physics. About 20% of the particles emitted in such reactions are composites, such as deuterons and alpha particles. Deuterons are produced through emission from the compound nucleus, as well as through two important direct reaction mechanisms - "pick-up" and coalescence. Iwamoto and Harada developed a semi-classical pre-equilibrium model that describes both direct mechanisms as a generalization of coalescence. We have implemented the Iwamato and Harada unified model of deuteron emission in Blann and Chadwick's hybrid Monte Carlo model. This implementation was made in order to analyse data of reactions of the type (p,d), that is, proton induced reactions having deuterons as emitted particles, but our previous results were not satisfactory. In order to find a new approach for the deuteron emission, we are investigating an eikonal approximation to the phase space of Iwamoto and Harada model. We are also comparing our angular distributions with the experimental ones using DWUCK4. Nevertheless, our results are not satisfactory yet and our work is under development.

1. Introduction

Nucleon-induced pre-equilibrium reactions are important in the description and modeling of fast reactors, accelerator-driven systems (ADS) and radiotherapy with particle beams. The exciton model of pre-equilibrium reactions assumes the excitation of a chain of particle-hole states of the pre-compound nucleus that results from the fusion of the incident particle with the target (two particles and one hole, three particles and two holes, etc.) [1]. To estimate emission from the stage of n+1 particles and n holes, it assumes that each state of this kind is equally probable. However, Bisplinghoff demonstrated that in general this hypothesis is satisfied only for the initial configuration of two particles and one hole states [2].

With the goal of defining a pre-equilibrium reactions model without this defect, Blann developed a model called the "hybrid Monte Carlo" model (HMS), which takes into account the chain of particles and holes states of the exciton model through independent excitations of two particles and one hole [3, 4]. A detailed comparison between both models shows that while the exciton model assumes that the interaction between the configuration of n+1 particle and n hole states is so strong that these reach equilibrium before making another transition, the "hybrid Monte Carlo" model neglects any interaction between the particle - hole states of each configuration. Obviously, the physical case should lie between these two extremes.

About 20% of the pre-equilibrium emissions in these reactions correspond to composite particles, such as deuterons and alpha particles. An important reaction mechanism for the

production of deuterons is "pick-up", in which an incident nucleon takes another nucleon from the target nucleus. Another pre-equilibrium deuteron production mechanism is coalescence [5, 6, 7], in which a deuteron is formed from two fast nucleons that are emitted close to one another in phase-space. In the context of the exciton model of pre-equilibrium reactions, Iwamoto and Harada developed a model that unifies these two mechanism of deuteron emission [8, 9, 10].

2. Iwamoto and Harada unified model

We started with the model proposed in Ref. [9], in which deuteron formation is represented by a quasi-classical phase space factor. As we were trying to reproduce their results, we found some inconsistencies in their calculations. With that, we tried to improve this model by making the necessary adjustments to implement it in Blann and Chadwick's model, [4]. This implementation would allow us to obtain more realistic results in pre-equilibrium nuclear reactions.

Even with the treatment of the inconsistencies in the Iwamoto and Harada model, our results were not satisfactory. Our values did not fit with the experimental values and the results of the deuteron formation mechanisms did not follow the same pattern as the experimental data. As an example, our ratio of the deuteron pick-up partial emission widths and proton partial emission widths decreased with the increase of the target mass while the experimental data kept the same ratio.

3. Eikonal phase space

We decided to investigate an alternative approximation to the phase space as a way to improve our last results. With that, we have begun to investigate an eikonal phase space.

To begin, we calculate the one-step distorted-wave Born approximation (DWBA) amplitude of a proton-induced (p,d) reaction in the following way:

$$\langle \vec{K}_d; h|T^{(1)}|\vec{K}_p\rangle = \int d^3r_d \int d^3r_p \phi_d^{\dagger}\psi_d^{\dagger(-)} V(\vec{r}_d - \vec{r}_p)\phi_n \psi_p^{(+)}, \tag{1}$$

where $\psi_d^{(-)}$ is the outgoing deuteron wave function and $\psi_p^{(+)}$ is the incoming proton wave function. Both of these include the information of the plane wave plus the spherical wave that reach the detector. ϕ_n is the neutron wave function and ϕ_d is the internal wave function of the deuteron.

4. Preliminary results

We started analyzing the differential cross section for the (p, d) reaction on ^{40}Ca in the $1d3/2$ ground-state. However, our simulations did not achieve the same pattern as the experimental data [13].

In order to see why the differential angular cross section did not fit with the experimental data, we searched for the cause of the difference between the results. At first, we tested the $t\rho$ potential against the optical potential that Ref. [13] uses.

In our work, the incident proton is subject to a potential represented by the $t\rho$ approximation,

$$U(\vec{r}) = -\frac{\hbar v}{2}\left[\sigma_{pp}^T(i+\alpha_{pp})\frac{Z}{A} + \sigma_{pn}^T(i+\alpha_{pn})\frac{N}{A}\right]\rho_m(\vec{r}). \tag{2}$$

with $\sigma_{n_1n_2}^T$ being the total cross section and $\alpha_{n_1n_2}$ a scattering phase factor, both energy dependent. $\rho_m(\vec{r})$ is the target density distribution, $v = \hbar k/\mu$, Z and N are the proton and neutron number of the nucleus of mass number $A = Z + N$. We interpolated the values found in Ref. [14] to obtain α and σ.

IOP Conf. Series: Journal of Physics: Conf. Series **1291** (2019) 012036 doi:10.1088/1742-6596/1291/1/012036

In Ref [13], a phenomenological optical potential is used. It is given by

$$V(r) = V_C(r_C) - V(e^x+1)^{-1} - i\left[W - 4W_D a' \frac{d}{dr}\right](e^{x'}+1)^{-1} + \left[\frac{\hbar c}{m_p c^2}\right]^2 V_{SO}\frac{1}{r}\frac{d}{dr}(e^{x''}+1)^{-1}\sigma I, \quad (3)$$

where $x = (r - R_0)/a_0$, $x' = (r - R')/a'$, $x'' = (r - R'')/a''$, with $R_0 = r_0 A^{1/3}$, etc., and the Coulomb potential V_C is that for a uniformly charged sphere of radius $R_C = r_C A^{1/3}$. W_0 and W_D are the volume and surface parts, respectively, of the imaginary potential, and V_{SO} is the real part of the spin-orbit potential, σ is the projectile spin and I is the orbital angular momentum. The values of the parameters are given in Ref. [13].

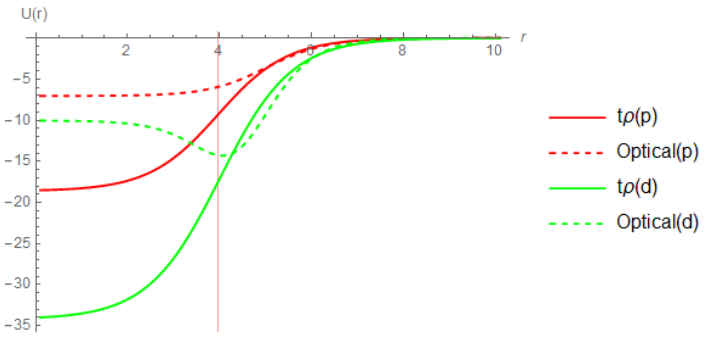

Figure 1. Comparison between the $t\rho$ approximation and the optical potential used in Ref. [13]. The abscissa represents the nucleus radius in fm and the ordinate represents the potential value in MeV. The red vertical line represents the target radius.

In Fig. 1, one can see that our potential is in a good agreement with the optical potential just at large radii but much deeper at smaller radii.

In Ref. [13], the distorted-wave Born approximation (DWBA) code DWUCK (Distorted Wave University of Colorado Kunz) [15] was used to analyze the differential cross section. As we are trying to build our code and using their experimental values as our source, we decided to compare results. In Fig. 2, one can see their experimental values (dots) and our calculations using their values input in DWUCK4 (line). In their work, they used an adiabatic potential for the deuteron channel but we did not include it in our input. It may be what causes the difference between our results, but such a conclusion is preliminary.

As our next step, we expect to conclude our comparison of the optical model potential and the $t\rho$ potential. With that, we expect to have a good idea of how the $t\rho$ approximation should behave in our differential cross section results. This step is important in order to validate the phase space that we are studying. Our hope is to improve the calculations of our model of deuteron emission in pre-equilibrium reaction.

5. Goal and Conclusion

Our ultimate goal is to implement a version of the Iwamoto and Harada model in the DDHMS module of the nuclear reaction code EMPIRE[11] which performs calculations of pre-equilibrium reactions within the HMS model, and then use it to analyze data of reactions of the type (p,d).

As our previous results using Iwamoto and Harada model were not satisfactory, we are analyzing the phase space of the "pick-up" reactions using an eikonal approximation. With that, we hope to get better results and to improve the Iwamoto and Harada model.

As next steps, we will investigate the relation between our transition matrix as function of the energy and of the nucleus radius. Achieving better results, we plan to implement the Iwamato and Harada unified model with our modifications in Blann and Chadwick's "hybrid Monte Carlo"

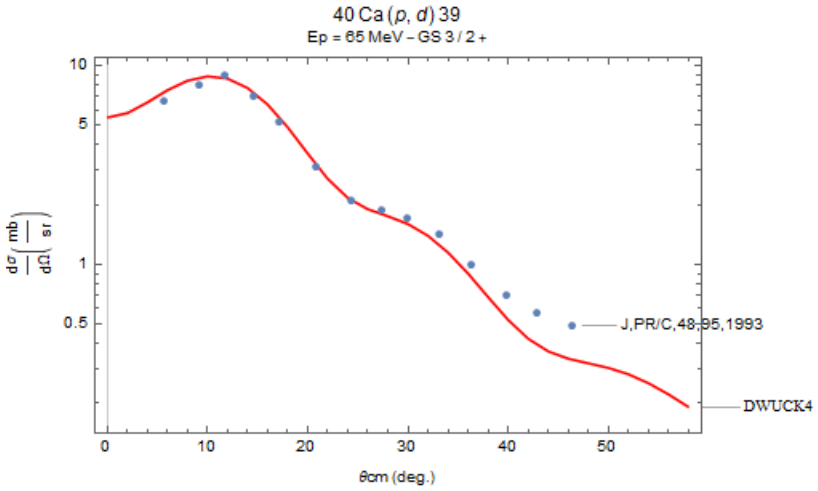

Figure 2. Angular distribution data of cross section for the ground state 3/2+ state in ^{40}Ca(p,d)^{39}Ca. The dots are the experimental values from Ref. [13] and the line are the predictions of the DWBA theory calculated using DWUCK [15].

model, to obtain a more physically-motivated description of pre-equilibrium deuteron emission. Inserting this result in the nuclear reactions code EMPIRE, we hope to improve the analysis of (p,d) reaction data.

Acknowledgments

E. A. Teixeira acknowledges support from the Coordenação de Aperfeiçoamento de Pessoal de Nível Superior - Brasil (CAPES) - Código de Financiamento 001. B. V. Carlson acknowledges support from grant 2017/05660-0 of the São Paulo Research Foundation (FAPESP) and grant 306433/2017-6 of the Brazilian National Council for Scientific and Technological Development (CNPq). The authors acknowledge support from the INCT-FNA project 464898/2014-5.

References

[1] Koning A and Duijvestijn M 2004 *Nucl. Phys.* A **744** (2004) 15.
[2] Bisplinghoff J 1986 *Phys. Rev.* C **33** 1569.
[3] Blann M 1996 *Phys. Rev.* C **54** 1341.
[4] Blann M and Chadwick M 1997 *Phys. Rev.* C **57** 233.
[5] Butler S and Pearson C 1961 *Phys. Rev. Lett.* **7** 69; 1963 *Phys. Rev* **129**, 836.
[6] Schwarzschild A and Zupancic C 1963 *Phys. Rev.* **129** 854.
[7] Nagle J, Kumar B, Kusnezov D, Sorge H and Mattiello R 1996 *Phys. Rev.* C **53** 367.
[8] Iwamoto A and Harada E 1982 *Phys. Rev.* C **26** 1821.
[9] Sato K, Iwamoto A and Harada E 1983 *Phys. Rev.* C **28** 1527.
[10] Konoboeyev A and Korovin Y 1996 *Kerntechnik* **61** 45.
[11] Herman M et al 2007 *Nucl. Dat. Sheets* **108** 2655.
[12] Hosono K et al 1980 *Nuclear Physics* A **343** p.234-248.
[13] Matoba M et al 1993 *Phys. Rev* C **48** p.95-104.
[14] Bertulani C, Campbell C and Glasmacher T 2003 *Computer Physics Communications* **152** p.317-340.
[15] Kunkz P, Maruhn J and Koonin E 1993 *Computational Nuclear Physics* 2 p.88-107.

Appendix B - Potentials used in the eikonal approximation

In this appendix, we discuss two potentials used in our studies with the eikonal approximation. This subject was introduced before in appendix A. One can also see our conclusion about the comparison between both potentials there.

B.1 t_ρ approximation

A possible choice for the nucleon-nucleus optical potential is the t_ρ approximation. The forward-angle nucleon-nucleon t-matrix is often parameterized as

$$t_{n_1n_2}\left(\vec{q}=0\right)=-\frac{2\pi\hbar^2}{\mu}f_{n_1n_2}\left(\vec{q}=0\right)=-\frac{\hbar v}{2}\sigma^T_{n_1n_2}\left(\alpha_{n_1n_2}+i\right), \tag{B.1}$$

where $f_{n_1n_2}$ is the n_1-n_2 scattering amplitude ($n_{1,2}=n,\,p$) and $\sigma^T_{pp}=\sigma^T_{nn}$ and σ^T_{pn} are the proton-proton, neutron-neutron and proton-neutron total cross-sections. In this case, we take for the proton-target optical potential

$$U\left(\vec{r}\right)=-\frac{\hbar v}{2}\left[\sigma^T_{pp}\left(i+\alpha_{pp}\right)\rho_p\left(\vec{r}\right)+\sigma^T_{pn}\left(i+\alpha_{pn}\right)\rho_n\left(\vec{r}\right)\right], \tag{B.2}$$

The total cross sections $\sigma^T_{n_1n_2}$ as well as the factors $\alpha_{n_1n_2}$ are energy dependent. We will assume that the cross sections and factors $\alpha_{n_1n_2}$ used in the optical potential also contain the effects of Pauli blocking in the nuclear medium. The position dependent quantities $\rho_p\left(\vec{r}\right)$ and $\rho_n\left(\vec{r}\right)$ are the target proton and neutron densities. These are often approximated as Z/A and N/A times the total nucleon density, $\rho_m\left(\vec{r}\right)$, where Z and N are the proton and neutron number of the nucleus of mass number $A=Z+N$.

Using $\rho_m(\vec{r})$, we can change $U(\vec{r})$ to

$$U(\vec{r}) = -\frac{\hbar v}{2}\Big[\sigma_{pp}^{T}(i+\alpha_{pp})\frac{Z}{A} + \sigma_{pn}^{T}(i+\alpha_{pn})\frac{N}{A}\Big]\rho_m(\vec{r}). \tag{B.3}$$

The total nucleon density $\rho_m(\vec{r})$ is given by

$$\rho_m(z,\vec{b}) = \int_0^\infty \frac{\rho_0}{1+\exp\Big[(\sqrt{b^2+z^2}-R)/a\Big]}dz, \tag{B.4}$$

with $\rho_0 \simeq 0.165$ nucleons$/F^3$, $R \simeq 1.25A^{1/3}$ F, and $a \simeq 0.55$ F. Inserting all these ideas in eq. (B.3), we get

$$U(\vec{r}) = -\frac{\hbar v}{2}\left[\sigma_{pp}^{T}(i+\alpha_{pp})\frac{Z}{A} + \sigma_{pn}^{T}(i+\alpha_{pn})\frac{N}{A}\right]\int_0^\infty \frac{\rho_0}{1+\exp\Big[(\sqrt{b^2+z^2}-R)/a\Big]}dz, \tag{B.5}$$

where $\mu c^2 = (A-1)mc^2/(A+1)$, $K_p = \sqrt{2\mu E_{cm}}/\hbar c$, $E_p = 65$ MeV, and $E_{cm} = (A \times E_p)/(A+1)$. For σ_{nn} and α_{nn}, we had used the values for $E_{lab} \leq 100$ MeV from (BERTULANI *et al.*, 2003) to get these constant values, as shown in table B.1. For $E_p = 65$ MeV, we interpolated the values to obtain $\alpha = 0.9772\, fm^2$, and $\sigma = 12.6745\, fm^2$.

TABLE B.1 – Parameters values from (BERTULANI *et al.*, 2003) for the nucleon-nucleon amplitude. The values are averaged over *pp* and *pn* collisions.

E$[MeV/nucl]$	$\langle\sigma_{NN}\rangle\,[fm^2]$	$\langle\alpha_{NN}\rangle$
30	19.6	0.87
38	14.6	0.89
40	13.5	0.90
49	10.4	0.94
85	6.10	1.00

As we are working with (p,d) reactions, the nucleons have to "feel" some Coulomb repulsion. We represent the Coulomb repulsion as

$$\exp\left[\frac{iZe^2}{(\hbar c)^2}(\Delta p + \Delta d)\right], \tag{B.6}$$

where Z is the proton number of the target nucleus, e is the electron charge, Δp and Δd are represented by

$$\Delta p(b) = \frac{\log(k_p b)\mu}{2k_p}, \qquad \text{and} \qquad \Delta d(b) = \frac{\log(k_d b)mc^2}{k_d}, \tag{B.7}$$

where μ is the reduced mass of the center of mass, mc^2 is the proton mass, k_p is the incident proton kinetic energy, and k_d is the deuteron kinetic energy. The kinetic energies are given by

$$k_p = \sqrt{\mu E_{cm}}/\hbar c, \qquad \text{and} \qquad k_d = \sqrt{4\mu E_d}/\hbar c, \tag{B.8}$$

with

$$E_{cm} = \frac{AE_{lab}}{A+1}, \qquad \text{and} \qquad E_d = E_{cm} + M_A + M_p - M_d - M_B - E_{lvl}, \tag{B.9}$$

where M_A is the mass of the target, M_p is the proton mass, M_d is the deuteron mass, M_B is the mass of the target less one neutron, and E_{lvl} is the level energy, which is given by experimental values. We used the mass excess instead of the real masses.

From this perspective, we can include eq. (B.6) in eq. (3.7) to have our final amplitude equation with all variables on it,

$$\begin{aligned}
\langle \vec{K}_d; h|T^{(1)}|\vec{K}_p\rangle = {} & 2\pi V_0 \int_0^\infty bdb \exp\left[\frac{iZe^2}{(\hbar c)^2}(\Delta p + \Delta d)\right] J_m(2kb\sin(\theta/2)) \\
& \times \int_{-\infty}^{\infty} dz Y_l^m(\theta_n, \phi_n)\left(\sqrt{\frac{m\omega}{\hbar}}\right)^{3/2} \\
& \times \left[\frac{1}{\pi^{1/4}}\sqrt{\frac{2^{l-(n+1)}(2n+2l-1)!!}{(n-1)!}}\frac{1}{(2l+1)!!}\right](\vec{b}+z\hat{z})^l \\
& \times \left[1 - \frac{(n-1)}{l+3/2}(\vec{b}+z\hat{z})^2 + \frac{(n-1)(n-2)}{(l+3/2)(l+5/2)}\frac{(\vec{b}+z\hat{z})^4}{2!}\right] e^{-(\vec{b}+z\hat{z})^2/2} \\
& \times \exp\left[\frac{i}{2}\left[\sigma_{pp}^T(i+\alpha_{pp})\frac{Z}{A} + \sigma_{pn}^T(i+\alpha_{pn})\frac{N}{A}\right]\rho_0\left(\int_{-\infty}^{z}\frac{1}{1+\exp\left[(\sqrt{b^2+z'^2}-R)/a\right]}dz'\right)_p\right. \\
& \left. + i\left[\sigma_{pp}^T(i+\alpha_{pp})\frac{Z}{A} + \sigma_{pn}^T(i+\alpha_{pn})\frac{N}{A}\right]\rho_0\left(\int_{z}^{\infty}\frac{1}{1+\exp\left[(\sqrt{b^2+z'^2}-R)/a\right]}dz'\right)_d\right].
\end{aligned} \tag{B.10}$$

Most of the variables were already defined. The second, third, and fourth lines come from the neutron radial function.

Eq. B.10 concludes our discussion about the t_ρ approximation. Using it on eq. **??** gives

us the differential angular distribution.

B.2 Optical potential

Another potential used in our calculations with the eikonal approximation is the optical potential used in (MATOBA *et al.*, 1993). We equate our U with their $V(r)$:

$$V(r) = V_C(r_C) - V(e^x+1)^{-1} - i\left[W - 4W_D a' \frac{d}{dr}\right](e^{x'}+1)^{-1} + \left[\frac{\hbar c}{m_p c^2}\right]^2 V_{SO}\frac{1}{r}\frac{d}{dr}(e^{x''}+1)^{-1}\sigma I, \tag{B.11}$$

where $x = (r - R_0)/a_0$, $x' = (r - R')/a'$, $x'' = (r - R'')/a''$, with $R_0 = r_0 A^{1/3}$, etc., and the Coulomb potential V_C is that for a uniformly charged sphere of radius $R_C = r_C A^{1/3}$. W_0 and W_D are the volume and surface parts, respectively, of the imaginary potential, and V_{SO} is the real part of the spin-orbit potential. The imaginary part of the spin-orbit potential was always set to zero in (MATOBA *et al.*, 1993) as they found that its value turned out to be very small in all cases. The other parameters are also given by them as

$$\begin{aligned}
V &= (49.9 - 0.22E_p + 26.4(N-Z)/A + 0.4Z/A^{1/3})\,\text{MeV},\\
r_0 &= 1.16\,\text{fm}, \quad a_0 = 0.75\,\text{fm},\\
W &= 1.2 + 0.09E_p\,(\text{MeV}),\\
W_D &= 4.2 - 0.05E_p + 15.5(N-Z)/A \text{ or } 0\ (\text{MeV}) \text{ (whichever is greater)},\\
r' &= 1.37\,\text{fm}, \quad a' = 0.74 - 0.0008E_p + 1.0(N-Z)/A\,\text{fm},\\
r'' &= 1.064\ \text{fm}, \quad a'' = 0.78\,\text{fm},\\
r_C &= 1.25\,\text{fm}, \quad V_{SO} = 6.04\,\text{MeV}.
\end{aligned} \tag{B.12}$$

The Coulomb potential given by

$$V_C(r_C) = \begin{cases} \dfrac{Ze^2}{4\pi\varepsilon_0 R_C}\left[1 + \dfrac{1}{2}\left(1 - \left(\dfrac{r_C}{R_C}\right)^2\right)\right] & \text{when } r_C < R_C,\\ \dfrac{Ze^2}{4\pi\varepsilon_0 r_C} \text{ when } r_C > R_C. \end{cases} \tag{B.13}$$

Inserting all these values in eq. B.11, we get

$$V(r) = V_C(r_C) - V(e^x+1)^{-1} - iW(e^{x'}+1)^{-1} - 4iW_D\frac{e^{x'}}{(e^{x'}+1)^2} - \left[\frac{\hbar c}{m_p c^2}\right]^2 V_{SO}\frac{1}{r}\frac{e^{x''}}{a''(e^{x''}+1)^2}\sigma I. \tag{B.14}$$

With $V(r)$ being our U, the exponential part of eq. 3.7 will change and the new transition amplitude will be given as

$$\langle \vec{K}_d; h|T^{(1)}|\vec{K}_p\rangle = V_0 \int d^3r \exp(i\vec{q}\cdot\vec{r})\psi_n \times \exp\left[-\frac{i\mu c^2}{(\hbar c)^2 k_p}\int V_p(r)dz' - \frac{imc^2}{(\hbar c)^2 k_d}\int V_d(r)dz'\right], \tag{B.15}$$

where V_p and V_d are the potential for proton and deuteron, respectively. The values used for each nucleon is given in table B.2.

TABLE B.2 – Parameters values used for the optical potential.

Parameter	Proton (p)	Deuteron (d)
Z	20	
A	40	
α	0.988	
σ	9.219	
ρ_0	0.165	
$\hbar c$	197.32	
a	0.75	0.779
R_0	3.9671	4.0013
k_n	1.7051	2.1412

We used the optical potential in all calculations performed on sec. 3.1.2.1, sec. 3.2 and in our proceedings paper published and available on appendix A

Appendix C - Redefining our phase space

Besides trying to find a new formulation to improve the unified model, we have also investigated its implications in more detail by looking more closely at the restrictions that are applied in the model. We start by using the ideas from (IWAMOTO; HARADA, 1982). One can see in Fig. C.1 a comparison between our attempt to calculate the amplitude T, eq. 3.13, using the unified model and the one from DWUCK. The DWUCK amplitude is multiplied by 3. The interesting thing to observe in this figure is that both results has the same behavior.

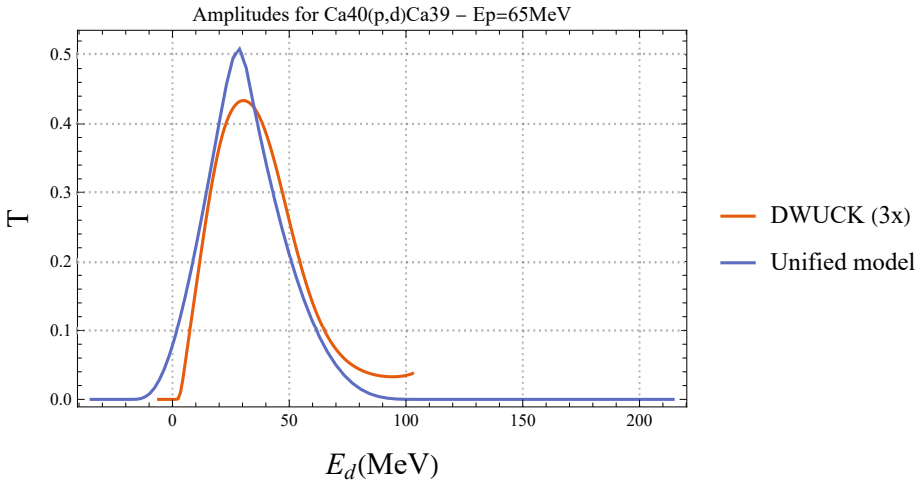

FIGURE C.1 – Comparison between the unified model amplitude and DWUCK for ^{40}Ca(p,d)^{39}Ca with $E_p = 65$ MeV. DWUCK is multiplied by 3.

C.0.1 Semi-classical pickup by Iwamoto and Harada

Consider a differential pickup rate consisting of the velocity at which protons pass a target nucleus times the differential phase space for a deuteron being emitted. We use

the semi-classical phase space approximation of Iwamoto and Harada. We write this as

$$\begin{aligned} d\lambda = \frac{p_p}{m}\theta\Big(\epsilon_0 - \frac{p^2}{2\mu} - \frac{\mu\omega^2 r^2}{2}\Big)\theta(p_{Fn} - |\vec{p}_n|)\delta\Big(\frac{|\vec{r}_p + \vec{r}_n|}{2} - R\Big) \\ \times \theta(R + \Delta - |\vec{r}_n|)\theta(R + \Delta - |\vec{r}_p|)\frac{d^3r_p d^3p_p}{(2\pi\hbar)^3}\frac{d^3r_n d^3p_n}{(2\pi\hbar)^3}, \end{aligned} \tag{C.1}$$

where R is the radius of the nucleus, Δ an adjustable length, p_{Fn} the neutron Fermi momentum, $\mu = m/2$, with m the nucleon mass, and ϵ_0 and ω are the parameters describing the deuteron phase space,

$$\vec{p} = \frac{1}{2}(\vec{p}_p - \vec{p}_n) \quad \text{and} \quad \vec{r} = \vec{r}_p - \vec{r}_n. \tag{C.2}$$

The deuteron momentum and position are given by

$$\vec{P}_d = \vec{p}_p + \vec{p}_n \quad \text{and} \quad \vec{R}_d = \frac{1}{2}(\vec{r}_p + \vec{r}_n). \tag{C.3}$$

The initial proton momentum is given and we would like to determine the pickup rate as a function of the deuteron momentum. We thus use the definition of the deuteron momentum to write

$$\vec{p}_n = \vec{P}_d - \vec{p}_p \quad \text{and} \quad \vec{p} = \vec{p}_p - \vec{P}_d/2. \tag{C.4}$$

These definitions place two constraints on $\vec{P}_d$, since $\vec{p}_p$ is given. These are

$$p_n^2 = \left(\vec{P}_d - \vec{p}_p\right)^2 \leq p_{Fn}^2 \quad \text{and} \quad p^2 = \left(\vec{p}_p - \vec{P}_d/2\right)^2 \leq 2\mu\epsilon_0. \tag{C.5}$$

We also transform the differential momentum volume as

$$d^3p_p d^3p_n \to d^3p_p d^3P_d. \tag{C.6}$$

It is interesting to analyze the momentum constraints on $\vec{P}_d$ independently of the additional coordinate constraints in the deuteron phase space factor. The constraints above furnish

$$\begin{aligned} P_d^2 + p_p^2 - 2P_d p_p \cos\theta_p \leq p_{Fn}^2, \\ P_d^2 + 4p_p^2 - 4P_d p_p \cos\theta_p \leq 8\mu\epsilon_0, \end{aligned} \tag{C.7}$$

or

$$\begin{aligned}(P_d - p_p\cos\theta_p)^2 &\leq p_{Fn}^2 - p_n^2\sin^2\theta_p,\\ (P_d - 2p_p\cos\theta_p)^2 &\leq 4(2\mu\epsilon_0 - p_p^2\sin^2\theta_p),\end{aligned} \tag{C.8}$$

where θ_p is the angle between the two momenta. These inequalities have solutions when

$$\sin^2\theta \leq \min(p_{Fn}^2, 2\mu\epsilon_0)/p_p^2. \tag{C.9}$$

In this case, we have

$$\begin{aligned}p_p\cos\theta_p - \sqrt{p_{Fn}^2 - p_p^2\sin^2\theta_p} \leq& P_d \leq p_p\cos\theta_p + \sqrt{p_{fn}^2 - p_p^2\sin^2\theta_p},\\ 2p_p\cos\theta_p - 2\sqrt{2\mu\epsilon_0 - p_p^2\sin^2\theta_p} \leq& P_d \leq 2p_p\cos\theta_p + 2\sqrt{2\mu\epsilon_0 - p_p^2\sin^2\theta_p}.\end{aligned} \tag{C.10}$$

Since both conditions must be satisfied simultaneously, we see that no solution will exist at sufficiently high initial momentum p_p. This will be the case when

$$p_p\cos\theta_p + \sqrt{p_{Fn}^2 - p_p^2\sin^2\theta_p} < 2p_p\cos\theta_p - 2\sqrt{2\mu\epsilon_0 - p_p^2\sin^2\theta_p}, \tag{C.11}$$

or

$$p_p\cos\theta_p > \sqrt{p_{Fn}^2 - p_p^2\sin^2\theta_p} + 2\sqrt{2\mu\epsilon_0 - p_p^2\sin^2\theta_p}. \tag{C.12}$$

Let us assume that this occurs at $\theta_p = 0$. Then, no solution will exist for

$$p_p > p_{Fn} + 2\sqrt{2\mu\epsilon_0}. \tag{C.13}$$

Using the Iwamoto and Harada value of $\epsilon_0 = 12.1$ MeV, $p_{Fn} = 270$ MeV, and $m = 938$ MeV, we find a limit of $p_p > 483$ MeV, which would correspond to $E_p > 124$ MeV. At this limiting value of the proton momentum, the only allowed value of the deuteron momentum would be $P_d = 753$ MeV, corresponding to an energy $E_d = 151$ MeV. Note that the restrictions on p_p and P_d are even tighter when $r^2 \neq 0$.

Turning now to the radii, which we will integrate, let us consider the vector $\vec{r}_n$ relative to $\vec{r}_p$, and write the constraint on the deuteron center-of-mass radius as

$$r_n^2 + r_p^2 + 2r_n r_p\cos\theta_n = 4R^2, \tag{C.14}$$

where we consider r_p fixed. As the definition of $\vec{r}$ gives

$$r^2 = r_n^2 + r_p^2 - 2r_n r_p \cos\theta_n, \tag{C.15}$$

we can use the center-of-mass radius to eliminate the cosine in the r^2, and write it as

$$r^2 = 2(r_n^2 + r_p^2 - 2R^2). \tag{C.16}$$

With $\cos\theta_n = 1$, we obtain the lower limit for r_n, as

$$r_{n,\min} = 2R - r_p \quad \text{with} \quad \cos\theta_{n,\min} = 1. \tag{C.17}$$

Its maximum value will be

$$r_{n,\max} = R + \Delta \quad \text{with} \quad \theta\cos_{n,\max} = \frac{4R^2 0(R+\Delta)^2 - r_p^2}{2(R+\Delta)r_p}. \tag{C.18}$$

Leaving out the deuteron phase space factor for the moment, which is independent of the angular variables ϕ_n and θ_n, the integral over $\vec{r}_n$ can be simplified as

$$\begin{aligned}\int d^3r_n \delta\Big(\frac{|\vec{r}_p + \vec{r}_n|}{2} - R\Big) &= 2\pi \int_{r_{n,\min}}^{r_{n,\max}} r_n^2 dr_n \int_{-1}^{1} dx \delta(f(x) - R) \\ &= 2\pi \int_{r_{n,\min}}^{r_{n,\max}} r^2 dr_n \frac{1}{f'(x)}\bigg|_{f(x)=R},\end{aligned} \tag{C.19}$$

where we have used the azimuthal symmetry to integrate over ϕ_n and written

$$f(x) = \frac{1}{2}\sqrt{r_p^2 + r_n^2 + 2r_n r_p x} \quad \text{with} \quad f'(x) = \frac{r_n r_p}{2f(x)}, \tag{C.20}$$

with $x = \cos\theta_n$, so that

$$\int d^3r_n \delta\Big(\frac{|\vec{r}_p + \vec{r}_n|}{2} - R\Big) = 2\pi \frac{4R}{r_p} \int_{r_{n,\min}}^{r_{n,\max}} r_n dr_n. \tag{C.21}$$

To make the $\vec{r}_p$ integral conform to the geometry of the collision, we write $d^3r_p = d^2b_p dz_p$,

so that

$$\begin{aligned} d\lambda =& \frac{p_p}{m}\frac{d^3p_p d^3P_d}{(2\pi\hbar)^6}\theta\left(p_{Fn} - |\vec{P}_d - \vec{p_p}|\right)(4\pi)^2 R \\ & \times \int_0^{R+\Delta=R_d} b_p db_p \int_{-z_{p,max}}^{z_{p,max}} \frac{dz_p}{r_p}\int_{2R-r_p}^{R_d} r_n dr_n \\ & \times \theta\left(\epsilon_0 - \frac{\left(\vec{p}_p - \vec{P}_d/2\right)^2}{2\mu} - \mu\omega^2(r_n^2 + r_p^2 - 2R^2)\right), \end{aligned} \tag{C.22}$$

with $\mu = m/2$, $r_p^2 = b_p^2 + z_p^2$, $z_{p,max} = \sqrt{R_d^2 - b_p^2}$, and p_p given by the problem. As-a-result, we can open up eq. C.22,

$$\begin{aligned} d\lambda =& \frac{(4\pi)^2 R}{m}\frac{d^3P_d}{(2\pi\hbar)^6}p_p \\ & \times \theta\left(p_{Fn} - \sqrt{P_d^2 - 2P_d p_p\cos\theta_{p_p,Pd} + p_p^2}\right) \\ & \times \int_0^{R_d} b_p db_p \int_{-z_{p,max}}^{z_{p,max}} \frac{dz_p}{r_p}\int_{2R-r_p}^{R_d} r_n dr_n \\ & \times \theta\left(\epsilon_0 - \frac{p_p^2 - P_d p_p\cos\theta_d + (P_d/2)^2}{2\mu} - \frac{mc^2}{2}\left(\frac{\omega\hbar}{\hbar c}\right)^2(r_n^2 + r_p^2 - 2R^2)\right), \end{aligned} \tag{C.23}$$

with

$$\cos\theta_d = \max\left(\frac{p_1^2 + P_d^2 - p_F^2}{2p_1P_d}, \frac{p_1^2 + P_d^2/4 - 2\mu\varepsilon_0}{p_1P_d}\right), \tag{C.24}$$

we get the final equation (remember that $\vec{P}_d$, eq. C.3, is constant here),

$$\begin{aligned} d\lambda =& \frac{R}{4\pi^4\hbar^6 m}p_p \times \frac{2\pi}{3}P_d^3 \\ & \times \theta\left(p_{Fn} - \sqrt{P_d^2 - 2P_d p_p\cos\theta_d + p_p^2}\right) \\ & \times \int_0^{R_d} b_p db_p \int_{-z_{p,max}}^{z_{p,max}} \frac{dz_p}{r_p} \\ & \times \int_0^{\theta_d} \sin\theta d\theta \int_{2R-r_p}^{R_d} r_n dr_n \\ & \times \theta\left(\epsilon_0 - \frac{p_p^2 - P_d p_p\cos\theta_d + (P_d/2)^2}{2\mu} - \frac{mc^2}{2}\left(\frac{\omega\hbar}{\hbar c}\right)^2(r_n^2 + r_p^2 - 2R^2)\right). \end{aligned} \tag{C.25}$$

We have calculated the differential pickup rate using the last equation. The result can be seen in Fig. C.2. Even though the rate has low values, we are interested in the behavior

of the result. One can observe that the curve starts to behave as the curve for the pickup formation factor, Fig. 2.8, but it drops abruptly and goes to zero after $\epsilon_d = 56$ MeV. This behavior is odd and needs to be investigated further.

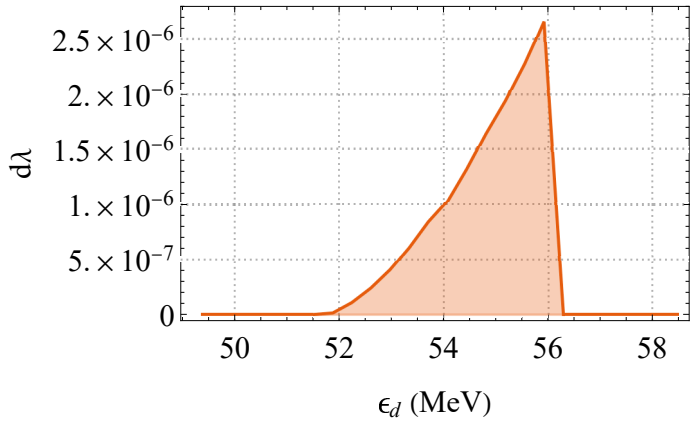

FIGURE C.2 – Differential pickup rate ($d\lambda$) for ^{40}Ca(p,d)^{39}Ca with $E_p = 65$ MeV by $\epsilon_d = E_d - 2\epsilon_F$ (where E_d is the deuteron energy, and ϵ_F is the Fermi energy).

Appendix D - Inelastic scattering with DWBA

D.1 One-step inelastic scattering

The one-step DWBA amplitude of a nucleon-induced reaction has the general form

$$T_{DWBA} = \int d^3r\, \psi_{k_f}^{(-)*}(\vec{r}) \left\langle B \left| \sum_{j=1}^{A} V(\vec{r} - \vec{r}_j) \right| A \right\rangle \psi_{k_i}^{(+)}(\vec{r}) \,, \tag{D.1}$$

where we have written the nucleon-nucleus interaction as a sum of nucleon-nucleon interactions $V(\vec{r} - \vec{r}')$. Any individual interaction can be written as

$$\left\langle \vec{k}_f;\, ph \left| T \right| \vec{k}_i \right\rangle = \int d^3r\, d^3r'\, \psi_{k_f}^{(-)*}(\vec{r})\; \psi_p^*(\vec{r}')\, V(\vec{r} - \vec{r}')\; \psi_h(\vec{r}')\; \psi_{k_i}^{(+)}(\vec{r}) \,, \tag{D.2}$$

where ψ_h is an occupied orbital in the initial nucleus (a hole state after the collision) and ψ_p is an unoccupied orbital or continuum state of the initial nucleus. There are three possibilities for the final state:

1. One of the two particles remains in the continuum while the second occupies a previously unoccupied bound state of the nucleus. This is the situation assumed in all multi-step direct models and corresponds to the amplitude given above.

2. At sufficiently high incident energy, both of the final particles can be in the continuum. The DWBA amplitude will then be

$$\left\langle \vec{k}_{f_1},\, \vec{k}_{f_2};\, h \left| T \right| \vec{k}_i \right\rangle = \int d^3r\, d^3r'\, \psi_{k_{f_1}}^{(-)*}(\vec{r})\; \psi_{k_{f_2}}^{(-)*}(\vec{r}')\; V(\vec{r} - \vec{r}')\; \psi_h(\vec{r}')\; \psi_{k_i}^{(+)}(\vec{r}) \,. \tag{D.3}$$

3. At extremely low energy, both of the particles can occupy previously unoccupied bound states of the nucleus. In this case, we would say that the incident nucleon was absorbed. The corresponding DWBA amplitude is

$$\left\langle p_1 p_2 h \left| T \right| \vec{k}_i \right\rangle = \int d^3r \, d^3r' \, \psi^*_{p_1}(\vec{r}) \, \psi^*_{p_2}(\vec{r}') \, V(\vec{r} - \vec{r}') \, \psi_h(\vec{r}') \, \psi^{(+)}_{k_i}(\vec{r}) \, . \tag{D.4}$$

To simplify the development of the possible amplitudes, we will assume that the nucleon-nucleon interaction can be well represented by a contact interaction,

$$V(\vec{r} - \vec{r}') \approx V_0 \delta(\vec{r} - \vec{r}') \, . \tag{D.5}$$

For the first case above, in which only one of the particles is in the continuum after the interaction, we have for the eikonal scattering amplitude,

$$\begin{aligned}
\left\langle \vec{k}_f ; \, ph \left| T^{(1)} \right| \vec{k}_i \right\rangle &= \int d^3r \, \psi^{(-)*}_{k_f}\left(z, \vec{b}\right) \, V_0 \, \psi^*_p\left(z, \vec{b}\right) \psi_h\left(z, \vec{b}\right) \, \psi^{(+)}_{k_i}\left(z, \vec{b}\right) \\
&= V_0 \int d^3r \, e^{i\vec{q}\cdot\vec{r}} \psi^*_p\left(z, \vec{b}\right) \psi_h\left(z, \vec{b}\right) \\
&\qquad \times \exp\left[-\frac{i}{\hbar v_f} \int_z^\infty U_f\left(z', \vec{b}\right) dz' - \frac{i}{\hbar v_i} \int_{-\infty}^z U_i\left(z', \vec{b}\right) dz' \right] \\
&= V_0 \int d^2b \, e^{i\vec{q}\cdot\vec{b}} e^{i\left(\delta_i(b) + \delta_f(b)\right)} \\
&\qquad \times \int_{-\infty}^\infty dz \, \psi^*_p\left(z, \vec{b}\right) \psi_h\left(z, \vec{b}\right) \\
&\qquad \times \exp\left[i q_z z + \frac{i}{\hbar v_f} \int_0^z U_f\left(z', \vec{b}\right) dz' - \frac{i}{\hbar v_i} \int_0^z U_i\left(z', \vec{b}\right) dz' \right] ,
\end{aligned} \tag{D.6}$$

with $\vec{q} = \vec{k}_i - \vec{k}_f$. We rewrite this as

$$\begin{aligned}
\left\langle \vec{k}_f ; \, ph \left| T^{(1)} \right| \vec{k}_i \right\rangle &= V_0 \int d^2b \, e^{i\vec{q}\cdot\vec{b}} e^{i\left(\delta_i(b) + \delta_f(b)\right)} \\
&\qquad \times \int_{-\infty}^\infty dz \, \psi^*_p\left(z, \vec{b}\right) \psi_h\left(z, \vec{b}\right) \exp\left[i q_z z - i\phi_f\left(z, \vec{b}\right) + i\phi_i\left(z, \vec{b}\right) \right] ,
\end{aligned} \tag{D.7}$$

where

$$\phi_m\left(z, \vec{b}\right) = -\frac{1}{\hbar v_m} \int_0^z U_m\left(z', \vec{b}\right) dz' \, , \tag{D.8}$$

and

$$\delta_m(b) = \lim_{z \to \infty} \phi_m\left(z, \vec{b}\right) \, . \tag{D.9}$$

The amplitude of the second case above, in which both final state nucleons are in the continuum, takes the form

$$\begin{aligned}\left\langle \vec{k}_{f_1},\, \vec{k}_{f_2}; h \left| T^{(1)} \right| \vec{k}_i \right\rangle &= V_0 \int d^3r\, \psi^{(-)*}_{k_{f_1}} \left(z,\, \vec{b}\right)\, \psi^{(-)*}_{k_{f_2}} \left(z,\, \vec{b}\right)\, \psi_h \left(z,\, \vec{b}\right) \psi^{(+)}_{k_i} \left(z,\, \vec{b}\right) \\ &= V_0 \int d^2b\, e^{i\vec{q}\cdot\vec{b}} e^{i\left(\delta_i(b)+\delta_{f_1}(b)+\delta_{f_2}(b)\right)} \\ &\qquad \times \int_{-\infty}^{\infty} dz\, \psi_h \left(z,\, \vec{b}\right) \exp\left[iq_z z - i\phi_{f_1}\left(z,\vec{b}\right) - i\phi_{f_2}\left(z,\vec{b}\right) + i\phi_i\left(z,\vec{b}\right)\right] .\end{aligned}$$

where we now have $\vec{q} = \vec{k}_i - \vec{k}_{f_1} - \vec{k}_{f_2}$.

The final amplitude, in which the interaction de-excites the incoming projectile to a bound state and there is no outgoing wave, can be written as

$$\left\langle p_1 p_2 h \left| T^{(1)} \right| \vec{k}_i \right\rangle = V_0 \int d^2b\, e^{i\delta_i(b)} \int_{-\infty}^{\infty} dz\, \psi^*_{p_1} \left(z,\, \vec{b}\right) \psi^*_{p_2} \left(z,\, \vec{b}\right) \psi_h \left(z,\, \vec{b}\right) \exp\left[ik_z z + i\phi_i\left(z,\vec{b}\right)\right] . \tag{D.10}$$

Appendix E - Energy levels used in DWUCK

In this appendix, we list all values used for the energy levels in DWUCK. One can see the values on Table E.1 through E.4. All binding energies were calculated using the Dirac-Hartree-Bogouliobov (DHB) method. The Q-value calculation is well known, but if the reader needs guidance to calculate it, we suggest the Q-Value online calculator (QCalc) from the National Nuclear Data Center (NNDC), developed by the Brookhaven National Laboratory, `https://www.nndc.bnl.gov/qcalc/`. By the time of publication of this thesis, the QCalc uses the 2020 Atomic Mass Evaluation by M. Wang et al.

Reaction	Target		Ground state orbital					
	A	Z	Orbital	Q (MeV)	n	l	j	Binding (MeV)
^{40}Ca(p,d)^{39}Ca	40	20	1d3/2	-13.4104	0	2	3/2	-16.470
^{40}Ca(n,d)39K				-6.1036				-8.911
^{120}Sn(p,d)^{119}Sn	120	50	2d3/2	-6.880	1	2	3/2	-8.383
^{120}Sn(n,d)^{119}In			1g9/2	-6.880	0	4	9/2	-11.254
^{208}Pb(p,d)^{207}Pb	208	82	3p1/2	-5.143	2	1	1/2	-7.857
^{208}Pb(n,d)^{207}Tl			3s1/2	-5.779		0		-8.356

TABLE E.1 – Energy levels used for our calculations in DWUCK for each reaction described on the Table.

^{40}Ca reactions orbitals data					
Orbital	n	l	2×j	(n,d) binding (MeV)	(p,d) binding (MeV)
s1/2	0	0	1	-47.248	-55.734
p1/2	0	1	1	-26.834	-34.892
p3/2	0	1	3	-31.136	-39.172
d5/2	0	2	5	-15.608	-23.225
2s1/2	1	0	1	-9.785	-17.333
d3/2	0	2	3	-8.911 (GS)	-16.464 (GS)

TABLE E.2 – Energy levels used for our calculations in DWUCK for the ^{40}Ca reactions. (n,d)/(p,d) represents the proton/neutron picked up at the orbital by the incident neutron/proton. Binding means the binding energy of the orbital. **GS** means the ground-state orbital.

^{120}Sn reactions orbitals data					
Orbital	n	l	2×j	(n,d) binding (MeV)	(p,d) binding (MeV)
s1/2	0	0	1	-53.127	-61.920
p1/2	0	1	1	-44.016	-52.396
p3/2	0	1	3	-42.724	-51.183
d5/2	0	2	5	-33.546	-41.504
2s1/2	1	0	1	-27.282	-35.390
d3/2	0	2	3	-30.584	-38.674
f7/2	0	3	7	-22.462	-29.916
f5/2	0	3	5	-17.532	-25.148
2p3/2	1	1	3	-14.918	-22.214
2p1/2	1	1	1	-13.497	-20.817
g9/2	0	4	9	-11.254 (GS)	-18.152
g7/2	0	4	7	–	-11.542
2d5/2	1	2	5	–	-10.477
2d3/2	1	2	3	–	-8.383 (GS)
3s1/2	2	0	1	–	-8.273

TABLE E.3 – Same as Table E.2 but for ^{120}Sn reactions.

^{208}Pb reactions orbitals data					
Orbital	n	l	2×j	(n,d) binding (MeV)	(p,d) binding (MeV)
s1/2	0	0	1	-50.538	-63.393
p3/2	0	1	3	-44.563	-56.605
p1/2	0	1	1	-43.853	-56.028
d5/2	0	2	5	-37.137	-48.483
2s1/2	1	0	1	-31.716	-43.896
d3/2	0	2	3	-35.513	-47.100
f7/2	0	3	7	-28.712	-39.386
f5/2	0	3	5	-25.808	-36.813
2p3/2	1	1	3	-21.205	-32.510
2p1/2	1	1	1	-20.061	-31.393
g9/2	0	4	9	-19.661	-29.666
g7/2	0	4	7	-15.234	-25.614
2d5/2	1	2	5	-11.086	-21.600
2d3/2	1	2	3	-9.308	-19.804
3s1/2	2	0	1	-8.356 (GS)	-19.132
h11/2	0	5	11	-10.267	-19.634
h9/2	0	5	9	–	-14.009
2f7/2	1	3	7	–	-11.455
2f5/2	1	3	5	–	-9.162
3p3/2	2	1	3	–	-8.771
3p1/2	2	1	1	–	-7.857 (GS)
i13/2	0	6	13	–	-9.614

TABLE E.4 – Same as Table E.2 but for ^{208}Pb reactions.

FOLHA DE REGISTRO DO DOCUMENTO

1. CLASSIFICAÇÃO/TIPO	2. DATA	3. DOCUMENTO Nº	4. Nº DE PÁGINAS
TD	25 de Janeiro de 2023	DCTA/ITA/TD-001/2023	142

5. TÍTULO E SUBTÍTULO:
Monte Carlo model of deuteron emission in pre-equilibrium nuclear reactions

6. AUTOR(ES):
Estevão Alves Teixeira

7. INSTITUIÇÃO(ÕES)/ÓRGÃO(S) INTERNO(S)/DIVISÃO(ÕES):
Instituto Tecnológico de Aeronáutica – ITA

8. PALAVRAS-CHAVE SUGERIDAS PELO AUTOR:
Nuclear reactions; pre-equilibrium; Monte Carlo;

9. PALAVRAS-CHAVE RESULTANTES DE INDEXAÇÃO:
Reações nucleares; Método de Monte Carlo; Equilíbrio; Reações por dêuteron; Partículas alfa; Física nuclear; Física.

10. APRESENTAÇÃO: (**X**) **Nacional** ( ) **Internacional**
ITA, São José dos Campos. Curso de Doutorado. Programa de Pós-Graduação em Física; Área de Física Nuclear. Orientador: Prof. Dr. Brett Vern Carlson. Defendida em 20/01/2023. Publicada em 2023.

11. RESUMO:
Pre-equilibrium reactions induced by nucleons are important in applications of nuclear physics, applications for aerospace technologies, atmospheric and space physics, as well as for astrophysics studies. One-fifth of the particles emitted in pre-equilibrium nuclear reactions are composites, such as deuterons, tritiums, and alpha particles. Iwamoto and Harada proposed a semi-classical model for pre-equilibrium nuclear reactions describing direct mechanisms. Deuterons can be produced by a direct reaction mechanism called pickup. Our goal is to implement their model of deuteron emission in the Blann Hybrid-Monte Carlo model to analyze data of proton-induced reactions having deuterons as emitted particles. The unified model phase-space is investigated to understand its restrictions. DWUCK and an eikonal approximation were used to compare with the unified model results. A semi-classical distorted-wave model is used to relate the unified model with the DWBA theory. The theoretical foundation for a Monte Carlo implementation is proposed. We compare our cross-section and angular distribution results with the ones from DWUCK4 for a ground-state to ground-state reaction and also for a sum of all orbits involved in each reaction. We have studied the (p,d) and (n,d) reactions for ^{40}Ca, ^{120}Sn, and ^{208}Pb. We can conclude that we have satisfactory results for all cases studied. The application of the Monte Carlo theoretical foundation and a deep understanding for the results obtained in this study are suggestions for future research.

12. GRAU DE SIGILO:
(**X**) **OSTENSIVO** ( ) **RESERVADO** ( ) **SECRETO**